Inter-calibration of accurate attitude instruments

Jørgensen, Peter Siegbjørn; Brauer, Peter; Jørgensen, John Leif

Publication date:
2002

Document Version
Publisher's PDF, also known as Version of record

Inter-calibration of accurate attitude instruments

Ph.D. dissertation

Peter Siegbjørn Jørgensen

Measurement & Instrumentation Systems
Ørsted·DTU
Technical University of Denmark

August 2002

Second edition, August 2002
First edition, April 2002

Printed at:
Measurement & Instrumentation Systems
Ørsted·DTU
Elektrovej
Building 327
Technical University of Denmark
DK-2800 Lyngby
Denmark

ISBN: 87-91184-12-6

This dissertation was typeset using LaTeX2e with the `book` documentcalss and compiled using the MiKTeX PC implementation of TeX.
Graphs have been produced in MatLab™ from Math. Works Inc.

This manuscript was prepared for a 80% A4 format.

Preface

This dissertation represents the final step towards obtaining the Ph.D. degree at the Technical University of Denmark. The work has been done within the Space Instrumentation Group at the Section for Measurement & Instrumentation (former Institute for Automation) at Ørsted·DTU. The group has been involved in development and construction of space qualified instrumentation for scientific satellites for several years. Primary instruments developed by the group are fluxgate vector magnetometers and Autonomous Stellar Compasses (star trackers). Launched missions include the Danish geomagnetic satellite Ørsted, the German CHAMP, the European PROBA, the U.S. GRACE and the Argentinean SAC-C. Several other are on the way to launch, and still others are on the drawing board.

As a result of this work, highly accurate attitude inter-calibrations of the instruments onboard a number of these satellites have been performed. Also the work has resulted in a software package (ASCfit) for achieving arc second astrometry on astronomical images. This tool is currently in use at the University of Hawai'i 2.2m telescope at Mauna Kea.

The work has been documented through a refereed publication on the inter-calibration of the SAC-C MMP [1], and a conference paper on the ASCfit package [2], both as primary author. Contributions to the work of the determining a main field model of the Earth's magnetic field have resulted in a co-authorship [3].

Acknowledgements

I am deeply thankful to my supervisors Associate Professor John L. Jørgensen, Senior Scientist Fritz Primdahl and Associate Professor Torben Risbo for their support and encouragement during this work. I also thank the Technical University of Denmark for funding this work.

During the thesis work half a year was spent abroad at the Institute for Astronomy at the University of Hawai'i. As result the ASCfit program package was developed and documented. I whish to extend my deep gratitude to Dr. Andrew Pickles who hosted my visit and provided formidable inspiration and support. Here I would also like to thank Troels Riis and Maurizio Bettto who did the founding work for ASCfit and Dr. Richard

Crowe for contributing with his CCD camera.

I would also like to thank Associate Professors Jose M.G. Merayo and Peter Brauer for many fruitful discussions and support during the duration of the work.

Also, I wish to acknowledge the work of E. Bertin in developing the Source-Extractor tool and the many people behind the development of the celestial reference catalogs, without which parts of this work would not have been possible.

This publication makes use of data products from the Two Micron All Sky Survey, which is a joint project of the University of Massachusetts and the Infrared processing and Analysis Center/California Institute of Technology, funded by the National Aeronautics and Space Administration and the National Science Foundation.

Finally I would like to thank my family and friends for their support throughout this work.

Peter Siegbjørn Jørgensen
April 2002, Lyngby, Denmark

Abstract

This text covers the subject of inter-calibration between highly accurate attitude sensing instruments. Inter-calibration in this respect means the determination of the relative attitude between the sensors of these instruments.

The outset is the inter-calibration of attitude sensing instruments used onboard satellites. However the methods studied here aim at a general applicability.

Various attitude representations (Euler angles, orthogonal matrices and quaternions) are presented and their applicability for inter-calibration is discussed.

The general theory for inter-calibration is introduced for cases with two or more attitude sensing instruments. The instruments can provide information about one, two or all three degrees of orientational freedom in ordinary 3D space. All types are considered, but only the two latter are exemplified.

The determination of absolute attitude with respect to a reference frame can be considered an inter-calibration between a model or reference "truth" and an instrument. This is exemplified in the determination of celestial coordinates on astronomical images.

Using the obtained relative attitudes between attitude sensing instruments, it is possible to improve the absolute attitude estimates by combining information from two or more sensors. A method for performing

this combined attitude estimate is presented.

The theory is applied to a number of real cases. The emphasis is on pre-flight inter-calibration of satellite instrumentation. Examples include the Ørsted and SAC-C satellites carrying instrumentation for mapping the magnetic field of the Earth.

The determination of absolute attitude is implemented in a program package and the results used to demonstrate the principle of an inter-calibration for a telescope guidance system.

Data from the German CHAMP satellite are used to demonstrate the method for improvement of the attitude estimate, by combining the measurements from two attitude sensors.

Resume

Denne tekst omhandler inter-kalibrering mellem højpræcisions, retningsbestemmende instrumenter. Inter-kalibrering betyder i denne sammenhæng bestemmelse af den relative orientering mellem disse instrumenters sensorer.

Udgangspunktet er inter-kalibrering af retningsfølsomme instrumenter på satelitter. Metoderne behandlet her sigter dog mod en generel anvendelse.

Forskellige repræsentationer af den rumlige orientering (Euler vinkler, orthonormale matrices og quaternioner) præsenteres og deres anvendelighed ved inter-kalibrering diskuteres.

Den generelle teori for inter-kalibrering introduceres for tilfælde med to eller flere retningsfølsomme instrumenter. Instrumenter kan give information om en, to eller alle tre frihedsgrader af den rumlige orientering. Alle typer betragtes, men kun de to sidste behandles med eksempler.

Bestemmelsen af den absolutte, rumlige orientering i forhold til et reference system kan betragtes som en inter-kalibrering mellem en model eller reference "sandhed" og instrumentet. Dette eksemplificeres ved bestemmelsen af astronomiske koordinater på billeder taget af stjernehimlen.

Ved hjælp af de fundne relative orienteringer mellem de retningsfølsomme instrumenter er det muligt at forbedre bestemmelsen af den absolutte orientering ved at kombinere informationer fra to eller flere sensorer. En metode til dette præsenteres.

Teorien anvendes på en række eksempler. Vægten ligger på pre-flight inter-kalibrering af satellit instrumnetation. Eksemplerne inkluderer Ørsted og SAC-C satellitterne, der er udstyret med instrumentation til kortlægning af jordens magnetiske felt.

Bestemmelsen af den absolutte orientering implementeres i en program pakke. Resultaterne anvendes til at demonstrere inter-kalibrerings princippet for et teleskop styresystem.

Data fra den tyske CHAMP satellit anvendes til at demonstrere metoden til at forbedre bestemmelsen af orienteringen ved kombination af målinger fra to retningsbestemmende sensorer.

Contents

List of Figures

List of Tables

Nonemclature

Synbols

In this work vector and matrix notation will be used extensively. In accordance with normal practice the following conventions are adopted.

Scalars are denoted by an italic lower case letter (latin or greek) e.g. r or ϕ. Greek letters are reserved for angles, unless else is stated angles are measured in degrees, whenever realizations are called for.

Vectors are denoted by a lowercase boldface letter e.g. $\mathbf{v}, \boldsymbol{\xi}$.

Matrices are denoted by uppercase boldface letters e.g. $\mathbf{R}, \boldsymbol{\Xi}$.

Rotations will be used often. When no specific representation is necessary the notation used is R_{S1}^{S2} signifying a transformation from system $S1$ to system $S2$. Three representations of rotations will be used: Euler angles (ϕ, θ, ψ), rotation matrices $\mathbf{R}$ and quaternions $\mathbf{q}$.

Abbrivations

2MASS	2-Micron All-Sky Survey
ASC	Advanced Stellar Compass
BFE	BrorFElde geomagnetic observatory
CCD	Charge Coupled Device
CHU	Camera Head Unit
CSC	Concentric Spherical Coils
CIS	Conventional Inertial System

CTP	Conventional Terrestrial Pole
CTS	Conventional Terrestrial System
DEC	DEClination
DPU	Data Processing Unit
EGSE	Electronic Ground Support Equipment
FITS	Flexible Image Transport System
GAST	Greenwich Apparent Sidereal Time
GPS	Global Positioning System
GSC	Guide Star Catalog
IC	Inter-Calibration
ICRF	International Celestial Reference Frame
ICRS	International Celestial Reference System
IERS	International Earth Rotation Service
ITRF	International Terrestrial Reference Frame
ITRS	International Terrestrial Reference System
LEO	Low Earth Orbit
LLR	Lunar Laser Ranging
LM	Levenberg-Marquardt
mas	milli arc second
MMP	Magnetic Mapper Probe
NED	North East Down
NM	Nelder-Mead
RA	Right Ascension
SIM	Star IMager
TGS	Telescope Guidance System
TMO	Table Mountain Observatory
USNO	United States Naval Observatory
VLBI	Very Long Baseline Interferometry
WCS	World Coordinate System

Terminology

Attitude: Specifies the orientation of an object or coordinate system. Can be either *absolute*, if the attitude is expressed with respect to a fixed reference frame or *relative*, if it is specified with respect to another non-constant object or coordinate system.

Epoch: A specific instant in time used as reference, e.g. the epoch J2000 is 12.00 UT on January 1^{st}, year 2000.

Inter-calibration The process of determination of the relative orientation between attitude sensors.

Meridian plane: Plane perpendicular to the equator, containing the coordinate origin, the pole and the point considered.

Rotation: The transformation from one system to another, under the condition that the origins of the two systems coincide, i.e. no translation.

Seeing: Astronomical term for the amount of atmospheric disturbance when conducting celestial observations from the ground. Little disturbance gives "good" seeing. Quantified by the *seeing angle* $\Delta\Theta = \lambda/r_0$, λ being the wavelength and r_0 being the radius of spatial coherence of the observed light.

Transformation: General term for changing from one coordinate system to another, can include translation, rotation and scaling.

Vernal Equinox (Υ)**:** Reference direction in celestial reference frames. The direction from the Earth to the Sun at the time of the vernal equinox (approximately March 22). Equivalently defined as the intersection between the Earth equator and the Earth ecliptic plane (i.e. the plane of the Earth's motion around the Sun).

Chapter 1

Introduction

1.1 Background and Motivation

This dissertation describes the development and analysis of methods for determining relative orientations between highly accurate attitude sensitive instruments.

The ever-progressing development of this type of instruments necessitates new methods for determining the relative orientations between them. New methods should comply with the increased accuracy and aim to simplify the implicated procedures, as the use of high accuracy instrumentation becomes more widespread.

In particular the outset for this thesis work was a series of geomagnetic mapping satellites (ASTRID II, ØRSTED, CHAMP and SAC-C) each carrying highly accurate instrumentation in the form of star cameras and vector magnetometers. Accurate determination of the relative orientation between these two instruments was needed in order to achieve the scientific goals of creating accurate models of the Earth's magnetic field (Magnetic Main Field Models).

The focus throughout this work has been on methods that will be generally applicable for relative orientation determination. Specific needs for satellite applications have been investigated through case studies. Other applications include e.g. alignment of telescope guiding systems and establishment of temporary geomagnetic observatories.

This first introductory chapter presents the attitude and inter-calibration framework and basic elements. Previous work within the field is summa-

rized and the delimitation of this work is given. Finally the outline of the dissertation is presented at the end of the chapter.

1.2 Attitudes

The term *attitude* will in this thesis be used to denote the three-dimensional orientation of an object (e.g. an instrument or a satellite) with respect to another object or a reference frame. In general, attitude will mean the orientation of one three-axis coordinate system with respect to another. In connection with attitudes the phrase *rotation* will be used to describe the transformation from one system to another. An attitude will thus be specified by the transformation, in the form of a rotation, between the systems. To fully specify such a rotation, or attitude, all three orientational degrees of freedom for ordinary three-dimensional space must be specified. The representation of attitude by rotating the coordinate system, which is applied here, is often referred to as the *passive* approach. In the complementary *active* representation the coordinate system is kept fixed while vectors are rotated. The passive approach has the mental advantage that physical vectors are not changed, it is only the description of the vector which changes.

Numerous representations of attitudes exist. A comprehensive summary is given in [4], while [5] presents a more compact introduction to attitude descriptions. The representations used in this work include: *Euler angles*, *orthonormal matrices* (sometimes called *rotational matrices*) and *quaternions*. These three representations of attitude are summarized in the following.

1.2.1 Euler angles

Euler angles are sets of three angles specifying rotations about three coordinate axes. An example is seen in Figure 1.1. This 3-2-3-Euler rotation is comprised of three consecutive rotations about the 3^{rd}, the 2^{nd} and finally the 3^{rd} coordinate axis. As seen in Figure 1.1 this takes the coordinate system through two intermediate positions before the final orientation is reached. This rotation is denoted by $R_{323}(\phi_1, \phi_2, \phi_3)$. ϕ_i being the angles of the three rotations. Euler angles are divided into symmetric and asymmetric sets according to whether a rotation axis is repeated or not. Hence

for $(i, j, k \in 1, 2, 3)$ $R_{iji}(\phi_1, \phi_2, \phi_3)$ are symmetric Euler rotations while $R_{ijk}(\phi_1, \phi_2, \phi_3)$ $(i \neq k)$ are asymmetric Euler rotations. The constraint $i \neq j$ and $j \neq k$ must be imposed to ensure completeness of the attitude representations.

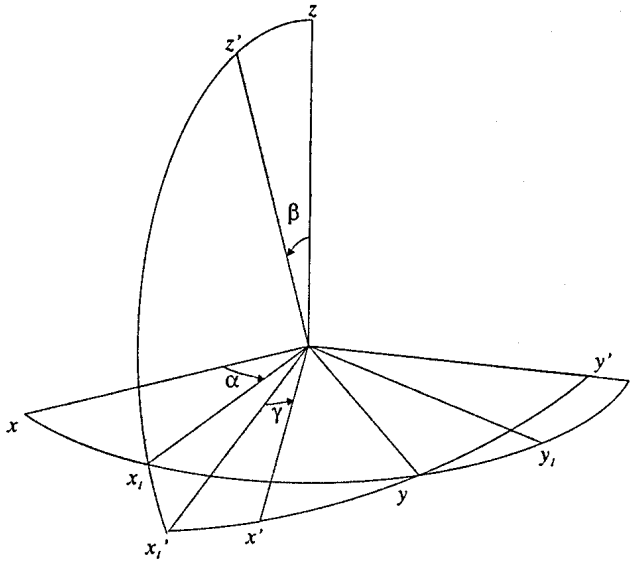

Figure 1.1: 323-Euler angle definition, figure from [6]

For each set of axes (i, j, k) a given attitude can be represented by at least one set of angles, thus each set gives a complete representation of the attitudes. In order to obtain unique representation using Euler angles, bounds are often put on the v_2 angle. By using $0 \leq v_2 \leq 2\pi$ for symmetric sets and $-\pi\backslash 2 \leq v_2 \leq +\pi\backslash 2$ in asymmetric cases a unique representation is obtained. Furthermore, Euler angles suffer from degeneracy in special cases. All the symmetric sets will be near degenerate when the second angle is close to zero. Asymmetric degeneracy occurs when the second rotation carries the first rotation axis into the third rotational axis. The degeneracy also plays a role when creating composed rotations from two or more sets of Euler angles. Consider a rotation comprised of two 323

Euler rotations $R = R_{323}(\phi_1, \phi_2, \phi_3)R_{323}(\theta_1, \theta_2, \theta_3)$. Here the two rotation angles θ_3 and ϕ_1 are about the same axis and thus only their sum is well determined.

Despite these drawbacks the Euler angle representation is useful and often chosen because its parameterization with three angles contains no redundant information for specifying attitudes, and because the rotations about coordinate axes are intuitively clear.

1.2.2 Orthonormal Matrices

Orthonormal matrices are characterized by having unit length and mutually perpendicular row and column vectors, i.e. if $\mathbf{R} = [\mathbf{v_1}|\mathbf{v_2}|\mathbf{v_3}]$ is an orthonormal matrix, then

$$\mathbf{v_i} \cdot \mathbf{v_j} = \delta_{ij} \tag{1.1}$$

Where δ_{ij} is the Kronecker delta symbol, defined by:

$$\delta_{ij} = \begin{cases} 0 & \text{if } i \neq j \\ 1 & \text{if } i = j. \end{cases} \tag{1.2}$$

Orthonormal matrices can represent attitudes by interpreting the column vectors as the coordinate vectors for the three coordinate axes of one system in the other. The definition used, is that a physical vector $\mathbf{r}$, that in a system (1) is represented by the coordinate vector $\mathbf{r}^1$, will be represented by the coordinate vector $\mathbf{r}^2$ in a second system (2) which is rotated with respect to the first system. If the column vectors of the orthonormal matrix $\mathbf{R}$ are the coordinate vectors for the three basis vectors of system (1) expressed in system (2) then the change of coordinates is represented by

$$\mathbf{r}^2 = \mathbf{R}\mathbf{r}^1. \tag{1.3}$$

Successive rotations can be composed from individual orthonormal matrices by simple matrix multiplication. If $\mathbf{S}$ also is an orthonormal matrix

$$\mathbf{r}^3 = \mathbf{S}\mathbf{r}^2 = \mathbf{S}(\mathbf{R}\mathbf{r}^1) = (\mathbf{S}\mathbf{R})\mathbf{r}^1. \tag{1.4}$$

Note the order of the matrices. The first rotation is the right most in equation (1.4). From basic linear algebra the product $\mathbf{SR}$ will also be an orthonormal matrix. Since matrix multiplication does not commute the

well-known fact that finite rotations do not commute can be seen from equation (1.4).

The three basic rotations around the coordinate axes are given by

$$\mathbf{R}_1(\alpha) = \begin{bmatrix} 1 & 0 & 0 \\ 0 & \cos(\alpha) & \sin(\alpha) \\ 0 & -\sin(\alpha) & \cos(\alpha) \end{bmatrix} \tag{1.5}$$

$$\mathbf{R}_2(\beta) = \begin{bmatrix} \cos(\beta) & 0 & -\sin(\beta) \\ 0 & 1 & 0 \\ \sin(\beta) & 0 & \cos(\beta) \end{bmatrix} \tag{1.6}$$

$$\mathbf{R}_3(\gamma) = \begin{bmatrix} \cos(\gamma) & \sin(\gamma) & 0 \\ -\sin(\gamma) & \cos(\gamma) & 0 \\ 0 & 0 & 1 \end{bmatrix} \tag{1.7}$$

From these, any of the Euler rotations can be build, e.g. the 323-Euler rotation will be represented by the orthonormal matrix

$$\begin{aligned} \mathbf{R}_{323}(\phi_1, \phi_2, \phi_3) &= \mathbf{R}_3(\phi_3)\mathbf{R}_2(\phi_2)\mathbf{R}_3(\phi_1) \\ &= \begin{bmatrix} \cos(\phi_3) & \sin(\phi_3) & 0 \\ -\sin(\phi_3) & \cos(\phi_3) & 0 \\ 0 & 0 & 1 \end{bmatrix} \begin{bmatrix} \cos(\phi_2) & 0 & -\sin(\phi_2) \\ 0 & 1 & 0 \\ \sin(\phi_2) & 0 & \cos(\phi_2) \end{bmatrix} \begin{bmatrix} \cos(\phi_1) & \sin(\phi_1) & 0 \\ -\sin(\phi_1) & \cos(\phi_1) & 0 \\ 0 & 0 & 1 \end{bmatrix} \end{aligned} \tag{1.8}$$

The orthonormal rotation matrix can also be found (see e.g. [4]) from the axis of rotation $\hat{\mathbf{v}}$ and the angle of rotation about this axis θ

$$\mathbf{R}_{\hat{\mathbf{v}}}(\theta) = \cos\theta\mathbf{I} + (1 - \cos\theta)\hat{\mathbf{v}}\hat{\mathbf{v}}^T + \sin\theta[[\hat{\mathbf{v}}]] \tag{1.9}$$

This expression is known as Euler's formula. The double bracket notation signifies the matrix used in connection with the cross product for 3-vectors i.e. $\mathbf{a} \times \mathbf{b} = -[[\mathbf{a}]]\mathbf{b}$, so that

$$[[\mathbf{a}]] = \begin{bmatrix} 0 & a_3 & -a_2 \\ -a_3 & 0 & a_1 \\ a_2 & -a_1 & 0 \end{bmatrix} \tag{1.10}$$

Orthonormal matrices are often used in the practical implementation when transforming coordinate vectors from one system to another. They have the advantage that an orthonormal matrix uniquely represents a given attitude. However, when several consecutive rotations are carried out, computations become cumbersome and care must be taken to keep the matrices orthonormal as numerical errors build up, e.g. by re-normalizing the matrices. Also the matrices carries redundant information with their nine parameters.

1.2.3 Quaternions

The third representation of attitudes used in this work is the *quaternions*. Quaternions (or *Euler-Rodriges symmetric parameters*) were originally developed by Hamilton in the early 1840s as a generalization of the complex numbers, and in 1845 Caley used the quaternion formalism to rotate 3D vectors. Quaternions are the extension of the complex numbers to four dimensions. A quaternion consists of four numbers (a, b, c, d) and is written as

$$q = a \cdot \hat{i} + b \cdot \hat{j} + c \cdot \hat{k} + d \tag{1.11}$$

where $\hat{i}, \hat{j}$ and $\hat{k}$ are the three complex quantities for which the following rules of multiplication apply:

$$\begin{gathered} \hat{i}^2 = \hat{j}^2 = \hat{k}^2 = -1 \\ \hat{j} \cdot \hat{k} = -\hat{k} \cdot \hat{j} = \hat{i}, \qquad \hat{k} \cdot \hat{i} = -\hat{i} \cdot \hat{k} = \hat{j}, \qquad \hat{i} \cdot \hat{j} = -\hat{j} \cdot \hat{i} = \hat{k} \end{gathered} \tag{1.12}$$

Note that the multiplication of quaternions does not commute. Inspired by complex numbers, vector and scalar parts are respectively defined by

$$Vq = a \cdot \hat{i} + b \cdot \hat{j} + c \cdot \hat{k} \tag{1.13}$$

$$Sq = d. \tag{1.14}$$

The conjugate, norm and inverse are similarly defined by

$$Kq = -Vq + Sq \tag{1.15}$$

$$Nq = \sqrt{(qKq)} \tag{1.16}$$

$$q^{-1} = \frac{Kq}{(Nq)^2}. \tag{1.17}$$

Rotations can be represented by quaternions with unit norm. In order to rotate a 3D coordinate vector $(\mathbf{r})$ a quaternion q_r is constructed by letting $\mathbf{r}$ be the vector part Vq_r and letting the scalar part be zero, i.e. $q_r = r_x\hat{i} + r_y\hat{j} + r_z\hat{k} + 0$. The rotation is then carried out by

$$q_r{}' = q\, q_r\, q^{-1} \tag{1.18}$$

$q_r{}'$ will also have zero scalar part and the vector part will be the coordinates of the vector in the rotated system.

A vector/matrix representation of quaternions also exists. Here the quaternion is written as a vector with four components

$$\mathbf{q} = (a, b, c, d)^T \tag{1.19}$$

In this notation quaternion multiplication can be represented by matrix multiplication

$$\mathbf{q}_2 \otimes \mathbf{q}_1 = \{\mathbf{q}_2\}_L \mathbf{q}_1 = \{\mathbf{q}_1\}_R \mathbf{q}_2. \tag{1.20}$$

Where the *left* and *right* multiplication matrices are given by

$$\{\mathbf{q}\}_L \equiv \begin{bmatrix} d & c & -b & a \\ -c & d & a & b \\ b & -a & d & c \\ -a & -b & -c & d \end{bmatrix} \qquad \{\mathbf{q}\}_R \equiv \begin{bmatrix} d & -c & b & a \\ c & d & -a & b \\ -b & a & d & c \\ -a & -b & -c & d \end{bmatrix} \tag{1.21}$$

The rotation represented by a quaternion can be envisaged by regarding the vector part (Vq) as an axis of rotation. The scalar part will then give the angle of rotation (θ) about this axis via $Sq = \cos(\theta/2)$.

Like the orthonormal matrices the quaternions carry redundant information in its four parameters, when used to represent rotations or attitudes, which are defined by only three parameters. This redundancy is removed by the unit norm demand. Thus, care must be taken to normalize quaternions when used in composite rotations. There is a non-uniqueness of the quaternion attitude representation since q and $-q$ represent the same attitude.

Quaternions are used extensively in real-time attitude control work and computer graphics, since compound rotations require fewer computations in the quaternion formulation than in the matrix formalism. However, this advantage of the quaternions is not crucial for this work.

The equations for going between the various attitude representations are given in [4].

1.2.4 Relative and absolute attitudes

In the following the terms *relative* and *absolute* attitudes will be mentioned. Their representations are the same, the difference lies in what the attitudes refer to. Relative attitudes describe the orientations of instrument systems with respect to each other, while absolute attitudes represent attitudes of instruments with respect to absolute reference systems

such as e.g. the geodetic WGS84 reference system or the International Celestial Reference Frame (ICRF).

Next the basic framework for the inter-calibration will be set up. For this, relative attitudes are of interest.

1.3 Inter-calibration

Inter-calibration is a widely used term, but here it will exclusively denote the process of determining the relative attitude (or orientation) between two or more instruments.

The representations of relative attitudes are the same as mentioned in the previous section. Here the emphasis is on the relative orientation between two or more coordinate systems.

Inter-calibrations are needed for several reasons. Traditionally, attitude control has relied on inter-calibrations. When determining the absolute attitude of a body (e.g. a spacecraft), with sensors of various types, it is essential to know the relative orientation of the sensors to the body. For scientific instrumentation, sensors are often divided into specialized units, some which measures physical quantities and others, which determine the absolute orientation with respect to some reference frame. In order to tie the measurements to the reference frames the relative attitude between the instruments must be known.

Procedures for highly accurate mechanical and optical measurement of angles do exist [1]. However such procedures are often cumbersome and the limited access to high precision measurement equipment limits the use of these methods. Furthermore, sensors are often build into or embedded in complex structures, which impede or prohibit high precision, mechanical alignment measurements. The final, and decisive reason why mechanical alignment measurement are not sufficient is that once instruments are commissioned, it will seldom be possible to take them back to the lab for alignment control. This especially applies to space instrumentation.

Thus, methods for inter-calibration, which rely only on the measurements, must be sought. This is the subject of this dissertation.

[1] At the National Physics Laboratory in UK angle measurement tables which can measure angles with accuracy down to 0.1 arcsec. exist.

1.3.1 Attitude sensors and instruments

In general, instruments will often be divided into a sensor unit and a data processing unit. Sensors can be characterized by the number of axes determined by the sensor and instruments by the number of degrees of rotational freedom which are resolved. In the following a characterization of sensor types is presented.

The number of coordinate axes specified classifies sensors. Sensors with zero to three axes will be considered. A 0-axis sensor is a scalar sensor (e.g. a proton precession magnetometer, [7]) which actually is not of interest for this work, since no attitude information can be gained from such a sensor, however it is mentioned here for completeness.

An example of a 1-axis sensor is the magnetic fluxgate rod sensor, which measures the projection of the magnetic field along a single axis. 2-axis sensors actually do not exist in their pure form, since it is always possible to construct a third axis perpendicular to the two axes specified. However sensors where the measurements are confined to a sensor-plane determined by to axes will be characterized as 2-axis sensors. An example is the 2-axis sun-sensor ([8], p. 161f). 3-axis sensors specify a full 3-axis coordinate system. Examples are the Compact Spherical Coils (CSC) magnetometer fluxgate sensor ([9]) and the Advanced Stellar Compass (ASC, [10]).

These types of sensors can be combined in instruments to give various types of attitude information. Instruments will, in this work, be classified by the number of degrees of freedom that they determine. The notation used will be On, where $n \in \{0, 1, 2, 3\}$. Thus $O0$ are instruments which fixe zero degrees of freedom, i.e. scalar instruments. Table 1.1 lists various sensors, their number of axes and the attitude information gained from the corresponding instrument.

Note that the number of axes does not always correspond to the number of degrees of freedom fixed by the instrument. E.g. the vector magnetometer has a 3-axis sensor and measures the full magnetic field vector, however the attitude of the sensor is only determined to within a rotation about this magnetic field vector and thus it is an $O2$ instrument.

Table 1.1: Sensor types, number of axes and attitude information.

Sensor type	Number of axes	Instrument type
Fluxgate rod sensor	1	$O1$
2-axes Sun sensor	2	$O2$
Earth horizon sensor	1	$O2$
Vector magnetometer	3	$O2$
Electric field probe	3	$O2$
Star tracker	3	$O3$

Showing the number of instrument axes and instrument type for various attitude sensing instruments.

1.3.2 Class of error terms

The errors in the inter-calibrations performed here will mainly be manifested as residuals between the quantity measured by the instrument and a reference value for this quantity. In general the measurements are to few for the residuals to give meaningful, spectral classification of the errors, so main emphasis will be on mean errors (biases) and magnitude (RMS) of these errors.

Errors will be treated at the instrumental level, i.e. each instrument will be described by a gathered error. Errors within the individual instrument will not be treated, but references to instrument calibrations and error estimates will be given whenever possible.

1.3.3 Time scales

The time scales over which inter-calibrations are studied vary from a few measurements, taken over the periods of minutes to long-term stability studies, which can last for the entire duration of a satellite mission (i.e. several years). Here the focus will be on short-term stability. Measurements are carried out over single or a couple of nights. It will, for some types of inter-calibrations, be possible to study relative attitude for the individual measurement, but in most cases, longer periods (several hours) of measurements will be used to establish the relative orientations.

1.3.4 Applications

Since this work has its origin in the recent geomagnetic satellites Ørsted, CHAMP, and SAC-C, the methods presented here find their most direct application with this type of satellite instrument packages. However the problem of determining relative attitude between instruments is often encountered and applications of the methods are numerous.

In general the methods are especially useful within space instrumentation, when direct measurements are inaccessible or inadequate. This is often the case in high precession space instrumentation, but also for on-ground instrumentation. One such example is the inter-calibration of a guidance system for an astronomical telescope, which is also studied in this work.

1.4 Previous work

Accurate alignment of instruments has been an important part of performing good scientific observations for several hundred years. From the early days of astronomy, instruments often needed to be tied to a reference system. The early precision astronomy instruments, some of which were refined by the Danish astronomer Tycho Brahe [11] during the sixteenth century, often used the local vertical as reference. Alignment of these instruments was accomplished by simple plumb line arrangements and knowledge of the local longitude and latitude. With these means Brahe achieved planetary observations with accuracy of 0.5 to 2 arc minutes[2].

Warfare is another field were accurate alignment instrumentation has been explored, especially for guiding artillery fire. Throughout the 15th and 16th century, numerous mechanical instruments for elevation determination were developed and deployed with varying success.

Later, in the 18th and 19th century the science of geomagnetism emerged. This required accurate alignment of the magnetometers with respect to a geo-based reference frame. With the establishment of fixed magnetic observatories came the need for formalized and uniform procedures for setting up observatories and for carrying out measurements. These included solar observations and optical alignments tools such as

[2] An excellent webpage with Tycho Brahe's astronomical instruments is provided by the Danish Royal Library at: http://www.kb.dk/elib/lit/dan/brahe/index-en.htm.

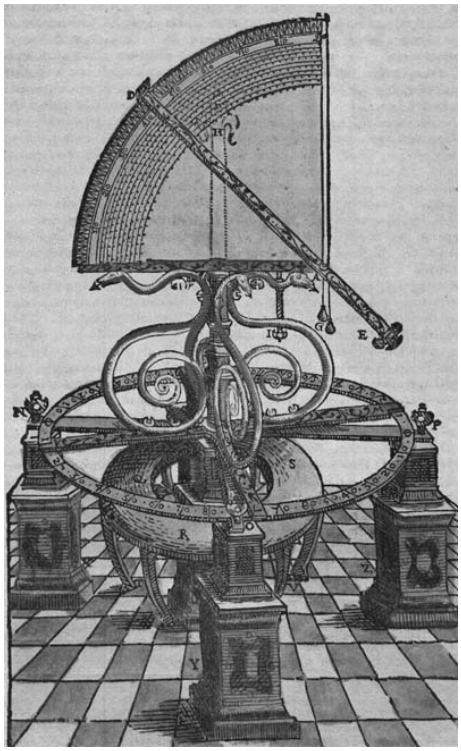

Figure 1.2: *Tycho Brahe's brass quadrant, for measuring the height above the horizon of celestial objects, illustration from [11].*

theodolites.

With the dawn of the space age in 1957 the development of autonomous instrumentation expanded and the need to perform alignment studies without having the instruments directly available arose. The need for alignment studies was dual since both attitude-sensing instruments, used for satellite control purposes, and scientific sensors had to be investigated.

According to [12] the first work on satellite instrumentation alignment seems to be [13] who studied in-flight sensor alignment of the Orbiting Astronomical Observatory using an un-weighted least-squares method. One of six star trackers was assumed to be perfectly aligned and relative atti-

tudes to the rest was determined using cosines of the angles between the sensors.

Later [14] studied the first dedicated geomagnetic satellite MAGSAT. In this work absolute sensor alignment was estimated by using the satellite attitude matrix. Thus, what was obtained was the absolute sensor alignments. In [15] magnetometer calibration parameters, including sensor misalignments, were estimated using a linear-regression method. It was demonstrated that satellite attitude determination from magnetometers improved significantly, from applying accurate sensor calibrations.

MAGSAT and Solar Maximum Mission (SMM) data were investigated by [16]. In this work sensor variances were estimated assuming unbiased errors on the measurements. Also, relative sensor misalignment was studied without the knowledge of satellite attitude.

This work is continued in [17], where the relative sensor alignment is estimated using a maximum likelihood method. Here redundancy of observations and measurement correlation is also taken into account. A factorized method (using SVD) for treating the redundancy problem is also presented.

Similar work was carried out by [18], who also included a description of the pre-flight alignment using optical reference cubes.

The previously mentioned work has all treated vector sensors exclusively. [19] expanded this work to include sensors with 2, 3 or 6 degrees of freedom.

Major contributions concerning attitude calibrations are provided by [12] and [20], which treat relative and absolute alignment calibrations respectively.

Later works include [21], where in-flight alignment of attitude instruments on the Compton Gamma Ray Observatory was investigated using methods similar to those of [12]. In this case drifts of sensor alignments of the order of several hundred arcsec. per year were observed.

An alternative method using an on-board filter approach has been investigated by e.g. [22]. Here a general Kalman filter is used to determine parameters, including sensor alignments, for an attitude system. A parameter observability study resulted in demanded maneuvers for complete observability of the parameters.

1.5 Delimitation of this thesis work

The main emphasis of this dissertation will be on the development, implementation and testing of methods for pre-flight inter-calibration between two or more attitude sensitive instruments. Special cases for satellite and ground equipment will be treated. Both cases with real and synthetic data will be included. In-flight calibration will also be treated theoretically, but due to lack of real data, in-flight calibrations will only be carried out using synthetic data.

1.5.1 New contributions

The methods presented here aim to simplify the calibration procedures e.g. by avoiding the use of optical alignment cubes, which is often cumbersome and relatively inaccurate. Furthermore, emphasis is on the simple setup for the pre-flight calibrations which facilitates the wider use of highly accurate attitude sensing instruments.

Finally this dissertation aims at presenting a relatively complete theoretical background for the determination of relative attitudes between all types of instruments ($O1, O2$ and $O3$). A theory that is easy to apply in future practical inter-calibration work will be sought.

1.6 Thesis outline

Following this introductory chapter, the theory of inter-calibrations is presented in chapter 2. First a general formulation is treated, followed by special cases of interest to this work. A few other subjects relevant for the data analysis will also be treated here.

Chapter 3 will introduce the specific instrumentation to be investigated in this work, i.e. vector magnetometers, star trackers and telescopes. Both single instruments and instrument packages are presented.

Chapter 4 describes considerations of the actual implementation as well as the data analysis and results for the studied cases.

Finally conclusions and suggestions for future work will be given in chapters 5 and 6.

Chapter 2

Theory

This chapter will introduce the main subjects of the theory used in this dissertation. First the inter-calibration between two instruments is described, generally and for special cases. This formalism is expanded to any number of instruments and a single special case (with four instruments) is presented. Hereafter the formalism for describing time and space dependencies of inter-calibrations is introduced. Then, in-flight calibrations and the choice of optimization method are discussed. Attitude error and a method for improving the error of an attitude estimate are introduced. In the final sections of this chapter some aspects of celestial observations (stellar matching, aberration, refraction and reference frames) are treated.

In this chapter the two first sections on the formulation of the inter-calibration and the section on the choice of optimization method describes original work. The attitude error representation is based on [4] while the application to for attitude refinement is a new approach. The section on stellar observations regards well-known facts that have all been implemented in order to carry out the inter-calibration.

2.1 Two-instrument inter-calibration

The inter-calibration (IC) between two instruments is a natural outset for the general theory of inter-calibration, since it is an often encountered situation and especially the case for the geomagnetic satellites Ørsted, CHAMP, SAC-C and Astrid-II, which were the starting points of this work.

The basis for the methods presented here is the Østerport method, which was described in [23], but "not convincingly demonstrated" by experiments. The key idea is to rotate an instrument sensor package (SEN), for example a satellite payload, such that the attitude sensing instruments goes through various positions, while an auxiliary reference instrument package (AUX), fixed with respect to a reference frame, records the natural variations of the quantities measured by the rotated instrument package. Figure 2.1 shows the setup in principle.

-

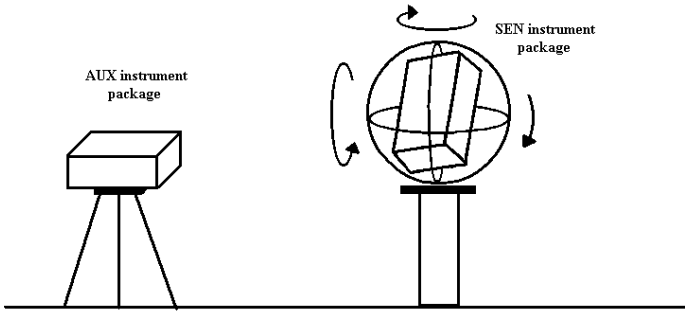

Figure 2.1: *Principle of two instrument inter-calibration.*

By minimizing the residual between measurements from the rotated instrument package and the auxiliary instruments, expressed in a common coordinate system, the relative attitude between the sensors in the instrument package can be determined.

For the two-instrument inter-calibration a distinction between packages with and without $O3$ instruments will be made. The reason being that the absolute attitude for configurations with $O3$ instruments will be measured directly, while the attitude has to be solved for in cases where no $O3$ instruments are present.

2.1.1 Two-sensor IC without $O3$ instruments

The schematic setup for a two-sensor inter-calibration where none of the instruments give the full $O3$ attitude, is shown in Figure 2.2. Displayed here are the two payload sensors SEN_A and SEN_B and the two corresponding auxiliary reference sensors AUX_A and AUX_B. Each pair (SEN_α and $AUX_\alpha, \alpha \in \{A, B\}$) are identical or at least similar instruments, e.g. two sun sensors or two magnetometers. The inter-calibration is performed by letting these instruments take simultaneous measurements. The auxiliary sensors remain fixed while the instrument package, which is to be inter-calibrated, is rotated to a number of positions. The aim is to rotate the measurements from the auxiliary sensor systems to the corresponding package systems. This is indicated in Figure 2.2 by the arrows connecting the coordinate systems.

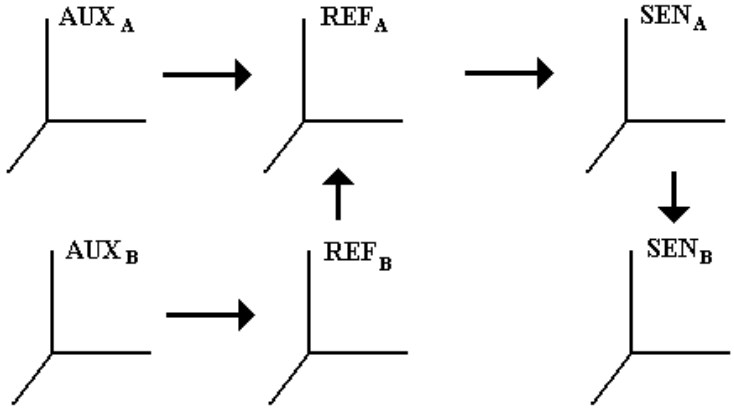

Figure 2.2: *Principle of two instrument inter-calibration, with no O3 instruments.*

The REF_α systems are reference systems for the two sensor types. This could be e.g. the Conventional Inertial System (ICRS) or a local North, East, Down system. The rotation from the auxiliary A system to the sensor A system can now formally be written as

$$R_{AUX_A}^{SEN_A} = R_{REF_A}^{SEN_A} R_{AUX_A}^{REF_A} \tag{2.1}$$

Here R_I^J represents the transformation from system I to system J. In principle both rotations in the above equation are unknown, and must be determined. $R_{AUX_A}^{REF_A}$ will be a fixed rotation, while $R_{REF_A}^{SEN_A}$ will change with every new setting. In a similar fashion, the rotation between the B systems can be written as

$$R_{AUX_B}^{SEN_B} = R_{SEN_A}^{SEN_B} R_{REF_A}^{SEN_A} R_{REF_B}^{REF_A} R_{AUX_B}^{REF_B}. \tag{2.2}$$

Here $R_{SEN_A}^{SEN_B}$ is the relative attitude, which is to be determined, while the transformation between the two reference systems $R_{REF_B}^{REF_A}$ is assumed to be known from theoretical considerations. $R_{AUX_B}^{REF_B}$ will be a fixed rotation and the attitude of the payload $R_{REF_A}^{SEN_A}$ reappears from equation (2.1).

The residual between the payload measurements and the auxiliary measurements expressed in the payload sensor systems, is formally written as

$$residual = \begin{bmatrix} M_{SEN_A} - R_{AUX_A}^{SEN_A} \circledast M_{AUX_A} \\ M_{SEN_B} - R_{AUX_B}^{SEN_B} \circledast M_{AUX_B} \end{bmatrix} \tag{2.3}$$

Where $R \circledast M$ denotes the transformation of a measurement M by the rotation R. The set of rotations that gives the minimum residual is determined by optimization techniques described in section 2.4.

The relative attitude between the payload sensors $R_{SEN_A}^{SEN_B}$ is the one of interest, but all the rotations have to be determined. The uniqueness of the solution found by this method is secured by the fact that rotations about different axes do not commute. Thus when a sufficient number of measurements have been taken it is not possible to obtain different solutions with the same minimum value of the residual in equation (2.3). There will however be an uncertainty in the obtained solution due to the finite accuracy of the measurements taken.

The number of unknowns to be determined will depend on the types of instruments used. If there are N settings of the payload there will be $3N$ unknowns for the payload attitude. Assuming 3-axis sensors there will furthermore be three unknowns for each of the rotations from the two auxiliary sensor systems to the corresponding reference systems. Finally, there will be the three unknowns for the relative attitude, which is to be determined. So in all there is $3N + 9$ unknowns. Still considering vector instruments, each observation will contribute with $2 * 3$ equations, so in all there will be $6N$ equations with residuals. Thus at least three linearly

independent observations must be taken before the inter-calibration can be solved for. However in practice more observations are needed due to the non-linear form of the observation equations, which are composed of rotations. The minimization of the residual vector of equation (2.3) is treated in section 2.4.

2.1.2 Two-sensor IC with one $O3$ instrument

If an $O3$ instrument is included in the instrument package the situation is somewhat simpler. The schematic setup is shown in Figure 2.3. In this

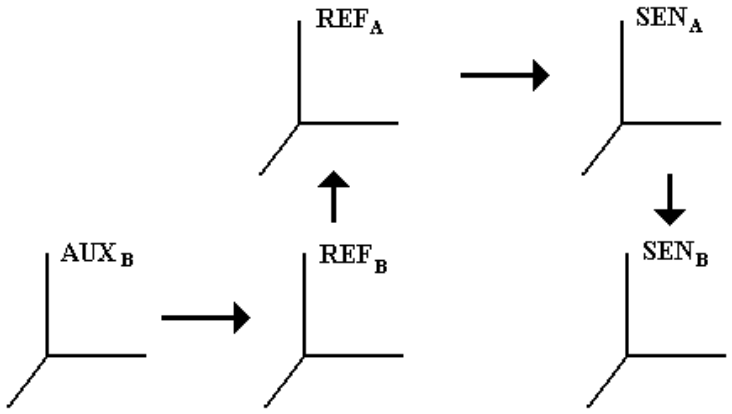

Figure 2.3: *Principle of two instrument inter-calibration with one O3 instrument.*

case there is no auxiliary sensor for the $O3$ sensor (SEN_A). The rotation from AUX_B to SEN_B is formally written as in equation (2.2).

$$R_{AUX_B}^{SEN_B} = R_{SEN_A}^{SEN_B} R_{REF_A}^{SEN_A} R_{REF_B}^{REF_A} R_{AUX_B}^{REF_B}.$$

However the instrument package attitude is now known since $R_{REF_A}^{SEN_A}$ is determined by measurements of sensor A. A residual vector is formed between the two B measurements expressed in the SEN_B system. The relative orientation between to two instruments ($R_{SEN_A}^{SEN_B}$) and the orientation of the auxiliary system in the REF_B system ($R_{AUX_B}^{REF_B}$) are determined by minimizing the residual given by:

$$residual = \left[M_{SEN_B} - R_{AUX_B}^{SEN_B} \circledast M_{AUX_B} \right] \tag{2.4}$$

The number of unknowns is less than for the case without the $O3$ instrument. Here only the relative sensor attitude $R_{SEN_A}^{SEN_B}$ and the orientation of the auxiliary sensor $R_{AUX_B}^{REF_B}$, have to be determined, in all six parameters.

For both the above cases, with or without $O3$ measurements, it is possible that there is an offset between the quantities measured by the corresponding sensor pairs. This can be included in the model by subtracting the offset from the auxiliary measurement before performing the rotations.

$O2$-$O3$ inter-calibration

A specific example of a two-instrument inter-calibration with an $O3$ instrument, is the inter-calibration between a CSC vector magnetometer ($O2$) and a star-tracker or (Advanced Stellar Compass) ($O3$). Together these constitute the geomagnetic mapping mission on board the Ørsted and SAC-C satellites[1]. Details of the various instruments are given in chapter 3.

Measurements for the inter-calibration of this instrument package is carried out by rotating the instrument package in the magnetic field of Earth, while a fixed reference magnetometer measures the natural variations of the Earth magnetic field.

Using the ASC measurements and theoretical knowledge about the Earth's rotation together with an estimate of the relative orientation between the CSC and the ASC, the measurements from the auxiliary magnetometer (AUX) are transformed from the coordinate system of AUX to the CSC coordinate system and expressed here. Thus the ASC plays the role of sensor A and the CSC the role of sensor B in Figure 2.3. By varying the estimate of the relative orientation the residual between the two measurements of the magnetic field, represented in the CSC system, can be minimized to obtain an optimum estimate of the relative orientation.

The relative orientation between ASC and CSC is parameterized by three Euler angles (α, β, γ), giving the rotations about three axes. Here a 323 representation of the Euler angles is chosen. Using the matrix

[1] The German CHAMP satellite also carries similar instrumentation. The inter-calibration of this satellite has been treated by [24].

representation $\mathbf{R}_{ASC}^{CSC}$ which transforms from the ASC system to the CSC system is expressed by

$$\mathbf{R}_{ASC}^{CSC} = \mathbf{R}_3(\gamma)\,\mathbf{R}_2(\beta)\,\mathbf{R}_3(\alpha) \tag{2.5}$$

The transformation of the vector measurements from the AUX system to the CSC system is done via a series of rotations going from AUX over the International Terrestrial Reference System (ITRS) and the International Celestial Reference System (ICRS also known as J2000) to the ASC system and finally on to the CSC system. The various reference systems are described below in section 2.6.3.

If the AUX system is aligned to a local North, East, Down (NED) system, as it is customary in the geomagnetic sciences, the rotation from NED to the Earth centered, Earth fixed ITRS system is expressed by

$$\mathbf{R}_{AUX}^{ITRS} = \mathbf{R}_3(-\Lambda)\,\mathbf{R}_2(90^o + \Phi) \tag{2.6}$$

Here Φ and Λ are astronomical longitude and latitude of the calibration site. If the reference system is not exactly aligned with the NED system a more general rotation in the form of a 232 Euler rotation is used for $\mathbf{R}_{REF}^{ITRF}$.

$$\mathbf{R}_{AUX}^{ITRS} = \mathbf{R}_2(\chi)\,\mathbf{R}_3(\zeta)\,\mathbf{R}_2(\eta) \tag{2.7}$$

As described in section 2.6.3 the transformation from ICRS to ITRS is given by

$$\mathbf{R}_{ICRS}^{ITRF} = \mathbf{SNP} \tag{2.8}$$

$$= \mathbf{R}_2(-x_p)\,\mathbf{R}_1(-y_p)\,\mathbf{R}_3(GAST)\,\mathbf{NP} \tag{2.9}$$

Here $\mathbf{R}_2(-x_p)\,\mathbf{R}_1(-y_p)$ represents the correction for the polar motion, $\mathbf{R}_3(GAST)$ is the Earth's rotation. Finally $\mathbf{N}$ and $\mathbf{P}$ corrects for the nutation and precession of the rotation axis of the Earth. Values for the polar motion (x_p, y_p) are found in the monthly Bulletin B from the International Earth Rotation Service (IERS). GAST (Greenwich Apparent Sidereal Time) is calculated using the formulas from [25], which also gives expressions for the nutation and precession as functions of time.

The ASC measurements consist of three angles (Ra, Dec, Rot) giving the rotation from the ICRS system to the ASC coordinate system. The

rotation from ICRS to the ASC system is given by[2]

$$\mathbf{R}_{ICRS}^{ASC} = \mathbf{R}_3\left(Rot\right)\mathbf{R}_2\left(90^o - Dec\right)\mathbf{R}_3\left(Ra\right) \tag{2.10}$$

All together the rotation from AUX to CSC is described by the matrix:

$$\begin{aligned} \mathbf{R}_{AUX}^{CSC} &= \mathbf{R}_{ASC}^{CSC}\mathbf{R}_{ICRS}^{ASC}\mathbf{R}_{ITRS}^{ICRS}\mathbf{R}_{AUX}^{ITRS} && (2.11)\\ &= \mathbf{R}_3\left(\gamma\right)\mathbf{R}_2\left(\beta\right)\mathbf{R}_3\left(\alpha\right)\mathbf{R}_{ICRS}^{ASC}\mathbf{R}_{ITRS}^{ICRS}\mathbf{R}_{AUX}^{ITRS} && (2.12)\end{aligned}$$

The two matrices, $\mathbf{R}_{ICRS}^{ASC}$ and $\mathbf{R}_{ITRS}^{ICRS}$, will vary from measurement to measurement, while $\mathbf{R}_{ASC}^{CSC}$ and $\mathbf{R}_{AUX}^{ITRS}$ will be constant since the ASC and CSC systems are locked together and since the reference magnetometer remains at a fixed orientation in the ITRS frame.

For each set of measurements a matrix of the type in equation (2.11) can be constructed and used to rotate the measurements from the AUX system to the CSC system. The parameters (α, β, γ) and (χ, ζ, η) are then varied by performing a least squares minimization on the residual vector $\mathbf{L}$, given by

$$\mathbf{L} = \begin{bmatrix} \mathbf{B}_{CSC}^{CSC,1} - \mathbf{R}_{AUX,1}^{CSC}\left(\mathbf{B}_{AUX}^{AUX,1} - \mathbf{O}\right) \\ \vdots \\ \mathbf{B}_{CSC}^{CSC,n} - \mathbf{R}_{AUX,n}^{CSC}\left(\mathbf{B}_{AUX}^{AUX,n} - \mathbf{O}\right) \\ \vdots \\ \mathbf{B}_{CSC}^{CSC,N} - \mathbf{R}_{AUX,N}^{CSC}\left(\mathbf{B}_{AUX}^{AUX,N} - \mathbf{O}\right) \end{bmatrix} \tag{2.13}$$

Here $\mathbf{O}$ is an offset in the magnetic field between the location of the reference magnetometer and the package magnetometer. This offset can either be determined by including the offset as parameters or can be chosen to have a predetermined fixed value.

Several variations of this method are feasible. The AUX orientation can be kept fixed at its theoretical value or be solved for. The offset can be fixed or solved for. Finally, the reference magnetometer can be used as a variometer to correct the magnetometer readings. These options are explored in section 4.3.1 and 4.3.2.

[2]This definition is for the SAC-C ASC. For the Ørsted ASC, $v_3 = 270^o - Rot$ should be used instead of Rot.

2.1.3 Two-sensor IC between two $O3$ instruments

For an instrument package with two $O3$ instruments the relative attitude can be determined directly as long as both instruments are measuring simultaneously. Figure 2.4 shows the principle. In this case no auxiliary instruments are necessary since the full orientation of both the instruments in the package are determined by their measurements. The Determination

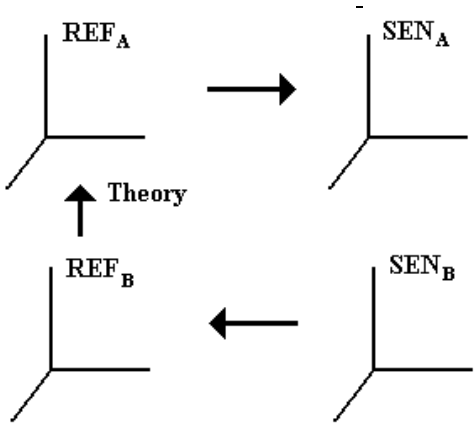

Figure 2.4: *Principle of two instrument inter-calibration with two $O3$ instrument.*

between the two instruments is formally written as

$$R_{SEN_A}^{SEN_B} = R_{REF_B}^{SEN_B} R_{REF_A}^{REF_B} R_{SEN_A}^{REF_A} \tag{2.14}$$

As in the previous cases the transformation between the two reference systems $R_{REF_A}^{REF_B}$ is assumed to be known form theoretical considerations. The two sensors might even have the same reference system, simplifying equation (2.14) even further. For two $O3$ instruments an estimate for the relative attitude might be obtained for each individual pair of measurements and this might be used for performing continuously updated inter-calibrations or for improving the absolute attitude estimates as described in the section 2.5.2.

2.2 N-instrument inter-calibration

The expansion to inter-calibration between N instruments is relatively straightforward. The distinction between weather or not $O3$ instruments are present also has to be made here.

2.2.1 N-sensor IC without $O3$ instruments

The schematic setup for inter-calibrating an instrument package without any $O3$ instruments is shown in Figure 2.5. Here the sensor SEN_A has

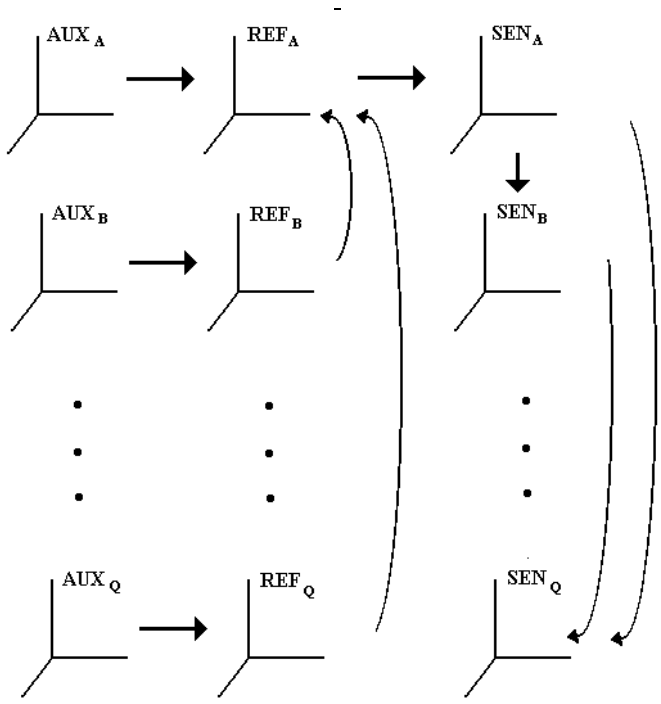

Figure 2.5: *Principle of N instrument inter-calibration, without O3 instruments.*

the specific role as the reference sensor for all the other sensors. Again the principle is to transform measurements from the auxiliary systems via the reference systems and SEN_A to the relevant system and construct the

residuals in the $SEN_\alpha, \alpha \in \{A, B...Q\}$ systems. Minimizing this residual will determine both the absolute attitude of SEN_a, the orientation of the auxiliary sensors with respect to their reference systems and the relative attitudes of the instrument package sensors.

The set of observation equations will have the following general appearance

$$residual = \begin{bmatrix} M_{SEN_A} - R_{AUX_A}^{SEN_A} \circledast M_{AUX_A} \\ M_{SEN_B} - R_{AUX_B}^{SEN_B} \circledast M_{AUX_B} \\ \vdots \qquad\qquad \vdots \\ M_{SEN_Q} - R_{AUX_Q}^{SEN_Q} \circledast M_{AUX_Q} \end{bmatrix} \tag{2.15}$$

where

$$R_{AUX_\alpha}^{SEN_\alpha} = R_{SEN_A}^{SEN_\alpha} R_{REF_A}^{SEN_A} R_{REF_\alpha}^{REF_A} R_{AUX_\alpha}^{REF_\alpha} \tag{2.16}$$

Among these rotations all but $R_{REF_\alpha}^{REF_A}$ are to be considered as unknowns. The total number of unknowns again depend on the type of sensors. In the worst case three parameters have to be determined for each sensor orientation

$$N_{unknown} = 3N_{inst} + 3N_{obs} + 3(N_{inst} - 1) = 3(2N_{inst} + N_{obs} - 1) \tag{2.17}$$

Still considering all the instruments as having three axes, the corresponding number of observation equations is

$$N_{eq.} = 3N_{obs}N_{inst} \tag{2.18}$$

Thus for $N_{obs} \geq 3$ there will be more equations than unknowns for three or more observations.

2.2.2 N-sensor IC with $O3$ instruments

If the package contains one $O3$ instrument the natural choice is to let this act as the reference system for the instrument package. This constitutes the natural expansion from the two-instrument case in section 2.1.2 and is shown in Figure 2.6.

If several $O3$ instruments are present, several options are possible. Either the inter-calibration procedure from the previous section can be performed for each of the $O3$ instruments. This will however give a lot of redundant information about the relative attitudes between the sensors.

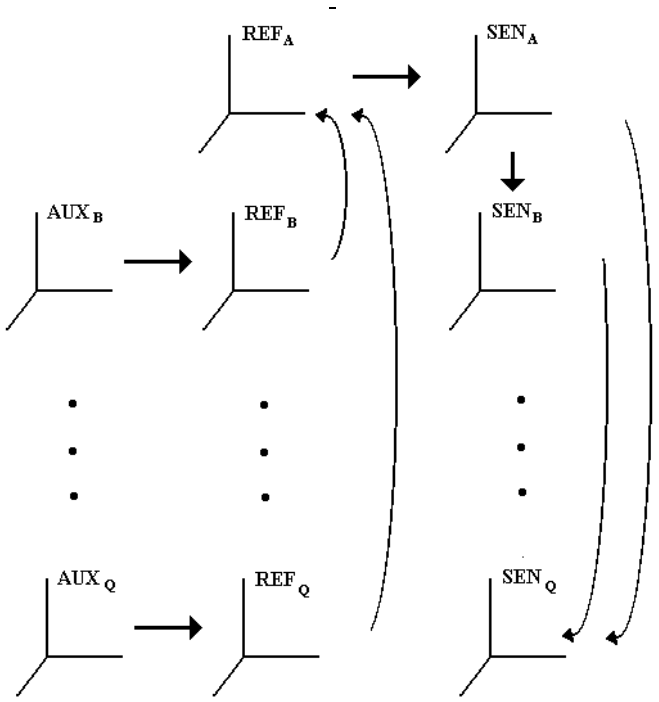

Figure 2.6: *Principle of N instrument inter-calibration, with one O3 instrument.*

Another possibility is to select one of the $O3$ systems as the primary reference system and determine the relative attitude to all the other instrument systems.

2.3 Space-time dependencies of inter-calibrations

Instrumentation packages are often designed to provide a fixed relative orientation between the instruments. However, the relative attitude will in many cases vary as the instrumentation is exposed to various conditions. Causes are numerous and may include temperature fluctuations, mechanical stresses, pressure variations and gravity release. The variations in the relative attitude may be expressed and modeled either as functions

of time, spatial position or spatial orientation. This is described in the following.

2.3.1 Modeling varying relative attitudes

When modeling relative attitudes some care must be taken in selecting a suitable representation.

Euler angles have the advantage that they posses no redundant information, and the three angles can thus be modeled individually. In disfavor of Euler angles is the discontinuities which appear around 0^o and 180^o. However, if variations are small this need not be a problem unless discontinuities are frequent.

Quaternions, with their four parameters, immediately seem somewhat less suited for modeling varying attitudes. The four components can be modeled individually, but care must be taken to keep the unit norm of the modeled quaternion at all times. In their favor the continuos nature of the quaternions must be mentioned. The double representation of attitudes by quaternions (i.e. q and $-q$ represent the same attitude) raises some problems in using quaternions for modeling varying inter-calibrations.

Rotational Matrices, with their 9 parameters, of which 6 are redundant, are not suited for modeling relative attitudes, this is in spite of their unique correspondence between rotational matrices and attitudes.

In this work the quaternion representation is used, whenever models of varying relative attitudes are called for. As described in section 4.3.4 a comparison of Euler angles and quaternions revealed the more agile applicability of the quaternion representation.

2.3.2 Temporal dependencies

The most general way to model changing inter-calibrations is to look at the temporal dependencies. If no specific information about the cause of the variations exist, a temporal model will still provide a valid description to some degree. In this context time dependencies will be modeled by some low order polynomial. In the case of quaternions the four components at

time $t - t_0$ will be expressed by

$$\begin{aligned} q_1 &= k_{10} + k_{11}(t - t_0) + k_{12}(t - t_0)^2 + ... \\ q_2 &= k_{20} + k_{21}(t - t_0) + k_{22}(t - t_0)^2 + ... \\ q_3 &= k_{30} + k_{31}(t - t_0) + k_{32}(t - t_0)^2 + ... \\ q_4 &= k_{40} + k_{41}(t - t_0) + k_{42}(t - t_0)^2 + ... \end{aligned} \tag{2.19}$$

Here the k_{ij} are the coefficients of the model at reference time t_0. The calculation of the parameters can be based on a traditional least square fit (described in brief in section 2.4). From estimates of these coefficients future developments in the relative attitude can be predicted to some extent, but in general such predictions become unstable and should be avoided. Thus, temporal models have their strength in interpolation, not in extrapolation.

When estimating time dependent models, for relative attitudes, over larger periods of time all collected information will not be equally relevant, for an attitude estimated at a given time. Often an exponentially decay with time, of the weight given to the data is applied.

2.3.3 Spatial position dependencies

In order to model eventual spatial position dependencies a representation of the spatial position must first be chosen. This can for instance be Cartesian, spherical or cylindrical coordinates.

For satellites in orbit, spherical coordinates are often advantageous. For example when regarding temperature variations, a coordinate system with the prime meridian either along the dawn-dusk or midnight-noon meridians is a natural choice.

For the spherical coordinates the spherical harmonics, described e.g. in [26], provide a natural set of orthogonal functions for modeling.

For small variations in spatial position Cartesian coordinates may provide the natural choice, performing polynomial modeling with respect to the three spatial coordinates instead of time, as in equation (2.19).

2.3.4 Spatial orientation dependencies

Relative attitudes may also vary with the spatial orientation of the instrument package. This could be caused by varying solar influx or changing

gravitational stresses. Again, several representations of the spatial attitude are possible. Already considered are the Euler angles and quaternions for representing the full three degrees of freedom for spatial orientation. Thus, quaternions can be modeled as functions of quaternions, e.g. in a linear form as

$$\begin{aligned} q_1 &= k_{10} + k_{11}q_1^0 + k_{12}q_2^0 + k_{13}q_3^0 + k_{14}q_4^0 \\ q_2 &= k_{20} + k_{21}q_1^0 + k_{22}q_2^0 + k_{23}q_3^0 + k_{24}q_4^0 \\ q_3 &= k_{30} + k_{31}q_1^0 + k_{32}q_2^0 + k_{33}q_3^0 + k_{34}q_4^0 \\ q_4 &= k_{40} + k_{41}q_1^0 + k_{42}q_2^0 + k_{43}q_3^0 + k_{44}q_4^0 \end{aligned} \tag{2.20}$$

Euler angles might be more suitable, since they have a more natural representation of the physical rotations actually carried out, but their discontinuities again limit their general applicability.

All three degrees of freedom are not always needed, two or even one might be enough. This is for instance the case for the telescope-ASC intercalibration considered in section 4.3.3. Here the mounting of the telescope allow only two degrees of freedom in its orientation. This orientation can be represented by the Azimuth and Zenith angles (A, z) as show in Figure 2.7. For this case, partly due to the insufficient number of data points, only a first order model in A and z is chosen.

2.4 Optimization

As stated in sections 2.1 and 2.2 the solution to the inter-calibration problem is found by minimizing residual functions like equation (2.3) or (2.15). In order to ensure that this is done in an optimal way, three methods of optimization are considered in the following: Linear inversion, Levenberg-Marquardt and Nelder-Mead. First some remarks about the demands to the optimization are given.

2.4.1 Requirements for the optimization

The residual equations are comprised of measurements and rotations of these measurements. The parameters of interest to this work, are the ones specifying the rotations of the relative attitudes. Depending on the parameterization chosen for the rotations these residual equations can

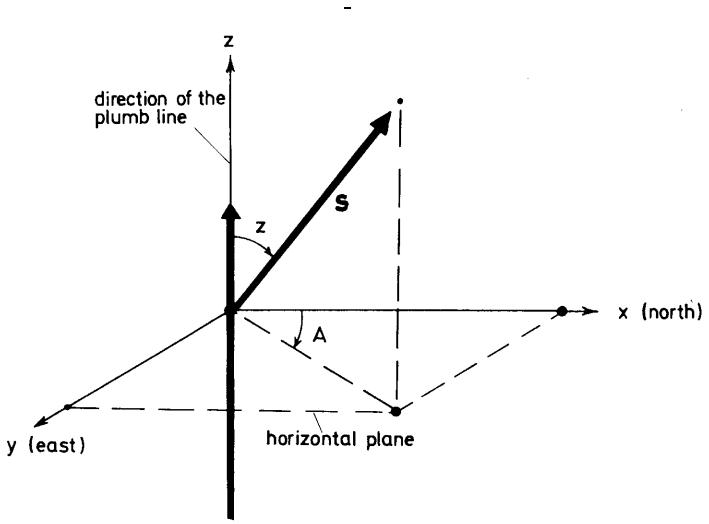

Figure 2.7: *Definition of the local astronomical Azimuth-Zenith coordinates (A,z). Note that the system is left-handed. Inverting the $\hat{z}$-axis gives the right-handed North, East, Down system discussed in section 2.6.3. Figure from [26].*

take various forms, but for all parameterizations the resulting residual equations will be non-linear in the rotation parameters. This is due to the fact that all three parameterizations (Euler angles, rotation matrices and quaternions) include matrix multiplication (3 by 3 or 4 by 4) of several matrices, each representing a rotation.

Furthermore when choosing the Euler-angle representation the equations will include trigonometric functions (cos and sin) of the parameters. Thus the residual equations are strongly non-linear in the parameters sought and iterative methods have to be applied to find the set of parameters that minimizes the residuals.

For most cases in inter-calibration, there will be a relatively good estimate of the relative attitude angles[3] which can provide a good initial guess for the optimization and thus very general search methods like the

[3]For instance the machine accuracy of the assembly in the Ørsted case was better than 1^o.

calculation heavy Monte-Carlo optimization and simulated annealing, can be avoided.

Another thing to take into consideration is the amount of data. For on-ground (or pre-flight) inter-calibrations the amount is often relatively modest. For typical calibration runs there are on the order of 100 measured positions, each including a number of observations. For example one measurement could consist of two magnetic field measurements (6 data) and one absolute attitude (3 data) bringing the total number of data to about 10^3. However when considering in-flight inter-calibrations the situation is quite different. Here data sets can comprise several days with measurements at one second intervals, bringing the number of data to the level of 10^6. Thus optimization methods demanding many calculations per data should be avoided in the in-flight cases.

When choosing an optimization method, the obtainable accuracy is of key interest. Methods often provide formal means of calculating the standard deviations, but in addition the robustness can be tested by comparing the results found using varying initial guesses.

In the following the three optimization methods that have been tested during this work are presented.

2.4.2 Linear inversion

Linear inversion is an iterative method based on the calculation of the gradient of the residual function with respect to the parameters sought. Since the residual equations are non-linear the use of this method relies on a sufficiently accurate initial guess for the linear approximation to be valid. The advantage of this method is that it is simple to implement. As will be seen, the direct calculation of the gradient of the residual is not overly cumbersome in the considered case. In the following the linear inversion method will be presented and afterwards some considerations about derivatives of composed rotations are given.

The iterative linear inversion can be envisaged as follows. The residual ($\mathbf{r}$) is the difference between sensor observations ($\mathbf{v}_{sen}$) and a model ($\mathbf{f}$) of these. The model based on reference observations ($\mathbf{v}_{ref}$), the current estimate of the model parameters ($\mathbf{m}_i$) and some additional, known parameters ($\mathbf{p}$)

$$\mathbf{r} = \mathbf{v}_{sen} - \mathbf{f}(\mathbf{m}_i, \mathbf{v}_{ref}, \mathbf{p}) \tag{2.21}$$

All quantities are expressed as column vectors. The residual is thus a function of the model parameters $\mathbf{m}_i$. In the following the explicit dependence of $\mathbf{f}$ on $\mathbf{v}_{ref}$ and $\mathbf{p}$ will be left out since these are considered to be constant. Within a small distance from $\mathbf{m}_i$ the residual function can be approximated by

$$\begin{aligned} \mathbf{r}(\mathbf{m_i} + \boldsymbol{\delta}\mathbf{m}) &= \mathbf{v}_{sen} - \mathbf{f}(\mathbf{m}_i + \delta\mathbf{m}) \\ &\approx \mathbf{v}_{sen} - \left[\mathbf{f}(\mathbf{m}_i) + \mathbf{f}'(\mathbf{m}_i)\delta\mathbf{m}\right] \\ &= \mathbf{r}(\mathbf{m}_i) - \mathbf{f}'(\mathbf{m}_i)\delta\mathbf{m} \end{aligned} \tag{2.22}$$

Where $\mathbf{f}'$ is the gradient of the model with respect to the parameters

$$\mathbf{f}'(\mathbf{m}) = \frac{\partial \mathbf{f}}{\partial \mathbf{m}} = \mathbf{f}_{\nabla \mathbf{m}}(\mathbf{m}) \tag{2.23}$$

By solving equation (2.22) for $\mathbf{r}(\mathbf{m_i} + \boldsymbol{\delta}\mathbf{m}) = 0$ the expression for the model update is found

$$\mathbf{f}'(\mathbf{m}_i)\delta\mathbf{m} = \mathbf{r}(\mathbf{m}_i) \tag{2.24}$$

Since $\mathbf{r}$ and $\mathbf{m}$ are column vectors with n_r and n_m elements respectively, the gradient $\mathbf{f}'(\mathbf{m}_i)$ is a $n_r \times n_m$ matrix. This matrix is denoted $\mathbf{F}$. For a sufficient number of independent observations ($n_r > n_m$) equation (2.24) is an over determined problem which can be solved by the standard least squares method (see e.g. [27])

$$\delta\mathbf{m} = (\mathbf{F}^T\mathbf{F})^{-1}\mathbf{F}^T\mathbf{r}(\mathbf{m}_i) \tag{2.25}$$

The new estimate of the parameters is then $\mathbf{m}_{i+1} = \mathbf{m}_i + \delta\mathbf{m}$. However it is often advantageous to take smaller steps in order to avoid overshooting by using $\mathbf{m}_{i+1} = \mathbf{m}_i + k \cdot \delta\mathbf{m}$ where k is a constant often chosen in the range 0.5 to 0.7.

A more elaborate version of equation (2.25) includes the possibility for weighting the data individually, via the data covariance matrix $\mathbf{C}_D$, as described in [27].

$$\delta\mathbf{m} = (\mathbf{F}^T\mathbf{C}_D\mathbf{F})^{-1}\mathbf{F}^T\mathbf{C}_D\mathbf{r}(\mathbf{m}_i) \tag{2.26}$$

Since the residual equations, like equation (2.3), are comprised of several rotations it is useful to find the general properties for derivatives of

composed rotations. First consider the matrix representation exemplified by the 323-Euler rotation

$$\mathbf{R}_{323}(\alpha,\beta,\gamma) = \mathbf{R}_3(\gamma)\mathbf{R}_2(\beta)\mathbf{R}_3(\alpha) \tag{2.27}$$

The derivative with respect to i.e. α is found by noting that the two leftmost matrices are independent of α so that

$$\begin{aligned}\frac{\partial \mathbf{R}_{323}}{\partial \alpha}(\alpha,\beta,\gamma) &= \mathbf{R}_3(\gamma)\mathbf{R}_2(\beta)\frac{\partial \mathbf{R}_3(\alpha)}{\partial \alpha} \\ &= \mathbf{R}_3(\gamma)\mathbf{R}_2(\beta)\frac{\partial}{\partial \alpha}\begin{bmatrix}\cos(\alpha) & \sin(\alpha) & 0\\ -\sin(\alpha) & \cos(\alpha) & 0\\ 0 & 0 & 1\end{bmatrix} \\ &= \mathbf{R}_3(\gamma)\mathbf{R}_2(\beta)\begin{bmatrix}-\sin(\alpha) & \cos(\alpha) & 0\\ -\cos(\alpha) & -\sin(\alpha) & 0\\ 0 & 0 & 0\end{bmatrix}\end{aligned} \tag{2.28}$$

Derivatives of the other components of the rotation can be found in a similar way

When using the quaternion notation for rotations it is noted that the derivative of multiplied quaternions is found as follows

$$\begin{aligned}\frac{\partial}{\partial q_{b1}}\left[\mathbf{q}_c \otimes \mathbf{q}_b \otimes \mathbf{q}_a\right] &= \frac{\partial}{\partial q_{b1}}\left[\{\mathbf{q}_c\}_L\{\mathbf{q}_b\}_L\mathbf{q}_a\right] \\ &= \{\mathbf{q}_c\}_L\frac{\partial\left[\{\mathbf{q}_b\}_L\right]}{\partial q_{b1}}\mathbf{q}_a \\ &= \{\mathbf{q}_c\}_L\frac{\partial}{\partial q_{b1}}\begin{bmatrix}q_{b4} & q_{b3} & -q_{b2} & q_{b1}\\ -q_{b3} & q_{b4} & q_{b1} & q_{b2}\\ q_{b2} & -q_{b1} & q_{b4} & q_{b3}\\ -q_{b1} & -q_{b2} & -q_{b3} & q_{b4}\end{bmatrix}\mathbf{q}_a \\ &= \{\mathbf{q}_c\}_L\frac{\partial}{\partial q_{b1}}\begin{bmatrix}0 & 0 & -1 & 0\\ 0 & 0 & 0 & 1\\ 0 & 1 & 0 & 0\\ 1 & 0 & 0 & 0\end{bmatrix}\mathbf{q}_a \\ &= \mathbf{q}_c \otimes [0,1,0,0]^T \otimes \mathbf{q}_a\end{aligned} \tag{2.29}$$

When carrying out rotations via the quaternion formalism using equation (1.18), it is noted that the product rule can be generalized to matrix multiplication in order to obtain

$$\frac{\partial}{\partial q_{ai}}\left(\mathbf{q}_a\begin{bmatrix}r\\0\end{bmatrix}\mathbf{q}_a^{-1}\right) = \frac{\partial \mathbf{q}_a}{\partial q_{ai}}\begin{bmatrix}r\\0\end{bmatrix}\mathbf{q}_a^{-1} + \mathbf{q}_1\begin{bmatrix}r\\0\end{bmatrix}\frac{\partial\left(\mathbf{q}_a^{-1}\right)}{\partial q_{ai}} \tag{2.30}$$

Along with equation (2.29), this gives all necessary ingredients for calculation of the gradients. As can be seen, the calculations of the partial derivatives are no more cumbersome than the actual rotations and many of the calculated matrices can be reused.

2.4.3 Levenberg-Marquardt

The Levenberg-Marquardt (hereafter LM) method is described in detail in [28] and only the main principles are presented here. The LM method uses a compromise between the linear inversion method given above and the solution found by a quadratic approximation to the residual function. The update of the model vector ($\delta\mathbf{m}$) is chosen to be close to the one found by linear inversion if the estimate is far from the correct solution. On the other hand if the estimate is close to the best solution, the update is chosen to be close to what is found from the quadratic approximation.

For the practical implementation of the LM method the standard MatLab routine *leastsq* is used. It features a numerical evaluation of the partial derivatives and thus there is no need for the equations of these.

2.4.4 Nelder-Mead

The Nelder-Mead (NM) or *downhill simplex* method is described in [28] and its main features are reported here.

The NM method requires only function evaluations no derivatives. The principle is to select $N + 1$ points in the N dimensional parameter space. The $N + 1$ points constitute what is called a simplex. Each iteration consists of moving the points one by one using either *reflection, expansion* or *contraction* to have the points converging on the set of parameters with minimum value of the residual function.

The NM method is relatively computational heavy requiring many function evaluations. For this work the MatLab implementation *fmins* of NM is used.

2.4.5 Choice of optimization method

The three methods are compared by applying them on a number of data sets. Typical results for a specific set (the first night of the TMO, SAC-C calibration from 1998) are presented in Table 2.1. As it is clearly seen the

Table 2.1: Performance test of optimization methods.

Optimization results				
Method	Δt [sec]	Flops [$\times 10^6$]	RMS [nT]	Iterations
Linear Inversion	145	148.6	26.4	1200
Levenberg-Marquardt	15	12.7	5.1	1200
Nelder-Mead	21	21.8	79.1	1200

Showing the obtained results for the three tested optimization methods. The 1200 iterations corresponds to 200$\times$ *the number of parameters determined for these tests.*

LM method if far superior in both convergence rate and computational speed. Similar results were obtained for other data sets. The Levenberg-Marquardt method is thus chosen as the optimization tool used throughout this work.

2.4.6 Error estimation

Estimation of the accuracy of the obtained results is important. In the current work two approaches have been used. The one uses the formal estimates of the standard deviations of the parameters found by the LM optimization routine. These estimated standard deviations are calculated using the inverse of the Jacobian matrix, calculated in the final iteration step of the optimization. The formal covariance matrix of the model parameters $\mathbf{m}$ thus becomes

$$\mathbf{P}_{mm} = \mathbf{J}^{-1} \tag{2.31}$$

Where $\mathbf{J}$ is the Jacobian matrix containing the second order partial derivatives of the residual function with respect to the model parameters (for details see [28]). The Jacobian matrix is directly available from the LM optimization routine.

The second approach is to find several estimates of the wanted parameters starting from a number of slightly deviating initial values. The standard deviation of the obtained results will then give an alternative estimate of the accuracy of the found parameters. Ideally a large number of initial values should be tested, in the studied cases some 15-20 different initial guesses have been tested. The drawback of this approach is that no estimate of eventual covariance between parameters is provided.

Results are reported in the data analysis chapter 4.

2.5 Attitude error and refinement

In order to treat error contributions correctly it is necessary to consider the description of errors in the various attitude representations. Also treated here is the incorporation of inhomogeneous errors in a combined attitude estimate from two instruments.

2.5.1 Attitude error representations

The description of attitude errors for the various representations is summarized in the following. This presentation owes a lot to the extensive treatment in [4].

Orthonormal matrices

If a true attitude, represented by the orthonormal matrix $\mathbf{A}$, is observed with a small error $\delta\mathbf{A}$, the resulting observed attitude is

$$\mathbf{A}^* = (\boldsymbol{\delta}\mathbf{A})\,\mathbf{A} \tag{2.32}$$

The general expression for a rotation through the angle θ, about the axis $\hat{\mathbf{v}}$ is, as stated in section 1.2.2, given by Euler's formula

$$\mathbf{R}_{\hat{\mathbf{v}}}(\theta) = \cos\theta\mathbf{I} + (1-\cos\theta)\hat{\mathbf{v}}\hat{\mathbf{v}}^T + \sin\theta[[\hat{\mathbf{v}}]] \tag{2.33}$$

For a rotation through a small angle equation (2.33) can be approximated by

$$\mathbf{R}_{\hat{\mathbf{v}}}(\theta) \approx \mathbf{I} + \boldsymbol{\theta}[[\hat{\mathbf{v}}]] \tag{2.34}$$

Regarding the error $\delta\mathbf{A}$ to be small it can be expressed by an angle ($\delta\theta$) and axis of rotation ($\hat{\mathbf{v}}$), which are combined to the error vector $\Delta\boldsymbol{\xi}$ according to

$$\delta\mathbf{A} \approx \mathbf{I} + \delta\theta[[\hat{\mathbf{v}}]] = \mathbf{I} + [[\Delta\boldsymbol{\xi}]] \tag{2.35}$$

It is expected that the error vector $\Delta\boldsymbol{\xi}$ is zero in mean i.e. $E\{\Delta\boldsymbol{\xi}\} = 0$. The covariance matrix of the error vector is defined by

$$\begin{aligned} P_{\xi\xi} &= Cov\{\Delta\boldsymbol{\xi}\} \\ &= E\{\Delta\boldsymbol{\xi}\Delta\boldsymbol{\xi}^T\} - E\{\Delta\boldsymbol{\xi}\}E\{\Delta\boldsymbol{\xi}^T\} \end{aligned} \tag{2.36}$$

The error in the elements of the attitude matrix are be found by

$$\Delta\mathbf{A} = \mathbf{A}^* - \mathbf{A} = (\mathbf{I} + [[\Delta\boldsymbol{\xi}]])A - A = [[\Delta\boldsymbol{\xi}]]A \tag{2.37}$$

The covariance of the of this error is calculated by

$$\begin{aligned} P_{AA} &= Cov\{\Delta\mathbf{A}\} \\ &= E\{\Delta\mathbf{A}\Delta\mathbf{A}^T\} - E\{\Delta\mathbf{A}\}E\{\Delta\mathbf{A}^T\} \end{aligned} \tag{2.38}$$

The connection between P_{AA} and $P_{\xi\xi}$ is not needed for this work but is reported for consistency. It is given by

$$P_{AA} = tr(P_{\xi\xi})\mathbf{I} - P_{\xi\xi} \tag{2.39}$$

Quaternions

In the quaternion representation of attitudes the error ($\delta\boldsymbol{\eta}$) on an attitude (η) is similarly described by

$$\boldsymbol{\eta}^* = \delta\boldsymbol{\eta} \otimes \boldsymbol{\eta} = \{\boldsymbol{\eta}\}_R \delta\boldsymbol{\eta} \tag{2.40}$$

The small rotation $\delta\boldsymbol{\eta}$ can also for quaternions be expressed by the error vector

$$\delta\boldsymbol{\eta} = \begin{bmatrix} \Delta\boldsymbol{\xi}/\mathbf{2} \\ 1 \end{bmatrix} + O(|\Delta\boldsymbol{\eta}|^2) \tag{2.41}$$

Again $\Delta\boldsymbol{\xi}$ expresses the rotation axis and its norm is the angle of rotation. The fourth component is approximately 1 since the angle of rotation for the error vector is assumed to be small. The error in the quaternion components is

$$\begin{aligned} \Delta\boldsymbol{\eta} &= \boldsymbol{\eta}^* - \boldsymbol{\eta} \\ &= \delta\boldsymbol{\eta} \otimes \boldsymbol{\eta} - \boldsymbol{\eta} \\ &= \{\boldsymbol{\eta}\}_R \begin{bmatrix} \Delta\boldsymbol{\xi}/\mathbf{2} \\ 0 \end{bmatrix} \\ &= \frac{1}{2}\boldsymbol{\Xi}(\eta)\Delta\boldsymbol{\xi} \end{aligned} \tag{2.42}$$

Where $\boldsymbol{\Xi}(\boldsymbol{\eta})$ is the 4 by 3 matrix identical to the first three columns of $\{\boldsymbol{\eta}_R\}$ given in equation (1.21)

$$\boldsymbol{\Xi}(\boldsymbol{\eta}) = \begin{bmatrix} \eta_4 & -\eta_3 & \eta_2 \\ \eta_3 & \eta_4 & -\eta_1 \\ -\eta_2 & \eta_1 & \eta_4 \\ -\eta_1 & -\eta_2 & -\eta_3 \end{bmatrix} \tag{2.43}$$

The inverse relation of equation (2.42) is

$$\Delta\boldsymbol{\xi} = 2\boldsymbol{\Xi}^T(\boldsymbol{\eta})\Delta\boldsymbol{\eta} \tag{2.44}$$

The covariance matrix for the error of the quaternion components is

$$P_{\eta\eta} = cov(\Delta\boldsymbol{\eta}) \tag{2.45}$$

With the transformation (2.42) the relation between the covariance matrices of the quaternion and the error vector is

$$P_{\eta\eta} = \frac{1}{4}\boldsymbol{\Xi}(\boldsymbol{\eta})P_{\xi\xi}\boldsymbol{\Xi}^T(\boldsymbol{\eta}) \tag{2.46}$$

Euler angles

In the Euler angle representation the set of three angles $(\phi, \theta, \psi) = \boldsymbol{\varphi}$ can be envisaged to have the observation errors $(\delta\phi, \delta\theta, \delta\psi)$. The connection to the error vector is according to [4] given by

$$\Delta\boldsymbol{\xi} = \mathbf{M}(\phi, \theta, \psi)\begin{bmatrix}\delta\phi\\ \delta\theta\\ \delta\psi\end{bmatrix} = \mathbf{M}_\varphi\begin{bmatrix}\delta\phi\\ \delta\theta\\ \delta\psi\end{bmatrix} \tag{2.47}$$

The inverse transformation is

$$\begin{bmatrix}\delta\phi\\ \delta\theta\\ \delta\psi\end{bmatrix} = \mathbf{M}_\varphi^{-1}\Delta\boldsymbol{\xi}\mathbf{M}_\varphi \tag{2.48}$$

Where $\mathbf{M}_\varphi$ is given in [4] and expressed by

$$\mathbf{M}_\varphi = \mathbf{M}(\phi, \theta, \psi) = \mathbf{R}(\hat{\mathbf{n}}_3, \psi)\mathbf{S}(\hat{\mathbf{n}}_1, \hat{\mathbf{n}}_2, \hat{\mathbf{n}}_3, \theta) \tag{2.49}$$

with

$$\mathbf{S}(\hat{\mathbf{n}}_1, \hat{\mathbf{n}}_2, \hat{\mathbf{n}}_3, \theta) = [\mathbf{R}(\hat{\mathbf{n}}_2, \theta)\hat{\mathbf{n}}_1|\hat{\mathbf{n}}_2|\hat{\mathbf{n}}_3] \tag{2.50}$$

where $\hat{\mathbf{n}}_i$ is the unit vector for the i^{th} axis of the Euler rotations expressed in the intermediate coordinate system. For the 323 Euler angles, which will be used later on, we thus have

$$\hat{\mathbf{n}}_1 = \hat{\mathbf{n}}_3 = \begin{bmatrix}0\\0\\1\end{bmatrix} \qquad \hat{\mathbf{n}}_2 = \begin{bmatrix}0\\1\\0\end{bmatrix} \tag{2.51}$$

The $\mathbf{M}_\varphi$ matrix is thus found by:

$$\begin{aligned}
\mathbf{R}(\hat{\mathbf{n}}_3, \psi) &= \begin{bmatrix} \cos\psi & \sin\psi & 0 \\ -\sin\psi & \cos\psi & 0 \\ 0 & 0 & 1 \end{bmatrix} \\
\mathbf{R}(\hat{\mathbf{n}}_2, \theta) \begin{bmatrix} 0 \\ 0 \\ 1 \end{bmatrix} &= \begin{bmatrix} \cos\theta & 0 & -\sin\theta \\ 0 & 1 & 0 \\ \sin\theta & 0 & \cos\theta \end{bmatrix} \begin{bmatrix} 0 \\ 0 \\ 1 \end{bmatrix} = \begin{bmatrix} -\sin\theta \\ 0 \\ \cos\theta \end{bmatrix}
\end{aligned}$$

$$\begin{aligned}
\mathbf{M}_\varphi &= \mathbf{R}(\hat{\mathbf{n}}_3, \psi)\mathbf{S}(\hat{\mathbf{n}}_1, \hat{\mathbf{n}}_2, \hat{\mathbf{n}}_3, \theta) \\
&= \begin{bmatrix} \cos\psi & \sin\psi & 0 \\ -\sin\psi & \cos\psi & 0 \\ 0 & 0 & 1 \end{bmatrix} \begin{bmatrix} -\sin\theta & 0 & 0 \\ 0 & 1 & 0 \\ \cos\theta & 0 & 1 \end{bmatrix} \\
&= \begin{bmatrix} -\cos\psi\sin\theta & \sin\psi & 0 \\ \sin\psi\sin\theta & \cos\psi & 0 \\ \cos\theta & 0 & 1 \end{bmatrix}
\end{aligned} \tag{2.52}$$

Similar to the previous section the covariance matrix for the Euler error angles can be found from

$$P_{\varphi\varphi} = \mathbf{M}_\varphi^{-1} P_{\xi\xi} = (\mathbf{M}_\varphi^{-1})^T. \tag{2.53}$$

2.5.2 Attitude refinement for two $O3$ instruments

When an instrument package contains two or more $O3$ instruments the attitude determination can be improved. Apart from the decreased risk of observation dropouts (simultaneous dropouts are less likely) the attitude accuracy can be improved above the accuracy of the individual instruments. This is done by combining the attitude measurements. This is especially useful in cases where the instruments have inhomogeneous noise distributions for the different instrument axes, as is the case for the star cameras treated in this work.

First the case with a fixed relative orientation between two $O3$ instruments (A_1 and A_2) is considered. Let the two instrument systems be $S1$ and $S2$. Their attitudes with respect to a common reference system are what is measured by the instruments and are R_{REF}^{S1} and R_{REF}^{S2} respectively. The relative attitude R_{S2}^{S1} between the two instrument systems is assumed to be fixed and known.

The principle is now to express the attitudes of the instruments in a common system, and by transforming information about the uncertainties to this system the correctly weighted average of the two attitudes can be found. Choosing $S1$ as the common system the attitude of the A_2

instrument is expressed by

$$(R_{REF}^{S2})_{S1} = R_{S2}^{S1} R_{REF}^{S2} \tag{2.54}$$

For the realization of these calculations the quaternion formalism for the rotations is chosen, since it is the best suited when the weighted average is to be calculated.

The formal standard deviations for the four quaternion components may be calculated using the equations from the preceding section.

Typically the uncertainty of the attitude measurements are given as standard deviations of a set of Euler angles. Assuming no cross-correlation between errors the covariance matrix becomes diagonal

$$\mathbf{P}_{\varphi_i\varphi_i} = \begin{bmatrix} (\sigma_{\phi_i})^2 & 0 & 0 \\ 0 & (\sigma_{\theta_i})^2 & 0 \\ 0 & 0 & (\sigma_{\psi_i})^2 \end{bmatrix} \tag{2.55}$$

Where i gives the instrument number ($i \in \{1, 2\}$). For the A_1 instrument these can be transformed to the standard deviations on the quaternion components by using equations (2.53) and (2.46)

$$\mathbf{P}_{\xi_1\xi_1} = \mathbf{M}_{\varphi_1} \mathbf{P}_{\varphi_1\varphi_1} (\mathbf{M}_{\varphi_1})^{-1} \tag{2.56}$$

$$\mathbf{P}_{\eta_1\eta_1} = \frac{1}{4} \mathbf{\Xi}(\mathbf{q}_1) \mathbf{P}_{\xi_1\xi_1} \mathbf{\Xi}^T(\mathbf{q}_1) \tag{2.57}$$

Here $\mathbf{M}_{\varphi_1}$ is given by equation (2.49) and $\mathbf{q}_1$ is the attitude quaternion of instrument A_1.

For the second instrument the relative attitude must be taken into account. Thus the covariance matrix of the A_2 measurement expressed in the $S1$ system is calculated according to

$$\left(\mathbf{P}_{\xi_2\xi_2}\right)_{S2} = \mathbf{M}_{\varphi_2} \mathbf{P}_{\varphi_2\varphi_2} (\mathbf{M}_{\varphi_2})^{-1} \tag{2.58}$$

$$\begin{aligned} \left(\mathbf{P}_{\xi_2\xi_2}\right)_{S1} &= \mathbf{M}_{rel} \left(\mathbf{P}_{\xi_2\xi_2}\right)_{S1} (\mathbf{M}_{rel})^{-1} \\ &= \mathbf{M}_{rel} \mathbf{M}_{\varphi_2} \mathbf{P}_{\varphi_2\varphi_2} (\mathbf{M}_{\varphi_2})^{-1} (\mathbf{M}_{rel})^{-1} \end{aligned} \tag{2.59}$$

$$\tag{2.60}$$

Here $\mathbf{M}_{rel}$ is the matrix for the transformation from $S2$ to $S1$, expressing the R_{S2}^{S1} rotation. Finally the covariance matrix of the quaternion from A_2 expressed in the S_1 system is

$$\left(\mathbf{P}_{\eta_2\eta_2}\right) = \frac{1}{4} \mathbf{\Xi}\left((\mathbf{q}_2)_{S1}\right) \mathbf{P}_{\xi_1\xi_1} \mathbf{\Xi}^T\left((\mathbf{q}_2)_{S1}\right) \tag{2.61}$$

Where $(\mathbf{q}_2)_{S1}$ is the $\mathbf{q}_2$ quaternion expressed in the $S1$ system. It is obtained by

$$(\mathbf{q}_2)_{S1} = \mathbf{q}_{rel} \otimes \mathbf{q}_2 \tag{2.62}$$

If more than two instruments are available their data and covariance matrices can be transformed to the common system similarly to the A_2 data. The weighted average can then be found using the reciprocal of the calculated standard deviations as the weights.

$$w = \frac{1}{\sigma^2} \tag{2.63}$$

It is chosen to perform this on each of the quaternion components individually. Regarding the i^{th} component and denoting the weight for the jth contribution by w_{ij}, the weighted average of the i^{th} component is calculated by

$$\langle(\mathbf{q})_i\rangle = k_i * \sum_{j=1}^{N} w_{ij}(\mathbf{q}_j)_i \tag{2.64}$$

Where the normalization factor k_i is given by

$$k_i = \left(\sum_{j=1}^{N} w_{ij}\right)^{-1} \tag{2.65}$$

Once the weighted average has been performed, the quaternion must be re-normalized to ensure a correct representation of the attitude.

If the relative orientation between the considered instrument systems is not constant, this must be taken into account by applying a time varying model for the relative attitude. An example of this is shown and discussed in the in the chapter on data analysis (section 4.3.4).

2.6 Stellar observations

The observation of stars play an important role as the basis for one type of attitude instruments used in this work, namely the star trackers as exemplified by the Advanced Stellar Compass (described in section 3.1.2). Therefore some aspects of stellar observations will be described in the following. First the effect of atmospheric *refraction*, which must be compensated for when observing from the Earth's surface is described. Secondly

the *aberration* of light is treated. Then various Earth based and celestial *reference systems*, used with stellar and other observations, will be described. Finally the principles of *stellar matching* are given.

2.6.1 Atmospheric refraction

The atmospheric refraction is described in great detail in [29]. Key points and the procedure for correcting for refraction will be given here.

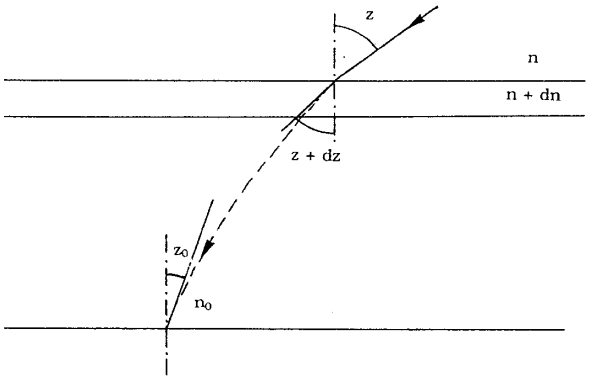

Figure 2.8: *Plane approximation for atmospheric refraction. Figure from [29].*

The effect of atmospheric refraction is caused by the variation of the refractive index (n) as the light from the observed stars passes down through the atmosphere. For a plane approximation, shown in Figure 2.8, Snell's law of refraction on differential form can be used to describe the effect of refraction

$$n \sin z = (n + \delta n) \sin(z + \delta z) \tag{2.66}$$

where z is the zenith distance of the ray path. This states that $n \sin z$ will be constant along the ray path. Since the refractive index outside the atmosphere is 1, the zenith distance on ground (z_0) which is the *apparent* zenith distance and the original zenith distance (z) are connected by

$$\sin z = n_0 \sin z_0 \tag{2.67}$$

The difference between these two zenith distances is called the refraction R and is given by

$$R = z - z_0 \tag{2.68}$$

Substituting $z = z_0 + R$ into equation (2.67) and neglecting second order effects yields

$$\sin z_0 + R\cos z_0 = n_0 \sin z_0 \tag{2.69}$$

$$R = (n_0 - 1)\tan z_0 \tag{2.70}$$

By taking into account the spherical shape of the atmosphere the following expression for the refraction is found (see [29])

$$R = \sin z_0 \int_1^{n_0} \frac{dn}{n\sqrt{(nr/n_0 r_0)^2 - \sin^2 z_0}} \tag{2.71}$$

Here r is the radii measured from the Earth center. By introducing the refractivity $\alpha = n_0 - 1$ and $\beta = L/z_0$, where L is the scale factor of the atmosphere, the following expression for the refraction, called the Laplace formula, is obtained

$$\begin{aligned} R =& \alpha(1-\beta)\tan z_0 - \alpha\left(\beta - \frac{\alpha}{2}\right)\tan^3 z_0 \\ R =& A\tan z_0 - B\tan^3 z_0 \end{aligned} \tag{2.72}$$

The coefficients A and B depend on the atmospheric conditions and are calculated relative to a normal atmosphere the conditions of which are listed in Table 2.2. For the normal atmosphere values the coefficients of

Table 2.2: The normal atmosphere for refraction.

Temperature	t_0	$= 15^o C (= 288.16\ K)$
Pressure	p_0	$= 101325$ Pa
Partial water vapour pressure	f_0	$= 0$ Pa
Wavelength	λ_0	$= 0.590 \mu$m
Altitude	h	$= 0$ m
Latitude	ϕ	$= 45^0$

Showing the defined conditions for the normal atmosphere, values are from [29].

the Laplace formula are given by

$$R_0 = A_0 tanz_0 - B_0 tan^3 z_0 = 57.''085 tanz_0 - 0.''0666 tan^3 z_0. \quad (2.73)$$

From these values for α and β can be calculated for the normal atmosphere

$$\begin{aligned} \alpha_0 &= 0.000277177 = 57.''1595 \\ \beta_0 &= 0.0013037 \end{aligned} \quad (2.74)$$

The dependence on temperature and pressure can be taken into account by modifying the values for α and β, but in practice an empirical formula is used

$$R_{t,p} = R_{t_0,p_0} \frac{1.0552126}{1 + 0.00368084t} \frac{p}{p_0} CE \quad (2.75)$$

where

$$\begin{aligned} C &= 1 - (0.003592(t - 15^o) - 0.0000055(t - 7.''5)) \\ E &= 1 + \left(0.943 \times 10^{-5}(p - p_0) - 0.78 \times 10^{-10}(p - p_0)^2\right) \end{aligned} \quad (2.76)$$

Finally effects of water vapor pressure and the chromatic aspects of refraction can also be included, but these effects are small and will not be included in this work.

The magnitude of the atmospheric refraction is depicted in Figure 2.9 for three special cases. It is seen that for sea level observations ($p = p_0 =$ 1013.25hPa) the refraction angle can be up to $100''$ for zenith distances of 65^o. At higher altitudes the refraction decreases. At 3km altitude ($p \approx p_0 * e^{-3/7.5} \approx$ 680hPa) the refraction is seen to be less than $50''$ for zenith angles less than 60^o. Temperature also has a noticeable effect, and must thus be taken into account.

Using the above equations the angle of refraction (R) can be calculated. The resulting effect of the refraction is that the light appears to come from a direction closer to zenith (apparent direction) than is actually the case (true direction). The correct zenith distance following equation (2.68) is

$$z = z_0 + R \quad (2.77)$$

Correction of the observed direction can be obtained by considering the unit vector $\hat{\mathbf{r}}_a$ along the apparent observed direction. Denoting the local

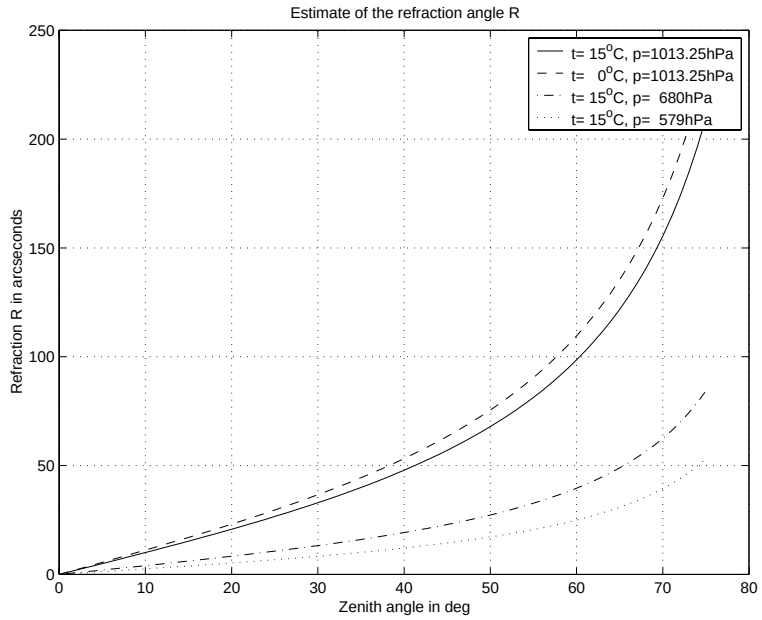

Figure 2.9: *Estimate of the atmospheric refraction angle for four special cases. $p = 680$ hPa corresponds to an altitude of approximately 3 km, while $p = 579$ hPa corresponds to 4.2 km.*

zenith $\hat{\mathbf{z}}$ the true direction of observation ($\hat{\mathbf{r}}_t$) can be obtained by rotating $\hat{\mathbf{r}}_a$ the angle $\theta = R$ about an axis perpendicular to both $\hat{\mathbf{r}}_a$ and $\hat{\mathbf{z}}$, namely

$$\hat{\mathbf{v}}_{rot} = \hat{\mathbf{z}} \times \hat{\mathbf{r}}_a \tag{2.78}$$

The true direction is then given by

$$\hat{\mathbf{r}}_t = \mathbf{R}_{\hat{\mathbf{v}}_{rot}}(\theta)\hat{\mathbf{r}}_a \tag{2.79}$$

where $\mathbf{R}_{\hat{\mathbf{v}}_{rot}}(\theta)$ is the 3×3 rotation matrix (to be distinguished from the refraction angle R). Equation (2.79) applies in any coordinate system as long as the coordinate vectors are represented in the same system.

For $O3$ attitude instruments the observation will not be a direction but the full attitude represented e.g. by a rotation matrix. In this case the correction can be obtained as follows.

In the passive description of rotations (used throughout this work) the column vectors of an attitude matrix ($\mathbf{A}$) are the coordinate vectors for the reference system basis vectors expressed in the instrument system. Likewise the column vectors of the inverse matrix $\left(\mathbf{A}^T\right)$[4] are the coordinate vectors for the instrument basis vectors expressed in the reference system. Changing the orientation of the instrument system by a small angel (refraction angles are indeed small) can be obtained by rotating each of the instrument basis vectors by the desired rotation. Denoting the attitude matrix by

$$\mathbf{A} = \begin{bmatrix} a_{11} & a_{12} & a_{13} \\ a_{21} & a_{22} & a_{23} \\ a_{31} & a_{32} & a_{33} \end{bmatrix} \tag{2.80}$$

the rotation of e.g. the first instrument axis, expressed in the reference system is given by

$$\left((\mathbf{A}')^T\right)_1 = \mathbf{R}_{\hat{\mathbf{v}}_{rot}}(\theta)(\mathbf{A}^\mathbf{T})_1 \tag{2.81}$$

$$= \mathbf{R}_{\hat{\mathbf{v}}_{rot}}(\theta) \begin{bmatrix} a_{11} \\ a_{12} \\ a_{13} \end{bmatrix} \tag{2.82}$$

Where the trailing subscript 1 refers to the first column vector. Using Euler's formula

$$\mathbf{R}_{\hat{\mathbf{v}}}(\theta) = \cos\theta\mathbf{I} + (1 - \cos\theta)\hat{\mathbf{v}}\hat{\mathbf{v}} + \sin\theta[[\hat{\mathbf{v}}]] \tag{2.83}$$

And its small angle approximation by equation (2.33)

$$\mathbf{R}_{\hat{\mathbf{v}}}(\theta) \approx \mathbf{I} + \theta[[\hat{\mathbf{v}}]] \tag{2.84}$$

The new direction of the first instrument axis is therefore expressed by

$$\begin{aligned} \left((\mathbf{A}')^T\right)_1 &= \mathbf{R}_{\hat{\mathbf{v}}_{rot}}(\theta)(\mathbf{A}^T)_1 \\ &= (\mathbf{I} + \boldsymbol{\theta}[[\hat{\mathbf{v}}_{\mathbf{rot}}]])(\mathbf{A}^T)_1 \end{aligned} \tag{2.85}$$

The full expression for the new attitude matrix is

$$\begin{aligned} (\mathbf{A}')^T &= \mathbf{R}_{\hat{\mathbf{v}}_{rot}}(\theta)(\mathbf{A}^T) \\ &= (\mathbf{I} + \boldsymbol{\theta}[[\hat{\mathbf{v}}_{\mathbf{rot}}]])(\mathbf{A}^T) \end{aligned} \tag{2.86}$$

[4] Rotation matrices are unitary and thus $\mathbf{A}^{-1} = \mathbf{A}^T$.

This is the general expression for transforming an attitude matrix by rotation through a small angle (θ) about the axis $\hat{\mathbf{v}}_{rot}$. It is of importance that the rotation axis coordinates be expressed in the reference system and that the operations carried out are on the inverse attitude matrix ($\mathbf{A}^T$).

2.6.2 Aberration

The aberration of light was first observed in 1728 by James Bradley, who correctly attributed the observed variation in star positions over the year to the velocity of the Earth around the Sun [30]. Later with the theory of relativity came a relativistic explanation of the phenomena via the Lorentz transformations (see e.g. [31]).

The aberration of light is due to the finite velocity of light and the relative motion between the emitting light source and the observer. The effect of aberration is to change the observed (apparent) direction to the star to be closer to the velocity vector of the observer (viewed in the rest frame of the source). The change in direction ($\delta\phi$) is found (see e.g. [32]) by

$$\frac{\sin\delta\phi}{v} = \frac{\sin\phi}{c} \tag{2.87}$$

Where v is the velocity of the observer, ϕ is the angle between the observer velocity and the apparent direction and c is the velocity of light. Using vector notation and noting that $\delta\phi \ll 1$ so that $\sin\delta\phi \approx \delta\phi$, equation (2.87) becomes

$$\delta\phi = \frac{|\mathbf{v} \times \hat{\mathbf{z}}_{appa}|}{c} \tag{2.88}$$

Where $\hat{\mathbf{z}}_{appa}$ is a unit vector in the direction of the apparent direction to the source.

The aberration is classified according to the velocity considered. When observing stars the ICRF reference frame (described below in section 2.6.3) is used and the motion of the stars with respect to this frame can be disregarded. Thus the velocity of interest is the motion of the observer with respect to ICRF. This consists of two parts. For an Earth-based observer the motion of the Earth around the Sun causes the *annual aberration*. The velocity of Earth in this motion $\mathbf{v}_E$ varies due to the excentric orbit. Methods for calculating it are found in [32] and [25]. The velocity is

approximately $30km/s$, so the effect of the annual aberration can be estimated, for the worst case where the apparent direction is perpendicular to the direction if motion ($\phi = 90^o$)

$$\delta\phi_{max} = \frac{v_E}{c} \approx \frac{29.7822km/s}{299792458m/s} \approx 9.93427259 \times 10^{-5} rad \approx 20.49'' \quad (2.89)$$

In addition to velocity of the Earth around the Sun there is the motion of the observer with respect to the Earth ($\mathbf{v}_O$). This gives rise to the *diurnal aberration*. Representative examples of this velocity is $0.46km/s$ for the on-ground observer at the Earth's Equator, $3.07km/s$ for a geostationary satellite and $7km/s$ for a Low Earth Orbit (LEO), giving rise to worst case aberrations of $0.31''$, $2.11''$ and $4.82''$ respectively.

Finally when observing objects with significant motions with respect to the reference frame i.e. planets or other satellites, the motion of these objects will give rise to the *planetary aberration* which can be taken into account by subtracting their velocity ($\mathbf{v}_P$). Gathering all terms the velocity to be used in equation (2.88) is

$$\mathbf{v} = \mathbf{v}_E + \mathbf{v}_O - \mathbf{v}_P \quad (2.90)$$

In order to correct an observed direction the calculated angle of aberration ($\delta\phi$) must be added to the angle between the apparent direction and the velocity vector. The apparent line of sight, expressed in the reference system, must be rotated the angle $\delta\phi$ about the direction determined by

$$\hat{\mathbf{r}}_{rot} = \frac{\mathbf{v} \times \hat{\mathbf{z}}}{|\mathbf{v}|} \quad (2.91)$$

When regarding full $O3$ attitudes the correction to the attitude matrix can be found by applying equation (2.86). Again it must be noted that is the corrections are performed on the attitude matrix expressing the transformation from instrument frame to reference frame.

2.6.3 Reference frames

For this work it is of importance to describe transformations between various reference frames[5]. In the following the relevant Earth-based and

[5]Sometimes a distinction between a reference *system*, which is a theoretical concept and a reference *frame*, which is the practical realization is made. Here the reference frames are of primary interest.

inertial reference frames will be presented along with the transformations between these.

Earth-based reference frames

Earth-based reference frames are useful for measurements carried out on the surface of the Earth. The primary Earth-based reference frame is the global International Terrestrial Reference Frame (ITRF), monitored and maintained by the International Earth Rotation Service (IERS). It is a geocentric frame, fixed to the surface of the Earth. Coordinates are determined by a series of stations carrying out observations using high accuracy techniques such as Very Long Baseline Interferometry (VLBI), Lunar Laser Ranging (LLR) and Global Positioning System (GPS) [33]. This Cartesian frame has its origin at the center of mass of the Earth, including the oceans and the atmosphere. The $\hat{z}$-axis is directed along the mean orientation of the Earth spin axis, also known as the Conventional Terrestrial Pole (CTP). The $\hat{x}$-axis lies in the mean equatorial plane perpendicular to CTP and is determined by the meridian through Greenwich. The $\hat{y}$-axis completes the right-handed frame. Positions in this system are either given by Cartesian (x, y, z) coordinates or by latitude (λ), longitude (ϕ) and distance from the origin (r). The positions of the reference stations are determined to 5 mm in each coordinate and have an overall consistency of the order of 1 cm. The GPS system provides instantaneous absolute positions accurate to the 1 m level and relative accuracies to 10^{-7} for fixed measurements of longer duration (a few days)[29].

Coordinates on the surface of the Earth can also be referred to by their astronomical coordinates, shown in Figure 2.10. These are defined by the direction of local plumb line. This direction is specified in the ITRF by the astronomical longitude and latitude (Φ, Λ).

In addition to the global ITRF, local reference frames are also used. The local astronomical reference frame (shown previously in Figure 2.7) is defined locally on each point of the Earth surface by choosing the $\hat{z}$-axis in the direction of the local plumb line directed outward from the Earth. The $\hat{x}$-axis is in the plane perpendicular to $\hat{z}$ pointing towards North. The $\hat{y}$-axis points towards East thus making the frame left-handed. Direction measurements in this local astronomical system are represented by two angles. The *azimuth* angle measured in the horizontal plane from the $\hat{x}$-axis in the clockwise direction. The *zenith* angle measured from the

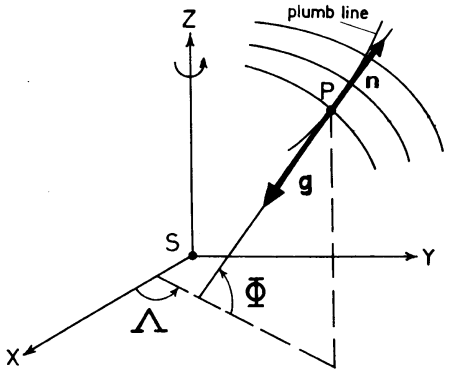

Figure 2.10: *Local astronomical coordinates. Figure from [26].*

$\hat{z}$-axis in the vertical plane containing the plumb line and the considered object (this angle will thus be restricted to $< 90^o$ for most practical cases. The accuracy of the realization of such systems depends on the available instruments, details of which can be found in [29]. Typically the realization is better than one arcsec.

The other local reference frame of interest to this work is the North, East, Down (NED) frame often used for geomagnetic purposes [7]. This is orientated with the $\hat{x}$-axis towards the North, the $\hat{y}$-axis towards east and the $\hat{z}$-axis pointing vertically downward (along the plumb line). In contrast to the local astronomical frame this is a right-handed frame. Apart from the Cartesian coordinates, measurements of the magnetic field in this frame are conventionally represented by declination, inclination and total intensity representing angle between North and horizontal component of the field, angle between the horizontal and the magnetic field direction and total intensity of the field respectively. Realizations of this type of frame rely on solar observations and fluxgate theodolites. The accuracy with which this frame can be realized is, according to [34], approximately $3''$.

Inertial reference frames

Inertial reference frames are frames wherein the Newtonian laws of motion apply. They are of use e.g. when considering the absolute motion of satellites and measurements obtained using instruments on board these. The primary inertial reference frame is the International Celestial Reference Frame (ICRF). This frame has its origin within astronomy and is defined through the position of approximately 200 very distant radio sources [35], shown in Figure 2.11. These are the defining reference sources of the

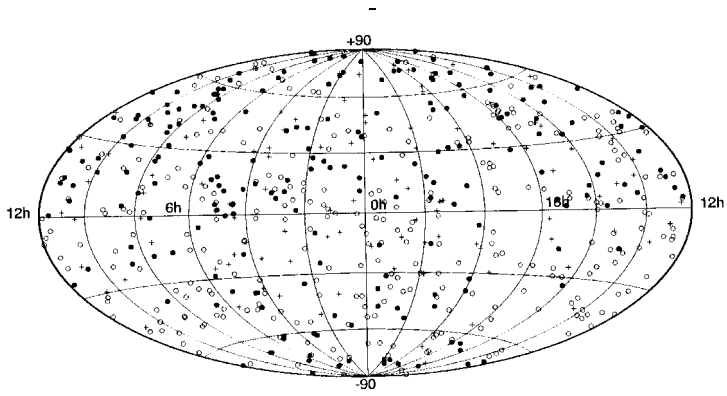

Figure 2.11: *ICRF sources. Filled circles are the defining radio sources. Figure from [35].*

ICRF. Using VLBI these can be positioned to better than 0.4×10^{-3} arcsec. (0.4 mas). The origin of this frame is chosen in the barycenter of the solar system, including the planets. The frame is orientated so that the $\hat{z}$-axis is as close as possible to the normal the mean equatorial plane at epoch J2000, i.e. the CTP at epoch J2000. Also when defining the coordinates it was aimed at having the $\hat{x}$-axis as close as possible to the vernal equinox at J2000.

The primary reference coordinates used in the inertial reference frame are the Right Ascension and Declination. Right Ascension (often denoted α and given in hours minutes and seconds, each hour corresponding to 15^o) counted in the xy-plane from the $\hat{x}$-axis in the counterclockwise direction. The Declination (δ) gives the angle from the xy-plane, counted positively

towards the North (the positive $\hat{z}$-direction) and negatively towards the south.

Since the defining reference sources of the ICRF are only accessible with full accuracy via VLBI, and because the defining reference sources are relatively few, a more dense set of optical reference sources have been tied to the ICRF by the Hipparcos mission. The resulting list of positions and proper motions 118.218 stars is the Hipparcos catalog. The positional accuracy of this catalog was 1 mas at the reference epoch (J1991.25). The accuracy of the annual proper motion is 1 mas/year. Further densified catalogs from the Hipparcos observations are available in the Tycho and Tycho-2 catalogs with approximately 1 and 2.5×10^6 reference sources respectively. A list of various reference catalogs and their accuracy with respect to the ICRF is given in Table 2.3.

Table 2.3: Stellar reference catalogs.

Catalog	Sources 10^6	Limiting magnitude V_{max}	σ_{pos} mas	$\sigma_{pos,2015}$ mas	σ_{μ} mas/year
Hipparcos	0.1	12.4	1	20	1
ACT	1	11	30	80	3
Tycho-2	2.5	12	30	80	2
UNSO A2	530	20	250	400	-
GSC II	500	18	250	400	20
2MASS	600	14	200	200	2

Optical and infrared reference catalogs. Columns list names, number of sources, the limiting magnitude, mean positional accuracy at observation and 2015 epoch along with the accuracy for the proper motion. Table extracted from [35].

Transformations between reference frames

For many purposes (e.g. the inter-calibration treated in this work) it is necessary to be able to transform between the various reference frames. In the following the transformation between Earth-based and the inertial reference frames are described. The transformations consists of rotations,

which in the practical implementation can be in any of the forms presented in section 1.2.

From the local, Earth-based NED frame the transformation to the global ITRF (or in general terms Conventional Terrestrial System, CTS) is given by two rotations

$$R_{NED}^{CTS} = R_3(-\Lambda)R_2(90^o + \Phi) \tag{2.92}$$

Here Φ and Λ are astronomical longitude and latitude at the origin of the local system.

The rotation from the global Earth-based frame to the inertial frame ICRF (or in general terms Conventional Inertial System, CIS) is comprised of several rotations. Traditionally these are grouped into three sets of rotations.

First there is a rotation taking care of the Earth spinning parameters. This is denoted S and takes care of the relative spinning of the two systems and corrects for the fact that the position of rotational axis of the Earth varies with time. S is given by

$$S = R_2(-x_p)R_3(-y_p)R_3(GAST) \tag{2.93}$$

Here x_p and y_p give the position of the instantaneous rotational axis of the Earth. These are monitored, predicted and published by the IERS on a monthly basis. GAST (Greenwich Apparent Sidereal Time) is the Greenwich hour angle of the (true) vernal equinox. It describes the spinning of the Earth and can be calculated by formulas given in [33] and [25]. Figure 2.12 show the three angles.

Next there is a set of rotations taking care of the nutation of the Earth spin axis. This rotation (denoted N) transforms from a system aligned with the *mean equator* at the time of the observation to a systems aligned with the *true equator* at the time of the observation.

Finally there is the rotation taking care of the precession of the Earth. This is denoted P and transforms from the mean equator at the *reference epoch* to the mean equator at the *epoch of the observation*. Expressions for both N and P can be found in [33] as well as in [25].

The above transformation can be gathered to the following expression for the transformation from the global Earth-based system (CTS) to the

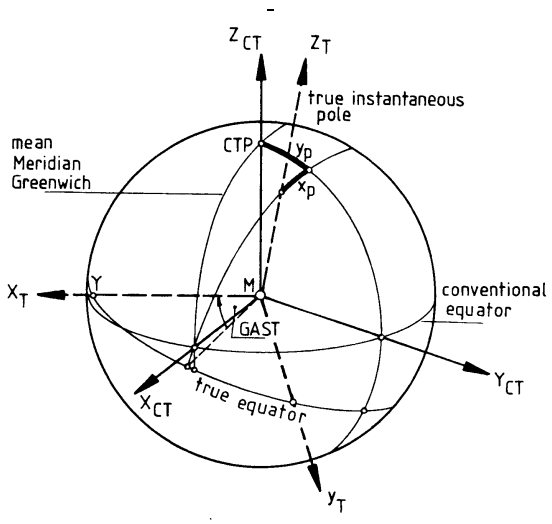

Figure 2.12: *True instantaneous and mean conventional terrestrial frames. Figure from [33].*

inertial system (CIS)

$$\begin{aligned} R_{CTS}^{CIS} &= P^{-1}N^{-1}S^{-1} \\ &= P^{-1}N^{-1}R_3(-GAST)R_1(y_p)R_2(x_p) \end{aligned} \tag{2.94}$$

For the overall transformation from the local NED frame to the inertial ICRF the following transformation applies

$$R_{NED}^{CIS} = P^{-1}N^{-1}S^{-1}R_3(-\Lambda)R_2(90^o + \Phi). \tag{2.95}$$

2.6.4 Stellar matching

For determination of the absolute orientation with respect to the inertial reference frame, the matching of observed stars with stars from reference catalogs (like e.g. Tycho) currently provides the most accurate method. The principal idea is to match the stars observed with the stars in the reference catalog and then calculate the parameters specifying the orientation of the observing instrument with respect to the reference frame.

This can be implemented in various ways, in the following the primary steps towards such an attitude determination are described.

An image of the night sky, may apart from the desired stars, contain other sources, e.g. galaxies and planets. The first step is therefore to determine which sources are stars and which are not. This can be done by methods described by [36]. The primary characteristic of a star is that stars have high peak intensities and that their light is concentrated in a narrow peak.

Once non-stellar objects have been removed the next step is to select a suitable subset of the stars which, based on a priori knowledge, are likely to have counterparts in the reference catalog. This can be based on knowledge of the typical magnitude of the catalog stars. The normal procedure is to select the n brightest of the stars detected in the image. This set must not be too large in order to avoid to extensive calculations when searching for matches.

Next, reference catalog and observed stars must be represented in some common frame, this can be done by transforming the reference catalog stars to the image plane using approximate a priori knowledge of the orientation along with a pinhole projection. There is no strict demand to know the orientation and scale of this transformation since methods exist (described by [37]) which can match the two set of stars even if the scale, orientation and axis directions are different. This method is based on the matching of triangles.

Finally when matching pairs between the reference catalog and the observed stars have been determined, a coordinate transformation specifying the relative attitude can be calculated.

The above scheme was followed in the implementation of the ASCfit (Automatic Stellar Coordinate fitting, described in section 4.2.1) package used for the inter-calibration between the UH 24-inch telescope and Advanced Stellar Compass. This instrument is described in section 3.2.4.

Chapter 3

Cases

In this chapter the instruments used in the case studies are introduced. First the individual instruments (magnetometer, star-tracker, telescope and CCD) are presented and then the instrument package configurations are given.

3.1 Individual instrument description

3.1.1 The CSC fluxgate vector magnetometer

The high accuracy fluxgate vector magnetometers used on the geomagnetic mapping missions (Ørsted, CHAMP and SAC-C) have all been manufactured at the Section for Measurement and Instrumentation, Ørsted·DTU, Technical University of Denmark. They are all of similar design and the prototype for the Ørsted mission has been described in great detail in [9]. Table 3.1, which is taken from [9], gives the principal technical data. Some additional key features are described below.

The CSC fluxgate vector magnetometer consists of a sensor unit and a data processing unit which are separated in order to avoid magnetic interference. The sensor unit is a compact spherical coil (CSC) vector feedback fluxgate sensor, in brief a CSC fluxgate. The review paper [38] and references herein describes the fluxgate principle while details on the CSC sensor can be found in [39]. In brief a single-axis fluxgate sensor operates by periodically driving two magnetic cores of ferromagnetic material, wound with excitation coils, into saturation in opposite directions.

Table 3.1: Technical data of the CSC vector magnetometer, from [9]

Power	
Electronics including AD converter and interface	940 mW
Tri-axial sensor	160 mW
Field range	±65536 nT
Resolution (18 bit)	0.5 nT
Linearity and accuracy	0.5 nT
Temperature range	-20 to +40 ^{o}C

In the absence of any external field the resulting field is zero. If an external field is present one core saturates before the other resulting in a detectable field. A detector coil surrounding the two cores picks up this field and its amplitude can be directly related to the external field, which is to be measured.

The CSC sensor unit consists of three single-axis fluxgate sensors, arranged orthogonally inside a spherical shell. The shell acts as support for three orthogonal sets of compensation coils used to obtain a zero-field inside the shell (see Figure 3.1). The 82 mm diameter spherical shell is made of carbon silicon carbide embedded in glass-bubble filled epoxy giving high thermal and mechanical stability, which is desirable for space missions. Other features of the shell are high electrical resistivity and very high temperature conductivity, which prevents induced currents and temperature gradients from building up in the shell material.

The three individual single-axis fluxgate sensors of the CSC are of the ringcore type, shown in Figure 3.2. Details of the ringcore sensor are given in [40]. The ring-shaped excitation core consists of the metallic glass $Co_{66.5}Fe_{3.5}Si_{12}B_{18}$. This material features low sensitivity to vibration and mechanical stresses (nearly zero magnetostriction) as well as a low Barkhausen noise. A toroidal excitation coil is wound around the ringcore to provide excitation of the core material. The ringcore is surrounded by a flat detector coil picking up the signal. The signals from the pickup coils of the three single-axis sensors are detected and amplified in the magnetometer processor unit and fed back into the compensation coils in order to maintain the zero field inside the CSC.

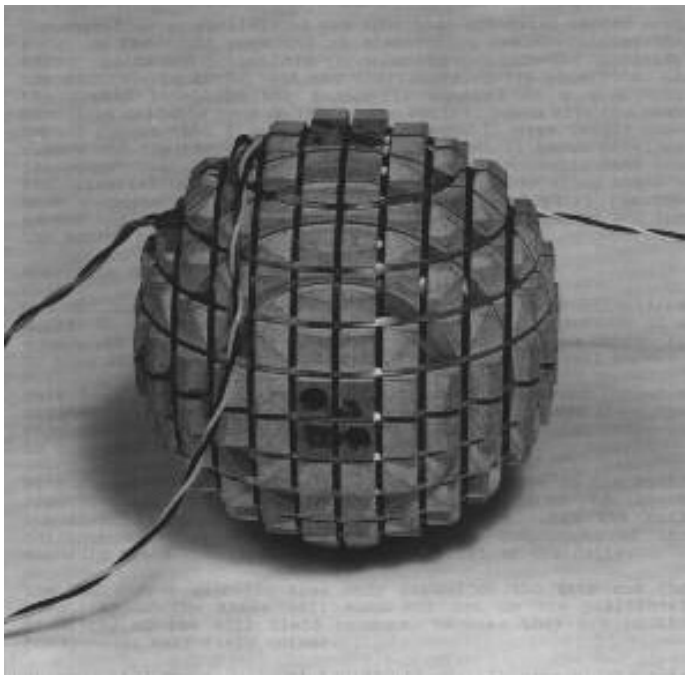

Figure 3.1: *The compact spherical coil (CSC) sensor. The three orthogonal spherical coils produce a homogeneous, compensating field inside the CSC. Figure from [39].*

The intrinsic noise of the CSC sensor is reported by [9] to be as low as 15 pT RMS at 0.06-10 Hz. The resolution of the magnetometer is therefore mainly limited by the 20 bit AD converter which in the Earth field of ±65000 nT gives a resolution of 0.125 nT.

A pulse-per-second (PPS) generated by a GPS (both onboard and during the on-ground experiments) controls the internal frequency of the magnetometer via a phase-locked-loop. On each data package, a timing synchronization information is sent in order to establish the magnetic field time.

For this work the CSC magnetometers will be considered as perfect, linear and orthogonal systems with homogeneous noise. This is possible since they have undergone extensive tests and calibrations as described in

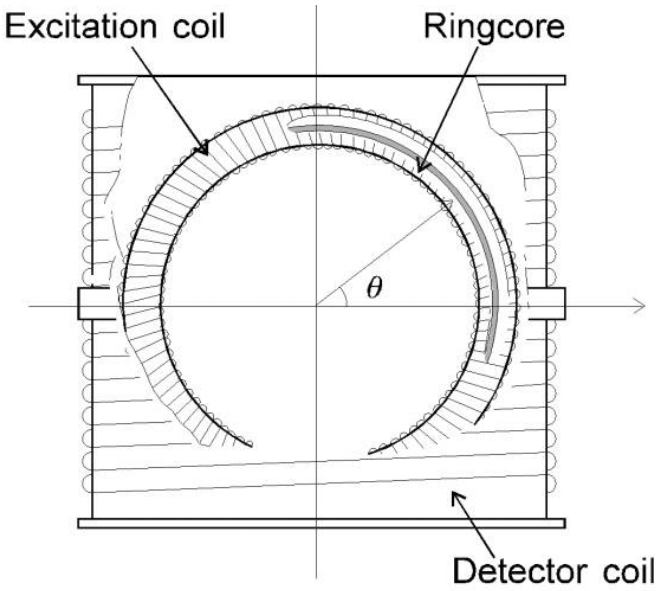

Figure 3.2: *The single axis ringcore fluxgate sensor. Figure from [40].*

[6], [41] and [42].

3.1.2 The Advanced Stellar Compass

The Advanced Stellar Compass (ASC, shown in Figure 3.3) is a newer model of the Star IMager (SIM), both developed at the Section for Measurement and Instrumentation, Ørsted·DTU. A variety of versions have been integrated and flown on various missions, some common key features are summarized here. Here no distinction between the two generations of instruments will be made. They will both be referred to as ASC.

The Ørsted ASC is described in [10]. The ASC is divided into one or more camerahead units (CHU) and a data processing unit (DPU). The separate sensor and processing units facilitate the placement of the sensor (camerahead) close to or together with other instruments, without the disturbing electromagnetic field from the DPU. The ASC provides accurate, real time attitude information by recognizing star constellations in a 28 degree field of view. The attitude is parameterized by three Euler

Figure 3.3: *Advanced Stellar Compass with one DPU and two CHU, baffles are also shown.*

angles, which are obtained with an accuracy of 20 arcsec. or better. The Euler angles give the direction of the camera boresight (two angles) with respect to the ICRF, and the rotation (one angle) about this boresight direction. Intrinsically the accuracy is a factor 5 better for the boresight direction than for the rotation.

The camera is fitted with a baffle to diminish stray light rays and reduce potential illumination from the Sun and the Moon. The baffle is designed individually for each mission, but most often consists of two sections to reduce thermal stresses between the outer part that is alternately heated by the Sun and cooled in the Earth's shadow and the inner part that is maintained at a more narrow temperature range.

A lens produces a defocused spot for a star of uniform size across the CCD. The CCD is a Sony ICX039BLA interline transfer type intended primarily for B/W video. The size is 7.95 x 6.45 mm (752 x 588 pixels). The CCD features high sensitivity, low smear, high antiblooming, micro lensing and low dark current. The exposure time is approximately 1 sec.

The CCD image is passed on to the ASC processor unit. Timing is established using a GPS signal. The processor unit is synchronized to GPS

time every second. The attitude is obtained either in an initial acquisition mode (without prior knowledge of attitude) or in a tracking mode (updating attitude based on prior attitude and known motion of the satellite). The ASC also features optional relativistic aberration corrections for Earth and satellite velocity.

3.1.3 The UH 24-inch telescope and Apogee CCD camera

The University of Hawai'i 24-inch (0.6 m) telescope was constructed near the top of Mauna Kea in 1969 and was the first permanent telescope there. The telescope is an equatorial mounted Smith telescope and is currently used for wide-field surveys and instrument development. The secondary mirror reflects the light to the primary focus where various instruments can be mounted.

The CCD camera used here has been developed by Richard Crowe at the Institute for Astronomy in Hilo, University of Hawai'i. The CCD is an Apogee Ap6ep, 1024 by 1024 array, with a physical size of 24-micrometer/pixel i.e. approximately 2.5 by 2.5 cm. The operating temperature is -40^oC. A number of filters (blue, v, red, infrared and green) are available. The typical exposure time is 5-10 minutes on bright galaxies.

3.2 Instruments packages

3.2.1 The Ørsted and SAC-C gondola

The Ørsted and SAC-C (a.k.a. Ørsted-2) satellites are both Earth observing satellites and carry highly similar instrument packages for observing the magnetic field of the Earth. The packages consist of a CSC vector fluxgate magnetometer and an ASC[1]. The principle is to measure the magnetic field vector with high accuracy (down to the nT level) and let the ASC determine the absolute attitude of the instrument package. By knowing the relative attitude between CSC and ASC it is possible to establish the absolute orientation of the measured magnetic field vector.

The two sensor units are placed together in a thermal and mechanical stable structure, which due to its shape is called the *gondola*. A schematic

[1]The star tracker on Ørsted and SAC-C are of the Star-IMager type, but as stated no distinction between ASC and SIM is made here.

drawing of this gondola is shown in Figure 3.4. This configuration provides a fixed relative orientation between the two sensors. By placing the data processing units away from the sensors, disturbing magnetic fields from the electronics are avoided. For the Ørsted satellite the gondola is placed on a boom 6 m away form the main body of the satellite. For the SAC-C satellite the distance from the gondola to the satellite body is approximately 2 m.

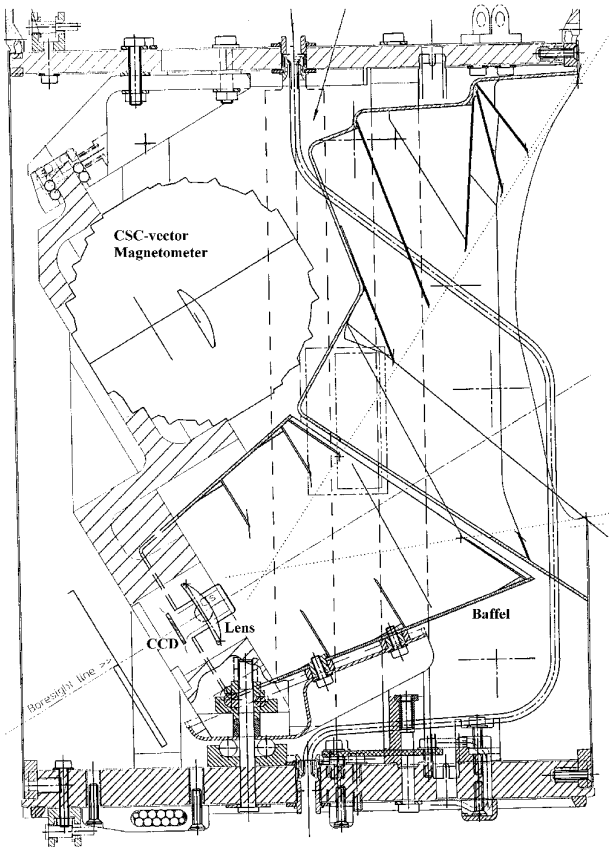

Figure 3.4: *Ørsted and SAC-C gondola with CSC vector magnetometer and camerahead unit of the ASC.*

3.2.2 The CHAMP optical bench

The German CHAMP (CHAllenging Minisatellite Payload) satellite, developed by the Geo-Forchungs-Zentrum Potsdam, is a multi-mission Earth observing satellite. The payload of interest to this work is the geomagnetic package consisting of two CSC vector magnetometers and two Advanced Stellar Compasses. These instruments are arranged on a structure called the *optical bench*, which is mounted on a deployable boom (see Figure 3.5).

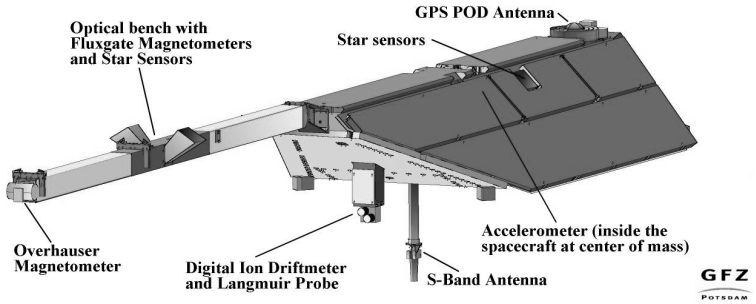

Figure 3.5: *The CHAMP satellite with optical bench containing two CSC magnetometers and two ASCs. Figure from the GeoForzhungsZentrum Potsdam website, http://op.gfz-potsdam.de/champ/.*

The principle is the same as for the Ørsted instrument package described above, here instrument doublets have been added to secure redundancy in case of instrument failure. Both ASCs operate simultaneously, but only one CSC is active at a time to avoid magnetic disturbances from the compensation coils.

3.2.3 The SWARM geomagnetic multi-satellite mission

To broaden the study of the geomagnetic field a multi-satellite mission called SWARM has been proposed. The mission will consist of 4 to 6 satellites each carrying identical payloads, measuring simultaneously the geomagnetic field at different locations thus simultaneous covering different local times. Apart from expanding the current studies of the geomagnetic field with increased accuracy and resolution, the simultaneous

observations from several spacecraft will allow for resolution of time-space variations of both internal and external sources to the geomagnetic field.

The instrumentation envisaged for each satellite consists of a high precision vector magnetometer and three star-trackers for attitude determination. A conceptual drawing of a SWARM satellite is shown in Figure 3.6.

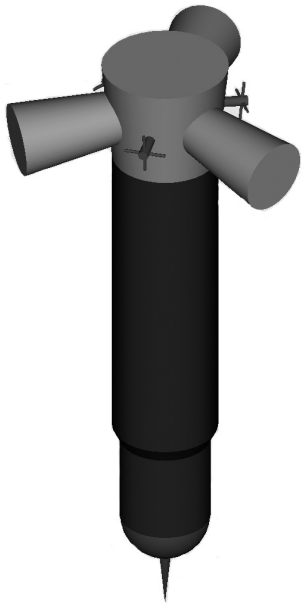

Figure 3.6: *Conceptual drawing of a SWARM satellite.*

The three star-trackers are pointing 15^o out of the plane of perpendicular to the long axis of the satellite and are equally spaced, 120^o apart. The magnetometer is mounted on the end of the spacecraft to avoid magnetic disturbances.

This instrument configuration is of interest to this work since it provides an excellent example of inter-calibration between several instruments.

3.2.4 UH 24-inch telescope guidance system

The University of Hawai'i telescope guidance system consists of an ASC mounted on the fixture for the secondary mirror of the UH 24-inch telescope (see Figure 3.7). The Apogee CCD camera (not shown in the Figure) is mounted at the primary focus, and is used for taking images of celestial objects. This constellation will make it possible to use the measurements

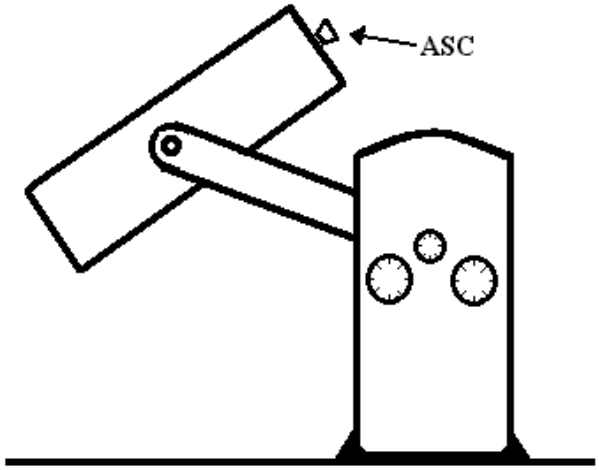

Figure 3.7: *UH 24-inch telescope guidance system. The size of the ASC CHU is exaggerated.*

from the ASC to give a highly accurate pointing direction of the telescope. The telescope motor drives can be controlled either manually or via a digital interface from a PC, thus making an automatic telescope guider possible.

Chapter 4

Data Analysis / Examples

This chapter describes examples of the inter-calibration methods presented in chapter 2. First some considerations about the implementation and computational costs are given. Following this, examples of stellar matching are shown. Hereafter examples of inter-calibration between two and more instruments are given. The cases studied are the ones presented in chapter 3.

The subjects and analysis described in this chapter have all been investigated during this thesis work. Especially the considerations on implementation and computational costs are new in this work. The ASCfit package is also a novel result of this work.

4.1 Implementation considerations

4.1.1 Implementation

Implementing the inter-calibration methods of chapter 2, two main approaches have been used. First the *specialized implementation* which is constructed for each case considering the specific features of the involved instrument packages. Second the *general implementation* which seeks the general solution to the problem of inter-calibration.

The specialized approach is highly adapted to the individual case.

The general implementation seeks to provide a common framework for the treatment of all instrument and sensor types. It utilizes replaceable modules for reading and selecting data, while the optimization is expected

to be performed by a fixed routine, which is able to consider all special cases. General error functions for the individual instrument types have been constructed and are used as input to the optimization routine. The general implementation of the inter-calibration is outlined in Figure 4.1.

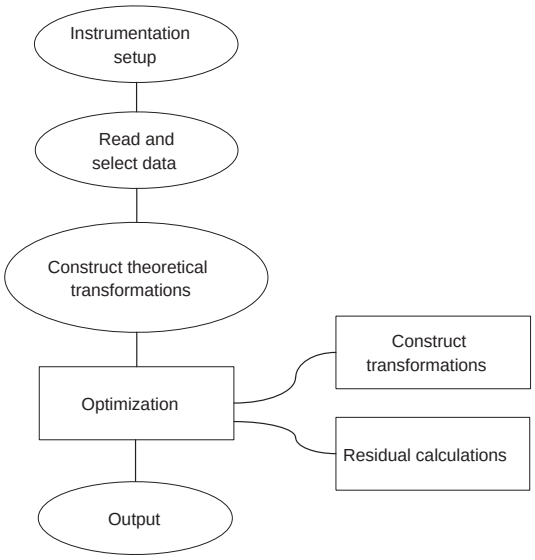

Figure 4.1: *General implementation of the inter-calibration. Ovals represent modules that are replaced for each new setup, while squares are non-changing elements of the inter-calibration routine.*

The outset was the specialized implementations for the Ørsted and SAC-C cases, later on the general method was constructed and used on the SWARM and Ørsted cases. Finally the specialized approach was also used for the UH-24-inch Telescope Guidance System (TGS).

Experience shows that it is often easier to perform a specialized implementation than to adapt the general implementation to the individual case.

4.1.2 Computational costs

When implementing the methods presented in chapter 2, some considerations about the computational burden should be made. The key to

understanding the computational cost of the optimization routines of section 2.4, is that they rely almost only on function evaluations. In this case evaluations of the residual functions like equation (2.4). The linear inversion also uses evaluations of the gradients of the residual functions. As shown in section 2.4.2 evaluating the gradient is very similar to evaluating the function itself when the residual function is comprised of successive rotations.

Thus the computational burden will mainly depend on the number of rotation to be composed and on the cost of composing individual pairs of rotations. Here the quaternion formalism has an advantage over the matrix notation. Multiplication of two 3×3 (unitary) matrices take 27 multiplications and 18 additions, while the composition of two quaternions by quaternion multiplication takes 16 multiplications and 12 additions. Thus when combining rotations approximately computation time can be reduced by approximately one third by using quaternions instead of matrices.

However there are also other considerations. For instance which representation the rotations are naturally given in. A general method for the change from matrix to quaternion representation is suggested in [43]. This method does not take many calculations (only 4 multiplications, 6 additions and 3 comparisons), but of cause this can constitute a significant computational burden if all rotations are to be taken from matrix notation to quaternion notation. Going the other way, from quaternions to matrices using equations by e.g. [4], takes 16 multiplications and 15 additions.

Having found the composite transformations it is also worth mentioning that the transformation of a vector is most efficiently carried out using the matrix notation of equation (1.3), which takes 9 multiplications and 6 additions. Using the quaternion formulation of equation (1.18) and considering the multiplication formulas of equation (1.20) it will take 32 multiplications and 24 additions to rotate a vector in the quaternion notation.

4.1.3 The representations used

In this work the specialized implementations of the Ørsted & SAC-C cases use the Euler angles as parameterization of the relative attitudes in order to obtain a non-redundant parameterization. For the calculations the

matrix notation is used. Though not the optimal choice the computational burden is not too extensive, since the data sets are relatively limited.

For the general implementation Euler angles are used only for in- and output. All internal representations use the quaternion formalism.

The Telescope guidance system, which was analyzed with a specialized implementation, uses a mixture of Euler angles and matrix representations.

Finally the attitude improvement of the two Advanced Stellar Compass on CHAMP use the quaternion formalism for calculations. However Euler angles are also used to estimate standard deviations of the raw data.

Before describing examples of the inter-calibration between two or more instruments the inter-calibration between one instrument and a model will be described.

4.2 One instrument

In general the modeling of data from one instrument can be regarded as an inter-calibration between the instrument and the model. In the following the fitting of astronomical coordinates onto astronomical images is described. This has been implemented in the ASCfit package, which is currently operating on the University of Hawai'i 2.2 m telescope. In addition to being an example of one instrument (inter-) calibration, this will later form the basis for the inter-calibration between an astronomical telescope and an Advanced Stellar Compass, used in the Telescope Guiding System.

4.2.1 Automatic Stellar Coordinate fitting package

ASCfit is a modular software package for automatically fitting astrometric world coordinates (WCS) onto raw optical or infrared astronomical images in the FITS format (described in [44]). Stars in the image are identified with stars in a reference catalog (USNO-A2 or 2MASS) and the celestial coordinates are given as a simple linear transformation from (X,Y) pixels to (RA,DEC). The coordinates can be fitted to the accuracy level of the reference catalog used. The tool has been implemented for images taken in the optical and infrared bands and allows for sidereal and non-sidereal tracking. In the following the ASCfit tool and its operation is described.

The ASCfit package

The ASCfit package was developed for the UH 2.2-m (88-inch) telescope on Mauna Kea, as a result of the ongoing collaboration between the Institute for Astronomy (IfA) at the University of Hawai'i and the Department for Measurement and Instrumentation at the Technical University of Denmark. The work has been done in cooperation with Dr. Andrew Pickles and builds on previous work by Troels Riis and Associate Professor Maurizio Betto. It was originally developed for use with 2K $\times$ 2K CCD images, but the modular structure of the package allows for other applications such as for 1K $\times$ 1K images from the infrared QUIRC camera (described in [45]) and the UH8K CCD Mosaic Camera (described in [46]). It has also been used on optical and infrared data from other telescopes and instruments. In the following an overview of the software package and its components is given. The method used to obtain the astronomical coordinates is discussed along with the complications introduced by non-sidereal tracking. Some examples are given and error sources are discussed.

As described the ASCfit package adds world coordinates to astronomical FITS images by matching stars found in FITS images to stars extracted from a reference catalog around the approximate telescope pointing coordinates. The coordinates are given by a simple affine transformation from (X,Y) pixels to world coordinates (WCS). The affine transformation is linear in its coefficients, thus they can be obtained from a single linear inversion. No further iterations are necessary.

The actual type of coordinates will be the same as in the reference catalog used. ASCfit operates on an image stored in the FITS format and will update the header with keywords describing the coordinate transformation, as suggested in [44] and listed in appendix A. This allows image viewing tools such as SAOimage (version ds9) to display world coordinates, and can assist with image registration and stacking. The ASCfit package (script and programs) can be obtained as a `tar` file from `http://www.ifa.hawaii.edu/users/pickles`.

The ASCfit script

The backbone of ASCfit is a script, which spawns a series of tasks. The layout of the script and the dataflow is shown in Figure 4.2. In the following the modules of the package are summarized.

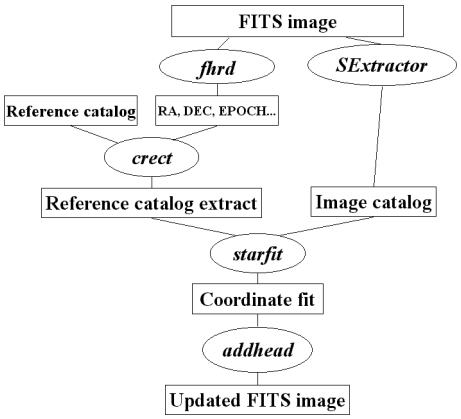

Figure 4.2: *Overview of the ASCfit package. Modules are represented in ellipses, while the squares represent data elements.*

- *fhrd* Extracts keyworded values from the FITS header, and writes them to `stdout` for use by other modules. The keywords read are listed in appendix A.

- *crect* Writes a list of stars centered on the pointing of the telescope and extracted from the USNO-A2.0 catalog to `stdout`. It is a modified C version of the USNO Fortran program *square*, and uses input values from *fhrd* for keywords RA, DEC, EQUINOX, WIDE_RA and WIDE_DEC, the latter derived from NAXISi and pixel scale information. ASCfit directs this subcatalog to `asc_ref.cat`.

- *msqbin* The ASCfit infrared option `-ir` branches the script to *msqbin*, which searches a compressed version of the infrared 2MASS point source catalog (currently second release) around the telescope pointing, and again writes the derived subcatalog to `asc_ref.cat`.

- *SExtractor* (Source-Extractor) A program by E. Bertin ([36]) which finds objects in the image, estimates relative magnitudes and identifies the objects by a galaxy/star parameter *diffuse* in the range [0..1]. Parameters of the GAIN, SECPIX or PIXSCAL and THRESHOLD keywords are fed to *SExtractor* from the script. Default parameters for *SExtractor* are given in the parameter file `ascfit.sex`. A cata-

log of identified objects is written to `asc_sextr.cat`. The layout of this catalog is given in `ascfit.par`.

- *starfit* Performs the actual matching and fitting of the stars and will be described in detail below. In brief *starfit* identifies matching stars between the two subcatalogs (`asc_ref.cat` & `asc_sextr.cat`) and calculates the parameters for the affine transformation. SECPIX/PIXSCAL and NAXISi are passed to *starfit* along with other parameters. A full list of the flags that can be used for *starfit* is given in appendix A. The parameters for the coordinate transformation are written to `param.dat` and to the commandline.

- *addhead* Updates the FITS header with the necessary keywords from `param.dat`. Keywords are updated if they exist or added before the "END" of the FITS header.

Running ASCfit

The syntax and flag options for running ASCfit are given in appendix A

Running ASCfit on the image shown in Figure 4.3 updates the FITS header with the keywords CTYPEi, CRPIXi, CRVALi and CDi_j, where $i, j \in \{1, 2\}$ and shows the result on a single line output as e.g.:

```
   ccd_023.fits:13h00:04.84+0.226X-0.0010Y ...
+13d53:23.2-0.219Y-0.0019X(10/22/46*,0.43"RMS)
```

The two expressions give RA and DEC as f(X,Y) respectively. The coefficients for X and Y are given on the output line in arcsec/pixel to provide easy visual verification. Numbers in the parentheses list number of stars matched, number of stars in the image, number of stars extracted from the reference catalog and the formal 1σ standard deviation for the obtained fit in arcsec. In the case that no satisfactory match could be found an error message is given and the FITS header is updated with zero values for the keywords to show that a fit has been attempted. For a successful fit the updated keywords can look as follows:

```
CTYPE1  'RA---CAR' 'R.A. '
```

```
CTYPE2  'DEC--CAR' 'DEC. '
CRPIX1  0 'Refpix of first axis'
CRPIX2  0 'Refpix of second axis'
CRVAL1  1.9502017455348E+02 'RA at Ref pix in decimal degrees'
CRVAL2  1.3889790298763E+01 'DEC at Ref pix in decimal degrees'
CD1_1   6.2714855856623E-05 'CD matrix'
CD1_2  -2.7932256640511E-07 'CD matrix'
CD2_1  -5.1539805080587E-07 'CD matrix'
CD2_2  -6.0829724272386E-05 'CD matrix'
```

From these values the transformation to the celestial coordinates is obtained by:

$$RA = \texttt{CRVAL1} + \texttt{CD1\_1}(x - \texttt{CRPIX1}) + \texttt{CD1\_2}(y - \texttt{CRPIX2}) \quad (4.1)$$

$$DEC = \texttt{CRVAL2} + \texttt{CD2\_1}(x - \texttt{CRPIX1}) + \texttt{CD2\_2}(y - \texttt{CRPIX2}) \quad (4.2)$$

Reference catalogs

The USNO-A2.0 from the US Naval Observatory ([47]) has been implemented for use with optical images. This catalog quotes a typical astrometric accuracy of 0.25 arcsec. and a photometric magnitude determination good to 0.25 mag, but photometric and scale errors for the B band are larger.

The 2MASS point source catalog (described in [48], currently second release) states an astrometric accuracy of < 0.2 arcsec. The roughly 300 bytes/star can be compressed with the auxiliary program *2mass_2bin* to 24 bytes/star (coordinates, shape, 4 colors) to produce files which can be quickly searched with *msqbin*.

The matching of stars

The *starfit* program performs the tasks of identifying matching stars among the two generated catalogs and finding the parameters of the coordinate transformation.

The first step is to select the stars to be searched for matching pairs. A color dependent (`-color` flag) estimate of magnitude is performed on the reference subcatalog `asc_ref.cat` before selecting the n brightest stars.

For the image subcatalog `asc_sextr.cat` an initial scan removes objects with too diffuse appearance (controlled by the `-diffuse` flag). In order to allow for non-sidereal tracking, elongated objects, which would be classified as galaxies by *SExtractor* will not be rejected if they have a common orientation in the image. Objects near the edge of the FITS image are also removed (controlled by the `-edge` flag) before the n brightest of the remaining stars are selected and transformed to pseudo world coordinates using a pinhole projection.

Now matches can be sought between these two sets using a triangulation method described by [37]. This includes the exclusion of multiple object identifications that are closer than 0.3% of the image width.

If at least six matches are found, the parameters for the affine transformation are fitted using the least squares linear inversion. A linear fit of the relation between image and reference catalog magnitudes is also performed. The reason for demanding six matches and not three, which would be sufficient to determine the transformation, is a wish to prevent a single false match from corrupting the fit.

From the initial match more matches are sought by searching for pairs of stars which fit the initial (X,Y) to (RA,DEC) transformation to within 1 arcsec. (in 2D distance) and the linear magnitude fit to within ± 3 magnitudes. The matches found in this second run are used to fit the final six parameters for the affine transformation.

Non-sidereal tracking

In the case of non-sidereal tracking, e.g. in observing comets or asteroids, stars will appear as trails across the image. Such trails are classified as galaxy-like objects due to their elongated shape and might thus be excluded from the search for matches. To avoid this the mean and standard deviation of the orientation of the objects rejected as galaxies are calculated. If a common orientation can be identified (i.e. standard deviation less than some limit and number of rejected stars larger than a lower limit to secure decent statistics) the objects having this common orientation to within the 1σ level will be accepted as stars. The centroid of trailed objects will be at the center of the trail (assuming an even non-sidereal tracking rate) and thus they and the fitted coordinates correspond to positions at the epoch of the middle of the exposure interval. These coordinates and epoch can be extracted from *ASCfit* fitted images with the auxiliary pro-

gram *xycoord*, e.g.:

```
xycoord qrc.fits 500 500
RA=197.869751 J2000 DEC= -1.349748 at X,Y= 500.0,500.0
RA=13:11:28.74 DEC=-01:20:59.1 at mid-UT +08:38:02.78
```

Examples and performance, Optical

In the following two examples from ASCfit are shown. Figure 4.3 show a 7 $\times$ 7 arcmin CCD image taken with the Tektronix 2K $\times$ 2K camera at the UH 2.2-m telescope. Due to a non-sidereal tracking rate (100mas/s in RA and 30mas/s in DEC) most objects appear elongated and are characterized as galaxies by *SExtractor*, having galaxy/star parameters < 0.01. However the trailed stars are retained due to their common orientation in the image. Some trailed stars are seen to be below the detection threshold set for *SExtractor*. Figure 4.4 show the corresponding reference catalog extract for the fit listed above. In this CCD image 10 of 22 objects were matched among the 46 stars extracted from the reference catalog. The resulting fit had a RMS of 0.43 arcsec.

Examples and performance, Infrared

When applying the ASCfit tool to infrared images, images can sometimes be fitted with stars extracted from the USNO-A2.0 optical catalog, but in general the success rate is low. This is partly due to using optical reference stars, which have significantly different magnitudes in the infrared, partly due to the small number of stars present in infrared images (with smaller fields), and sometimes due to a lack of stars in dark regions. An example of a single, raw 60 second QUIRC image (3 $\times$ 3 arcmin) around the Abell 1689 cluster is shown in appendix A, Figure A.1. Astrometry is difficult for this small field with faint objects, so the threshold has to be lowered. Figure A.2 shows the corresponding reference stars from the optical USNO-A2.0 catalog, mainly in the R-band magnitude range 17–18. For this image 8 out of 11 objects found matches among the 31 optical reference stars, with an RMS of 0.24 arcsec.

```
ascfit irfile -threshold 2
irfile:13h11:35.14-0.190X-0.0011Y -01d22:33.9+0.189Y+0.0007X
```

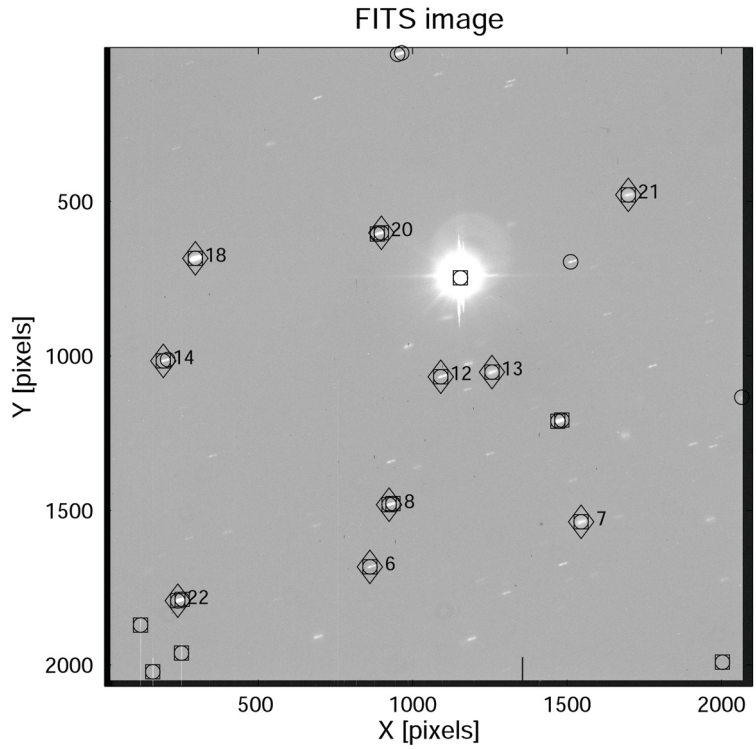

Figure 4.3: *A FITS image taken by the 2K × 2K Tektronix camera. Detected stars are marked by circles, brightest stars by squares and the matched stars by diamonds.*

```
8/11/31*,0.24"RMS)
```

Infrared images can be fitted instead with infrared reference stars if the 2MASS catalog covers that part of the sky. In this case 8 out of 11 objects found matches among the 35 infrared reference stars, mainly in the H-band magnitude range 15–16, with a formal RMS of 0.08 arcsec.

```
ascfit irfile -ir -threshold 2
irfile:13h11:35.03-0.189X+0.0005Y -01d22:33.9+0.189Y+0.0006X
8/11/35*,0.08"RMS)
```

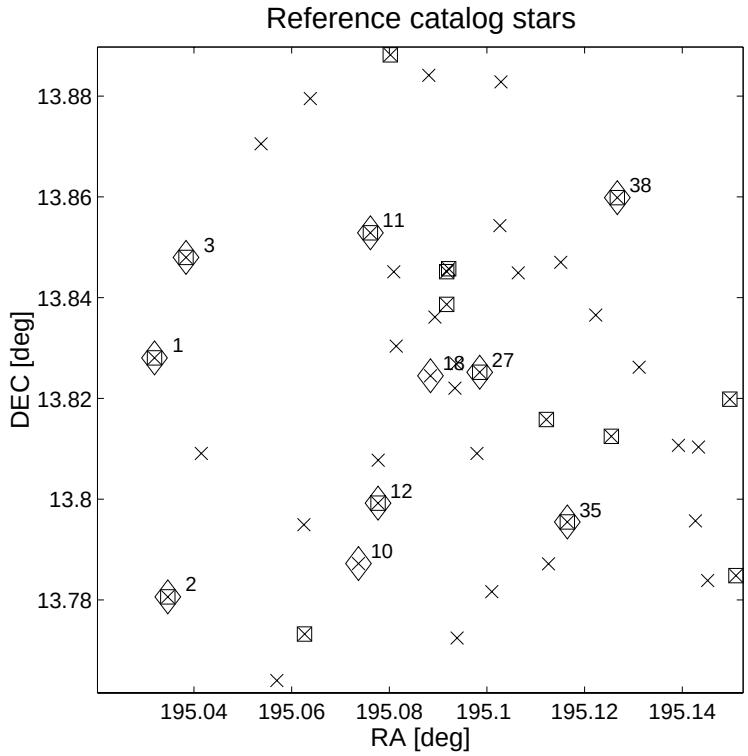

Figure 4.4: *The reference catalog stars (crosses). Brightest stars are marked by squares and matched stars by diamonds.*

As infrared detectors get bigger, fits become correspondingly easier. The 3-color SIRIUS camera from Nagoya University produces simultaneous J, H and Ks images of a 5 × 5 arcmin field on the UH 2.2-m telescope, almost 3 times the areal coverage compared to QUIRC, and hence easier to fit with ASCfit.

The execution time on a 450MHz PentiumII linux machine is typically 12 seconds for a 2K × 2K image. Most of this time (10 seconds) is spent on image object detection by *SExtractor*. In star-rich regions increasing the threshold of detection can reduce execution times.

Error sources

In general the accuracy level of the obtained fit, calculated as the RMS distance between reference stars and observed stars in (RA,DEC) coordinates, is < 0.4 arcsec. This is to be compared with the generally quoted typical astrometric error of 0.25 arcsec. for the USNO-A2.0 catalog. Additional error may arise from stars with significant proper motion since the USNO-A2 observation epoch. The 2MASS astrometric error is slightly better than the USNO-A2, and less subject to proper motion. Best results (0.1 arcsec) are obtained when a high percentage of the objects are fitted and in star rich images.

ASCfit is designed to work automatically most of the time, even in difficult fields. Failure to find a fit generally occurs in images with very few (<10) stars, in fields around bright stars where the reference catalog may miss stars, or very confused images with many (>1000) stars. The reason for the latter being the high possibility of selecting wrong stars for the initial match due to poor knowledge of the magnitude of the stars in the reference catalog.

4.3 Two instruments

Two-instrument inter-calibration constitutes the bulk of the examples treated in this work. There are several two instrument packages with instruments build at the Technical University of Denmark. Data from various calibration measurements have thus been available and the need to determine the relative attitudes between the instruments an important motivation for this work.

4.3.1 Ørsted

For the pre-flight inter-calibration of the Ørsted gondola two datasets exist. The two datasets are sufficiently similar to be treated in parallel in the following. The first set was taken at the geomagnetic observatory Brorfelde (BFE) in Denmark in March 1996[1]. The second set was taken at the Table Mountain Observatory (TMO), CA. USA, in October 1996.

[1] The data treated here are from the second Brorfelde calibration. The first Brorfelde calibration will not be considered since the relative attitude between the instruments is expected to have changed between the two Brorfelde calibrations.

Calibration setup and data description

BFE: The Brorfelde inter-calibration was carried out on the night of March 18, 1996. The geomagnetic observatory is situated at astronomical coordinates $(11.6729^o E, 55.62494^o N)$ at a height of 80 m above the sea. The Ørsted gondola was placed on a turntable mounted on a non-magnetic pillar outside and close by the house containing the geomagnetic observatory magnetometer. The readings from this magnetometer were recorded while the gondola was rotated to various positions. In all 60 positions were covered, each position was observed for 20 seconds and an average over these 20 seconds was formed for the magnetometer readings. The ASC boresight zenith distance was kept below 24^o to avoid substantial optical refraction and blinding from adjacent objects (trees and buildings). The Brorfelde calibration site is far from optimal for this type of calibrations since weather often prevents celestial observations and even when the weather is clear, the seeing is relatively poor.

TMO: The TMO inter-calibration was carried out on the night of October 24, 1996. The Table Mountain Observatory is an astronomical observatory under JPL, which has extended its capabilities to perform magnetic calibrations. It is situated at astronomical coordinates $(242.34490^o E, 34.38185^o N)$, at a height of 2353 m. At TMO there is no permanent geomagnetic reference station, instead a temporary reference station was established [34]. Two non-magnetic pillar acts as support for this reference magnetometer and for the turntable on which the gondola was mounted and rotated to various positions. The available dataset covers 23 positions.

Calibration procedure

For both sets, the reading from the gondola magnetometer have to be calibrated using the methods and constants described in [42]. This calibration corrects for non-orthogonalities, scale factors, zero offsets and temperature effects for the magnetometers as described in detail in [49]. For the Brorfelde set the reference magnetometer need no calibration since it is a part of the global network of geomagnetic reference stations which are periodically calibrated to international standards. The TMO reference magnetometer data are calibrated following the descriptions in [34].

The ASC data must also be reduced before use. Since the orientation

of the ASC drifts across the sky due to the Earth's rotation over the 20 seconds, it is not sufficient to take the average of the ASC data. Instead a first order line is fitted to the ASC data and this line is extrapolated to the time associated with this measurement. For the Ra parameter (giving the Right ascension of the ASC boresight) it is necessary to take out the Earth rotation of approximately 15 arcsec/second when fitting the line, in order to avoid its dominant but well determined influence. An example of the extrapolation of the ASC orientation is shown in Figure 4.5.

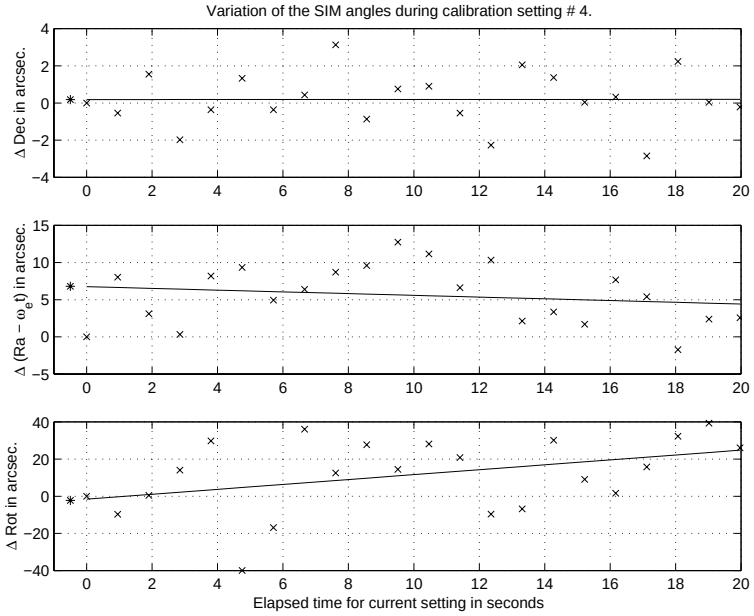

Figure 4.5: *Fitting and extrapolating ASC data. Crosses mark observations, which are extrapolated to the time associated with the measurement, marked by the asterisk.*

The fluctuations about the estimated line are regarded as being the noise level, either internally in the instrument or externally due to e.g. the wind stress, seeing and clouds which might not be negligible. From instrumental considerations the *Rot* angle is expected to have a higher internal noise level than the *Dec* and *Ra* angles. This is observed in Figure 4.5.

After this reduction the ASC data are be corrected for atmospheric refraction and for aberration using the equations from section 2.6. These corrections are of the order of 10-20 arcsec. aberration for the and 50-100 ascsec. for the refraction.

Several variations are possible when performing the inter-calibration. The choice is which parameters to solve for and which to assume to be known and constant. Furthermore there is the possibility to let the reference magnetometer work only as a variometer (thus disregarding its absolute values). Eight possible combinations in varying absolute or variometer reference magnetometer, fixed or variable reference magnetometer orientation and fixed zero offset or variable offset were investigated.

A plot of a typical set of the obtained residuals is shown in Figure 4.6.

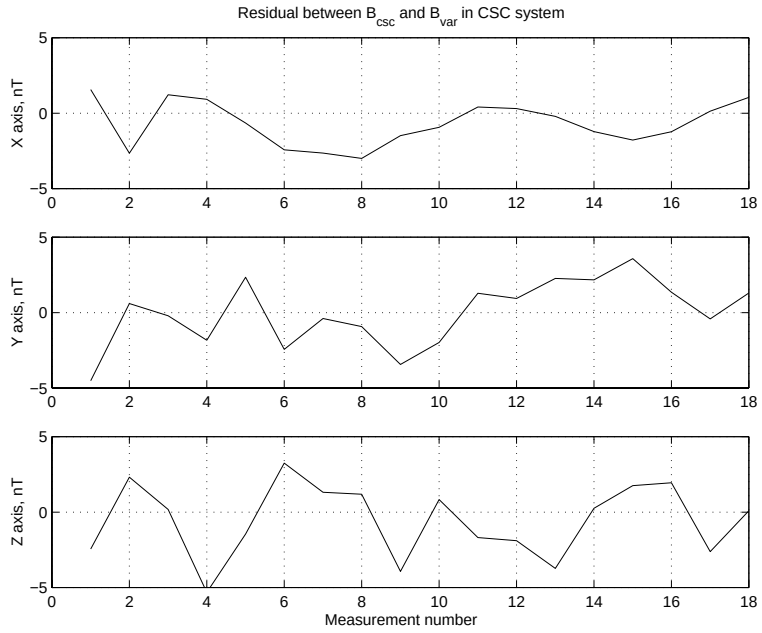

Figure 4.6: *Obtained residuals for the Ørsted instrument package. This example is for absolute reference measurements, fixed orientation of the reference magnetometer, and no offset determination.*

Results

The results are summarized in Tables 4.1 and 4.2. The first column describes the choice of options used for that calibration. 000 signifies absolute reference magnetometer, known fixed reference magnetometer orientation, and a magnetic offset kept fixed at zero. 111 signifies a variometer reference magnetometer, varying reference magnetometer orientation and varying offset. Combinations in between describe the various combinations.

Columns 2 to 4 give the 323 Euler angles (α, β, γ) of the relative attitude between the ASC and the CSC systems. Columns 5 to 7 give (η, ζ, ξ), which are the 232 Euler angles for the orientation of the reference magnetometer in the Conventional Terrestrial System (CTS). Finally (O_1, O_2, O_3) give the offset in the magnetic field vector (in nT), between the reference pillar and the calibration pillar. This is expressed in the fixed system of the reference magnetometer.

The variances have formally been calculated using the methods described in section 2.4, and are listed below each of the determined parameters.

	Euler angles in deg.			REF orientation angles in deg.			Offsets in nT.			RMS in nT
	α	β	γ	η	ζ	χ	O_1	O_2	O_3	
BFE										
000	-91.2656	-91.0007	-1.0091	145.6249	-11.6729	0.0000	0.00	0.00	0.00	8.37
	0.0004	0.0002	0.0002	-	-	-	-	-	-	
001	-91.2497	-91.0029	-1.0061	145.6249	-11.6729	0.0000	7.67	-6.01	-3.17	6.70
	0.0009	0.0002	0.0002	-	-	-	0.13	0.29	0.13	
010	-91.2495	-91.0029	-1.0061	136.4367	-10.6035	9.3524	0.00	0.00	0.00	6.69
	0.0009	0.0002	0.0002	4.2693	0.4721	4.3481	-	-	-	
011	-91.2494	-91.0029	-1.0061	134.8735	-10.4617	10.9415	-0.63	-3.14	-0.11	6.68
	0.0009	0.0002	0.0002	4.6012	0.5603	4.6253	402.04	334.44	148.40	
100	-91.2503	-91.0025	-1.0061	145.6249	-11.6729	0.0000	0.00	0.00	0.00	6.44
	0.0008	0.0002	0.0002	-	-	-	-	-	-	
101	-91.2501	-91.0025	-1.0061	145.6249	-11.6729	0.0000	$\approx 10^3$	$\approx 10^3$	$\approx 10^3$	6.23
	0.0009	0.0002	0.0002	-	-	-	$\approx 10^3$	$\approx 10^3$	$\approx 10^3$	
110	-91.2486	-91.0031	-1.0056	96.5185	-23.8234	62.3199	0.00	0.00	0.00	6.23
	0.0009	0.0002	0.0002	3.7715	1.0539	2.5137	-	-	-	
111	-91.2486	-91.0030	-1.0056	93.6086	-22.7209	69.2608	$\approx 10^3$	$\approx 10^3$	$\approx 10^3$	6.17
	0.0009	0.0002	0.0002	4.8588	1.5715	3.2623	$\approx 10^3$	$\approx 10^3$	$\approx 10^3$	

Table 4.1: Results of the Ørsted BFE inter-calibrations.
Showing the obtained results for the Ørsted gondola inter-calibration. The first column describes the type of calibration, as explained in the text.

	Euler angles in deg.			REF orientation angles in deg.			Offsets in nT.			RMS in nT
	α	β	γ	η	ζ	χ	O_1	O_2	O_3	
TMO										
000	-91.2328	-90.1386	0.0958	124.3841	-242.3209	0.0000	0.00	0.00	0.00	2.07
	0.0005	0.0003	0.0003	-	-	-	-	-	-	
001	-91.2178	-90.1402	0.0999	124.3841	-242.3209	0.0000	0.00	-7.18	0.89	1.58
	0.0023	0.0004	0.0007	-	-	-	0.32	1.04	0.24	
010	-91.2178	-90.1402	0.0999	123.5976	-242.2400	-1.3732	0.00	0.00	0.00	1.59
	0.0023	0.0004	0.0007	3.8615	0.4308	6.7367	-	-	-	
011	-91.2178	-90.1402	0.0999	124.0311	-242.2858	-0.6010	-6.82	-1.96	4.06	1.58
	0.0024	0.0004	0.0007	4.1280	0.8902	6.8998	732.46	708.17	402.56	
100	-91.2255	-90.1390	0.0986	124.3841	-242.3209	0.0000	0.00	0.00	0.00	2.08
	0.0023	0.0004	0.0007	-	-	-	-	-	-	
101	-91.2146	-90.1407	0.1005	124.3841	-242.3209	0.0000	$\sim 10^3$	$\sim 10^3$	$\sim 10^3$	1.53
	0.0027	0.0004	0.0008	-	-	-	$\sim 10^3$	$\sim 10^3$	$\sim 10^3$	
110	-91.2230	-90.1394	0.0990	110.3164	-238.8520	4.6931	0.00	0.00	0.00	1.96
	0.0024	0.0004	0.0007	10.2098	13.1298	12.8496	-	-	-	
111	-91.2228	-90.1395	0.0991	110.1129	-238.9161	4.4568	$\sim 10^3$	$\sim 10^3$	$\sim 10^3$	1.94
	0.0028	0.0004	0.0008	27.0332	13.5518	15.8489	$\sim 10^3$	$\sim 10^3$	$\sim 10^3$	

Table 4.2: Results of the Ørsted TMO inter-calibrations.
Showing the obtained results for the Ørsted gondola inter-calibration. The first column describes the type of calibration, as explained in the text.

When studying the results, a number of things can be observed. For the BFE set the result of the first inter-calibrations is significantly different from the rest, with differences up to 55 arcsec. This result also has a higher RMS value of the residual and it seems reasonable to assume that too few parameters are available for modeling the actual situation in this case. This is also seen, but to a lesser extent in the TMO measurements.

A common feature is that the offset determination fails for the cases where the reference magnetometer is used as a variometer magnetometer. This is due to the fact that the absolute level of the variometer and thus the offset between the two magnetometers is not taken into consideration for this type of optimization. However it can be observed that the solutions obtained for the inter-calibration angles are close to what is found in the cases with an absolute reference magnetometer. This is of significance since, absolute reference magnetometers are not always available.

Another feature of the cases where the reference magnetometer is a variometer is the poor determination of its orientation. This is due to the fact that the orientation of the reference magnetometer, with respect to the Earth reference system, is primarily determined by the measured magnetic field vector, when only the variations are available orientation is poorly determined. However again this does not influence the solution for the inter-calibration angles.

When comparing the results for the two sets a significant difference of close to one degree in the third inter-calibration angle (γ) is evident. This difference is believed to be caused by a change in the calibration parameters for the ASC [50]. Following in-flight tests have shown the values from the BFE inter-calibration to be closest to the in-flight values.

Finally it is important to note that the formally determined variances does not cover the observed variations in the found angles. The variances are seen to be a factor between 2 and 7 too low.

4.3.2 SAC-C

The MMP aboard the Argentinean SAC-C satellite (also known as Ørsted-2) was the successor to the Ørsted satellite. The pre-flight calibration was carried out in September 1998, at the TMO facility.

Calibration setup and data description

The inter-calibration of the SAC-C MMP was very similar to the Ørsted inter-calibration since the two instrument packages were almost identical. The main difference was that no geomagnetic reference station was established for the SAC-C inter-calibration. Instead the flight spare magnetometer was used as the reference magnetometer. This was of equally high quality, as the instrument package magnetometer, but it was not carefully aligned with the local NED-system, thus when performing the inter-calibration the reference magnetometer orientation must be solved for. The SAC-C inter-calibration measurements were conducted over two nights (September 10 and 12, 1998) and each night 90 positions were measured each for 20 seconds.

A plot of the obtained results is shown in Figure 4.7.

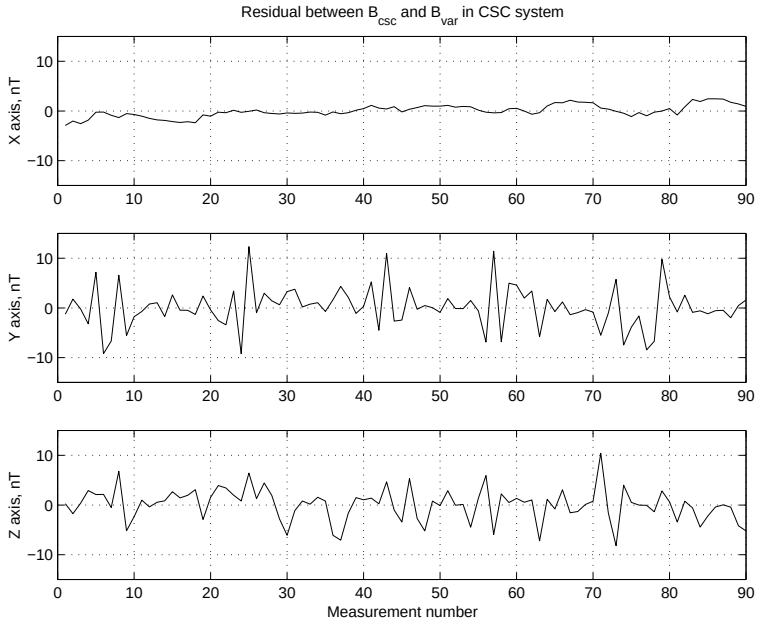

Figure 4.7: *Obtained residuals for the SAC-C instrument package. This example is for absolute reference measurements, variable orientation of the reference magnetometer, and includes offset determination.*

Another plot of the obtained residuals when using the reference magnetometer as a variometer is shown in Figure 4.8.

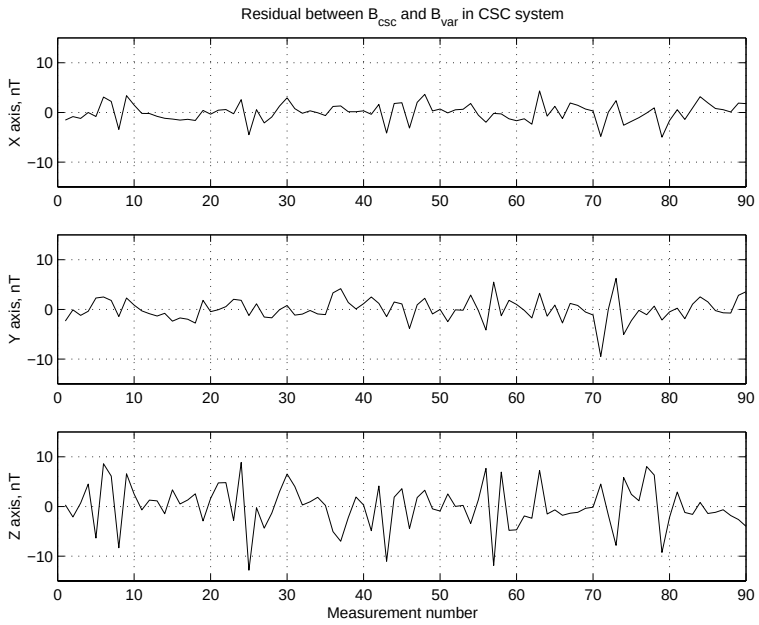

Figure 4.8: *Obtained residuals for the SAC-C instrument package. This example is for variometer reference measurements, variable orientation of the reference magnetometer, and includes offset determination.*

Results

The calibration procedure is the same as that applied to the Ørsted data. Constants for both the SAC-C and Flight Spare magnetometers can be found in [6]. The obtained results for the inter-calibration are shown in Table 4.3. Table columns show the same as for the Ørsted case above.

	Euler angles in deg.			REF orientation angles in deg.			Offsets in nT.			RMS in nT
	α	β	γ	η	ζ	χ	O_1	O_2	O_3	
TMO, night 1										
010	-90.45187	-90.43993	0.45732	39.33238	-57.02618	30.12922	0.00	0.00	0.00	5.06
	0.00088	0.00014	0.00037	1.62746	1.03979	3.35031	-	-	-	
011	-90.45188	-90.43993	0.45733	39.11279	-57.16815	30.60317	0.63	6.98	-10.43	3.11
	0.00088	0.00014	0.00037	1.76871	1.09638	3.44584	$\sim 10^3$	$\sim 10^3$	$\sim 10^3$	
110	-90.45259	-90.44001	0.45766	0.29693	-60.69731	78.76064	0.00	0.00	0.00	3.12
	0.00089	0.00014	0.00037	5.91099	4.33522	8.61799	-	-	-	
111	-90.45264	-90.43993	0.45766	-3.59486	-61.47123	78.20104	$\sim 10^3$	$\sim 10^3$	$\sim 10^3$	3.02
	0.00090	0.00014	0.00038	6.60409	5.85447	11.17881	$\sim 10^3$	$\sim 10^3$	$\sim 10^3$	
TMO, night 2										
010	-90.45368	-90.43930	0.45841	83.74279	-61.71788	-54.26930	0.00	0.00	0.00	5.85
	0.00088	0.00014	0.00037	1.08861	0.87700	2.39102	-	-	-	
011	-90.45368	-90.43931	0.45842	83.98751	-61.95041	-54.82690	5.07	4.53	-7.12	4.14
	0.00088	0.00014	0.00037	1.14033	1.01987	2.36536	$\sim 10^2$	$\sim 10^2$	$\sim 10^2$	
110	-90.45201	-90.43912	0.45807	143.39691	-153.38965	10.95765	0.00	0.00	0.00	4.07
	0.00088	0.00014	0.00037	10.66852	2.67517	9.94410	-	-	-	
111	-90.45205	-90.43910	0.45802	144.33590	-142.47076	0.39031	$\sim 10^3$	$\sim 10^3$	$\sim 10^3$	3.02
	0.00088	0.00014	0.00038	15.19142	4.10732	14.11658	$\sim 10^3$	$\sim 10^3$	$\sim 10^3$	

Table 4.3: Results of the SAC-C, MMP inter-calibrations at TMO. Showing the obtained results for the SAC-C gondola inter-calibration. The first column describes the type of calibration, as explained in the text.

First it is noted that only four different methods have been used for the SAC-C inter-calibration, since it is not possible to assume a fixed orientation for the reference magnetometer.

For the three Euler angles the spread over all the obtained results is 6.5, 3.4 and 4.0 arcsec. respectively. It is seen that the spread is somewhat larger for the results from the second night than for the first night. In general there is a good agreement between the formal standard deviations and the spread obtained using the various calibration procedures. However again the formal estimate of the standard deviation is too low, by a factor between 2 and 7.

As for the Ørsted case the orientation of the reference magnetometer is poorly determined when using it as a variometer. However its orientation can be determined to within a few deg when using the full absolute measurement of the reference magnetometer.

Offset determination is only possible in one case (it fails when using the variometer since no absolute values are available). For both nights the determined offset has a norm of approximately 10 nT.

4.3.3 UH 24-inch TGS

The purpose of the inter-calibration between the UH-24-inch telescope and the ASC is to establish the basis for a working Telescope Guidance System (TGS), using the highly accurate output from the ASC to steer the telescope.

In order to make this operational an accurate determination of the relative attitude between the ASC and the telescope coordinate system is necessary. The telescope system is defined by the pointing of the telescope axis and the orientation of the two edges of the CCD in the camera mounted on the telescope.

It is expected that the relative orientation between the two systems might vary since no single rigid structure exists to support the ASC.

The inter-calibration can be performed in two modes $O2$-$O3$ or $O3$-$O3$. Both modes use the accurate coordinates obtained by the ASCfit package, described in section 4.2.1, along with the ASC data. The $O2$-$O3$ inter-calibration only utilizes the pointing of the telescope as defined by the center coordinates of the image, while the $O3$-$O3$ inter-calibration uses the full attitude information regarding the CCD.

Calibration setup and data description

The measurements for the inter-calibration were performed on the night of July 9, 2001 at the UH-24-inch telescope, near the top of Mauna Kea on Hawai'i. The telescope is positioned close by the UH-88 telescope and its position ($19.8261^oN, 155.4722^oW$, height: 4214 m) is therefore adopted for the following calculations.

The ASC was continuously sampling at approximately 1 second intervals and the attitudes were recorded to a file. The telescope was pointed to a number of relatively bright stars and a manual, optical confirmation of target was performed. In all 14 images were registered on the Apogee CCD and saved in the FITS format. Starting times of the exposure intervals were noted in a log. A summary of the obtained images is given in appendix B, Table B.1. The approximate pointing of the telescope optical axis during the measurements, expressed in local Az-Ze (Azimuth-Zenith distance) coordinates, are shown in Figure 4.9.

Initial data reduction

CCD Images: Each image was inspected with the GAIA display tool and an attempt to derive the astronomical coordinates with ASCfit was done. Unfortunately this was only possible for two of the images. The problem being that the central bright star used for positioning the telescope in most cases was too bright to distinguish any other stars. Thus the pattern matching of ASCfit is not applicable. However from the two images that could be matched the scale and orientation, which is expected to be the same for all the exposures, can be used to determine the values for the center of the remaining images. These can be used in the $O2$-$O3$ IC as described below. In all eleven of the obtained images were deemed suitable for the inter-calibration procedure. These are shown in Figure 4.9. The others disqualified for various reasons mainly over or under exposure.

More data would have been desirable if a thorough determination of the relative attitude for the TGS is to be obtained. Unfortunately there was not enough time to perform any more observations. Thus the treatment in the following sections must be considered as a study of the method rather than an actual calibration.

In addition new inter-calibration might have to be performed each time the camera is mounted or adjusted. A study comparing relative attitudes

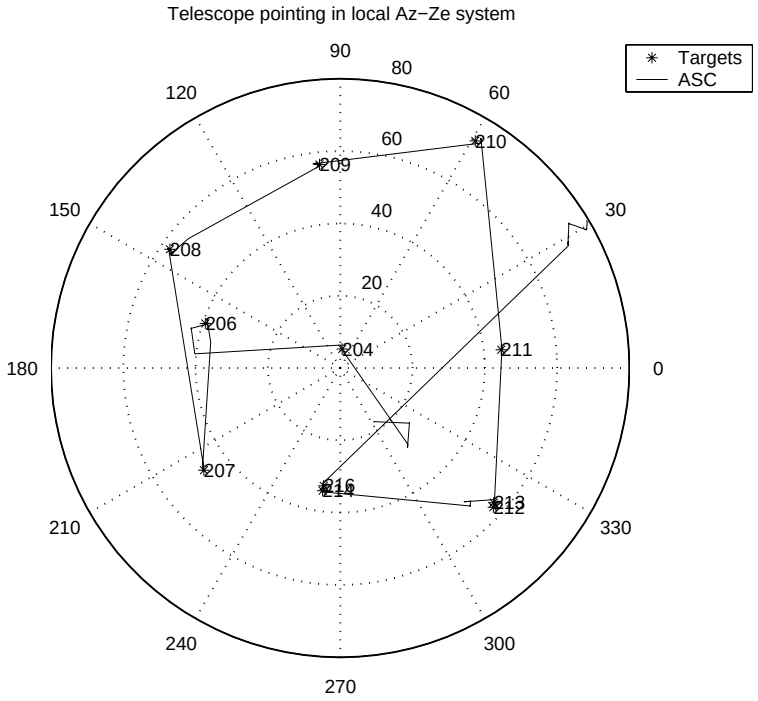

Figure 4.9: *Telescope pointing and ASC data in local Az-Ze coordinates. The Ox axis is directed towards South, Azimuth increases towards the West. The solid line gives the ASC readings and the asterisks indicate the coordinates of the valid images.*

between remounting of the camera could be an interesting follow-up investigation.

ASC data: For each of the valid images the ASC data covering the exposure interval are extracted and first order lines are fitted to the three angles as described in section 4.3.1. An example of the fitting of ASC data is shown in Figure 4.10. Since the ASC in this case is mounted on the telescope, which follows the motion of the stars across the nightsky, the Right Ascension shall not be corrected for the 15 arcsec/second Earth

rotation. No correction for refraction and aberration has been applied. The refraction is negligible due to the high altitude of the observation site and the aberration is deemed to be significantly less than the variation caused by the mechanical flexures.

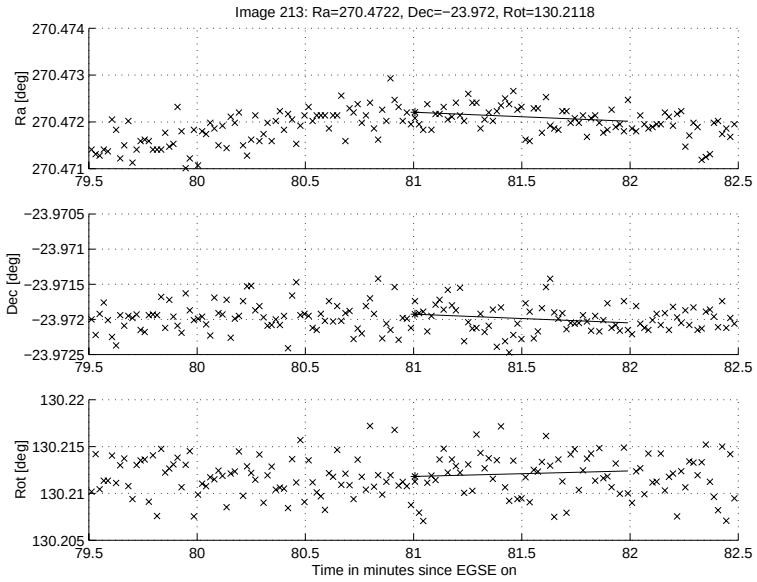

Figure 4.10: *Fitting ASC data. Crosses mark observations, which for the interesting time interval are fitted by the line and estimated at the time associated with the measurement, marked by the asterisk.*

*O*2-*O*3 Calibration procedure

For the images where only the center of the frame can be determined it is only possible to determine two of the three angles specifying the relative attitude between telescope and ASC. Formally this can be expressed by the following equations. In the matrix notation the telescope and ASC attitudes are connected by

$$\mathbf{R}_{REF}^{TEL} = \mathbf{R}_{ASC}^{TEL}\mathbf{R}_{REF}^{ASC} \tag{4.3}$$

The pointing of the telescope optical axis in the reference system is therefore

$$\mathbf{r}_p = (\mathbf{R}_{REF}^{TEL})^{-1} \begin{bmatrix} 0 \\ 0 \\ 1 \end{bmatrix} = (\mathbf{R}_{ASC}^{TEL}\mathbf{R}_{REF}^{ASC})^{-1} \begin{bmatrix} 0 \\ 0 \\ 1 \end{bmatrix} = \begin{bmatrix} \cos(Ra)\cos(Dec) \\ \sin(Ra)\cos(Dec) \\ \sin(Dec) \end{bmatrix} \tag{4.4}$$

The final equality is due to the convention used for the astronomical coordinates. Inverting equation (4.4) gives

$$\mathbf{R}_{REF}^{ASC}\mathbf{r}_p = (\mathbf{R}_{ASC}^{TEL})^{-1} \begin{bmatrix} 0 \\ 0 \\ 1 \end{bmatrix} = \begin{bmatrix} r_{11} & r_{12} & r_{13} \\ r_{21} & r_{22} & r_{23} \\ r_{31} & r_{32} & r_{33} \end{bmatrix}^T \begin{bmatrix} 0 \\ 0 \\ 1 \end{bmatrix} = \begin{bmatrix} r_{31} \\ r_{32} \\ r_{33} \end{bmatrix} = \mathbf{r}_{tel} \tag{4.5}$$

This vector is the telescope optical axis expressed in the ASC system. It can be obtained since $\mathbf{R}_{REF}^{ASC}$ is known from the ASC observations and $\mathbf{r}_p$ is known from the determined center coordinates of the images. By calculating $\mathbf{r}_{tel}$ for the various positions it is possible to study how the relative attitude between ASC and telescope changes.

O3-O3 Calibration procedure

When the complete absolute attitude of the CCD image is available, it is possible to calculate the full attitude matrix for each position by

$$\mathbf{R}_{ASC}^{TEL} = \mathbf{R}_{REF}^{TEL}\,(\mathbf{R}_{REF}^{ASC})^{-1} \tag{4.6}$$

where

$$\mathbf{R}_{REF}^{TEL} = \mathbf{R}_3(90-\beta)\mathbf{R}_2(90-Dec)\mathbf{R}_3(Ra) \tag{4.7}$$

Here β is the angel giving the orientation of the CCD about the optical axis of the telescope. Assuming orthogonality of the CCD axis, β can be found from equation (4.1) and is determined by the transformation parameters from ASCfit by

$$\beta = \arctan\left(\frac{CD1\_2}{CD1\_2}\right) \tag{4.8}$$

Again $\mathbf{R}_{REF}^{ASC}$ is known from the ASC observations, and the full $\mathbf{R}_{ASC}^{TEL}$ attitude can thus be calculated.

Results

In spite of the sparse data the derived relative attitudes for the two methods will be given in the following.

O2-O3: Figures 4.11 and 4.12 show the obtained telescope axis expressed in the ASC system. Since it is expected that possible flexures stems from gravitational stresses, the telescope the relative attitudes are depicted as function of the local (Az, Ze) coordinates. For the available data it is

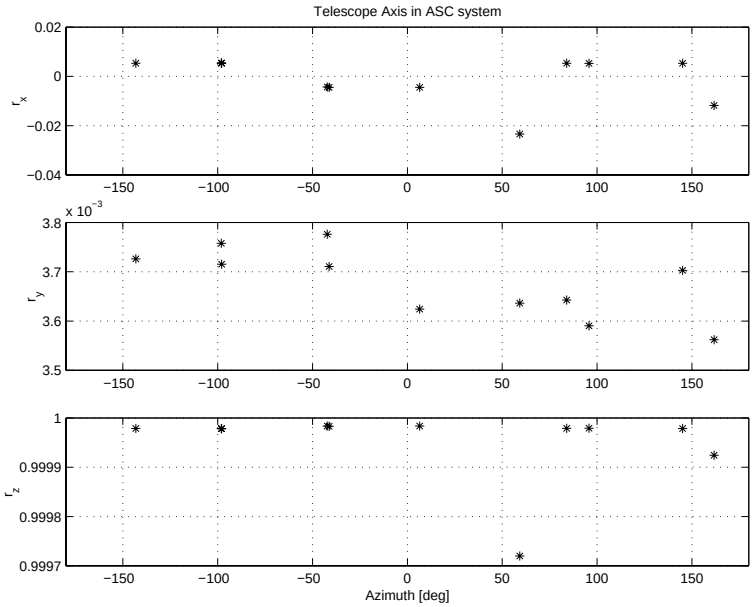

Figure 4.11: *Telescope optical axis in ASC system for the O2-O3 intercalibration as function of the Azimuth angle.*

hard to claim any systematic features. One might see a shift of the level of r_y between positive and negative Azimuth values, i.e. when the telescope changes between eastward and westward pointing in local coordinates. The angle between the two systems z-axis is depicted in Figure 4.13. The bulk of the angles are in an interval of 0.06 deg around the 0.35 mean value. Two points (images 206 and 210) have significantly different values

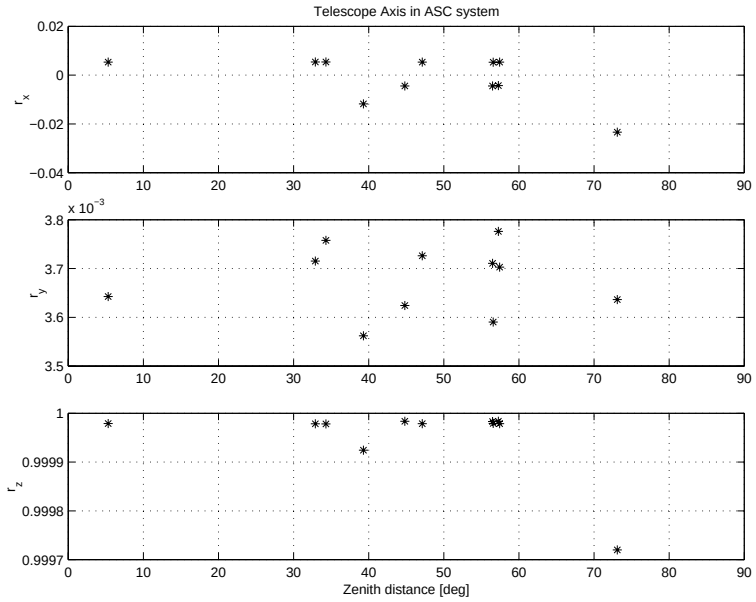

Figure 4.12: *Telescope optical axis in ASC system for the O2-O3 inter-calibration, as function of the Zenith distance.*

for the inter-calibration angle, 0.7 and 1.4 deg respectively[2]. It is not relevant to speak of outliners with the amount of data, but the two points do deviate from the rest of the determined relative attitudes.

O3-O3: The obtained results are listed in Appendix B. Since only two data points are available no real conclusions can be drawn. It can be seen that the two obtained sets differ by 0.05 arcsec in the angle between the two z-axes, but actually there is a rotation of 1.15^o between the two solutions.

For both the *O2-O3* and *O3-O3* inter-calibrations the data are too sparse to try any form of modeling of the relative attitude, and this is therefore left for future studies.

[2]Image 210 is actually not on the plot with the chosen axes.

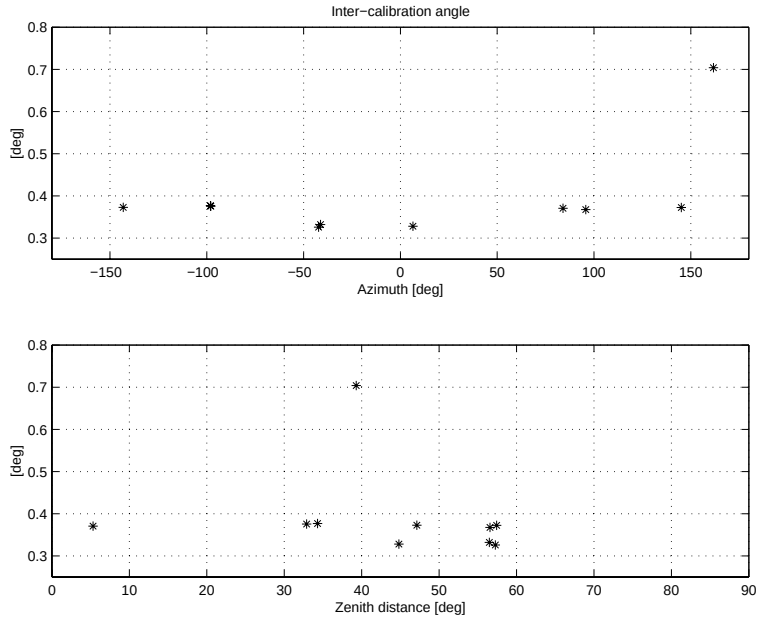

Figure 4.13: *Angle between the z-axis of the ASC system and the telescope optical axis for the O2-O3 inter-calibration.*

4.3.4 CHAMP

The study of CHAMP data concerns the inter-calibration between two $O3$ instruments and the improvement in attitude determination by combining such two instruments. The CHAMP satellite described in section 3.2.2. Methods for inter-calibration and attitude refinement are given in sections 2.1.3 and 2.5.2 respectively.

Calibration setup

The data consists of attitudes from the two ASCs onboard the CHAMP satellite. The data considered here are from March 18, 2001 (the 77^{th} day of that year), covering the period from 15:54:27 UT to 18:42:05 UT. The raw attitudes in the form of three Euler angles from each of the two ASCs (ASC1 and ASC2) and the matching timestamps. Information on validity and quality of the attitudes is also in the data. A plot of the valid data is shown in Figure 4.14.

At the considered time CHAMP was flying at an altitude of approximately 450 km making each orbit 93 minutes long. This period is clearly evident in the data. Structures in the data on small scale are also recognizable from one orbit to the next. This demonstrates the high degree of stability of the CHAMP satellite's attitude. Data gaps, especially in ASC2, are mainly due to solar blinding as the ASC2 boresight passes close by the solar disc. For this study only periods where both ASCs provide valid data are of interest. Thus the period from approximately 16:02 UT to 16:53 is selected. Other periods with data from both ASCs have been studied and give similar results. This is to be expected because of the high inter-orbit similarity.

Calibration procedure

As stated, there are two main objectives with the CHAMP data analysis. First the determination of the *relative attitude* between the two ASCs. Since the relative attitude varies, a smoothly varying model has to be determined. This model is utilized for the second objective, namely the *improvement of the attitude estimate*, which is performed by combining the measurements from the two ASCs. In the following the methods used are summarized and afterwards results and discussions are given.

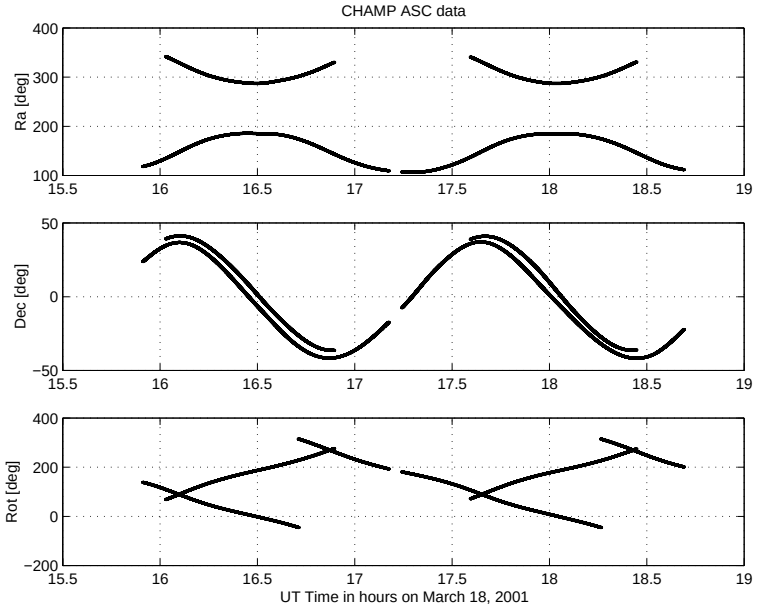

Figure 4.14: *Raw CHAMP ASC data. Shown are the valid data for ASC1 and ASC2. Note the clear periodicy. The data gaps, mainly for the ASC2, are due to solar blinding.*

Determination of relative attitude: Since both instruments are $O3$, the full relative attitude is easily obtainable by

$$R_{ASC2}^{ASC1} = R_{REF}^{ASC1} \left(R_{REF}^{ASC2}\right)^{-1} \tag{4.9}$$

Here it is understood that the two measurements are simultaneous. This is the case for the majority of the data, but exceptions do occur. Besides, in a more general setting, data from different types of attitude instruments will surely not be simultaneous. Thus it is chosen to fit polynomial models to each of the ASC attitudes. From these models the estimate of the relative attitude can be calculated at any desired instant of time within the regarded interval.

When fitting models to the individual attitudes it is possible to either

determine models for the individual Euler angles or determine models for each of the four quaternion components. Both methods work, but the quaternion approach gives the most stable results.

Improvement of attitude estimate: The improvement in attitude estimate relies on the determined model for the relative attitude and on the formalism described in section 2.5.2. The procedure is as follows. For each of the ASCs the standard deviation of each of the Euler angles is determined by determining the spread of the data around the fitted polynomial model. Using the estimated model of the relative attitude, the measurements and standard deviations of ASC2 are transformed to the system of ASC1. A weighted average of the two attitudes is then performed, resulting in a combined estimate of the attitude of the ASC1 system with respect to the reference system. The standard deviation of this new estimate is calculated by considering the spread around a polynomial fit to the new attitude. Depending on the length of the data interval considered and the order of the polynomial fit used varying improvements in the standard deviation of the attitude is obtained.

Results

Determination of relative attitude: Since most of the ASC data have identical timestamps it is possible to estimate the relative attitude directly for these using equation (4.9). An example of this is shown in Figure 4.15. For the determination of the relative attitude model the first step is to fit polynomial models to the individual ASC attitudes. Fits using various orders (from 2 to 10) have been tried, result vary with the length of the considered interval and the variability of the ASC attitudes. An example is given in Figure 4.16 and 4.17, which shows the residuals obtained from a 5^{th} order polynomial fit to the quaternion components and the Euler angles respectively. It has been observed that there is no significant difference between the models obtained using quaternions or Euler angles, when using higher order (>4) fits. However it is observed that quaternions numerically better suited for fitting models of lower order since the range of variation is smaller for the quaternions than for the Euler angles.

Using the polynomial model limits the applicability since the analysis is restricted to intervals where only smooth attitude variations occur, i.e. no thruster firerings or attitude maneuvers. Also the polynomial fit must be

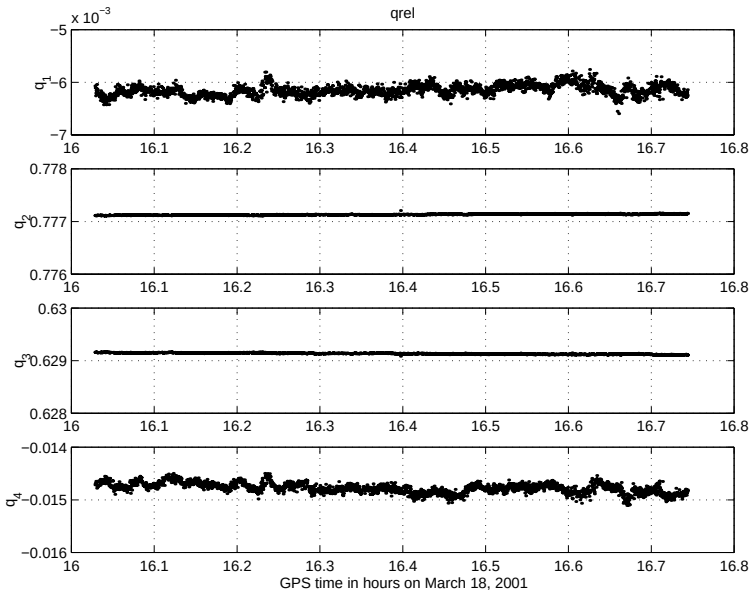

Figure 4.15: *Quaternion for the relative attitude between the two ASC coordinate systems, based on raw simultaneous measurements.*

broken up between periods where discontinuities in either of the attitude representations occur.

From the determined models of the individual ASC attitudes the relative attitude between the two instruments can be determined. An example using the quaternion to parameterize this is given in Figure 4.18, which shows the quaternions for this smooth model of the relative attitude imposed on top of the data from Figure 4.15. It is clearly seen that there are different noise levels on the various quaternion components, this is due to the intrinsic difference in the accuracy of the three Euler angles as described in section 3.1.2.

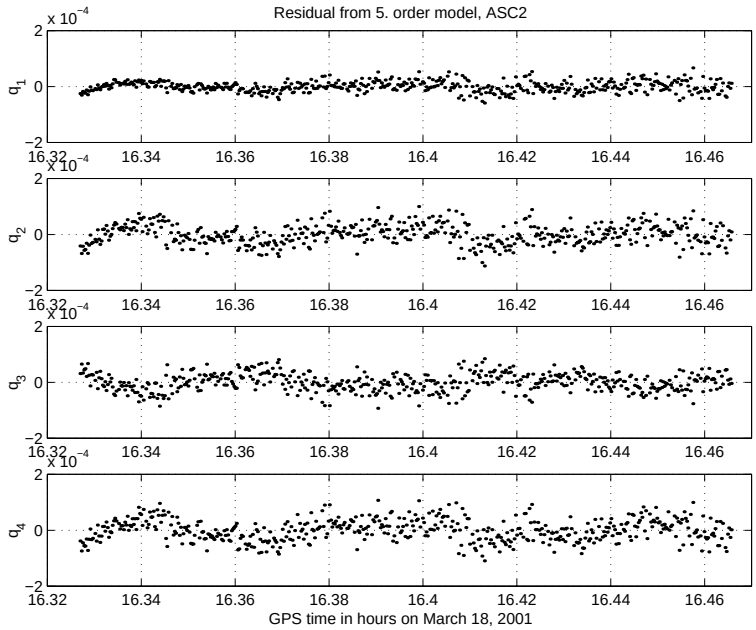

Figure 4.16: *Residual for single ASC attitude model, quaternions.*

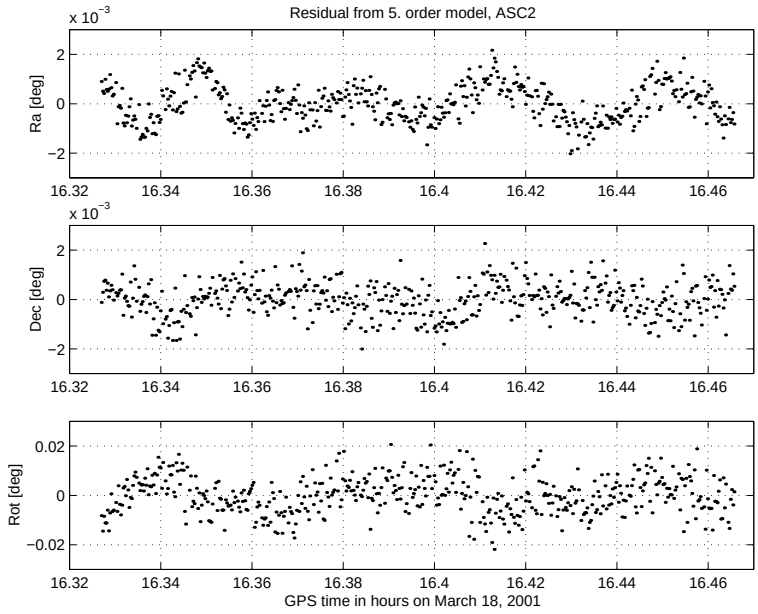

Figure 4.17: *Residual for single ASC attitude model, Euler angles.*

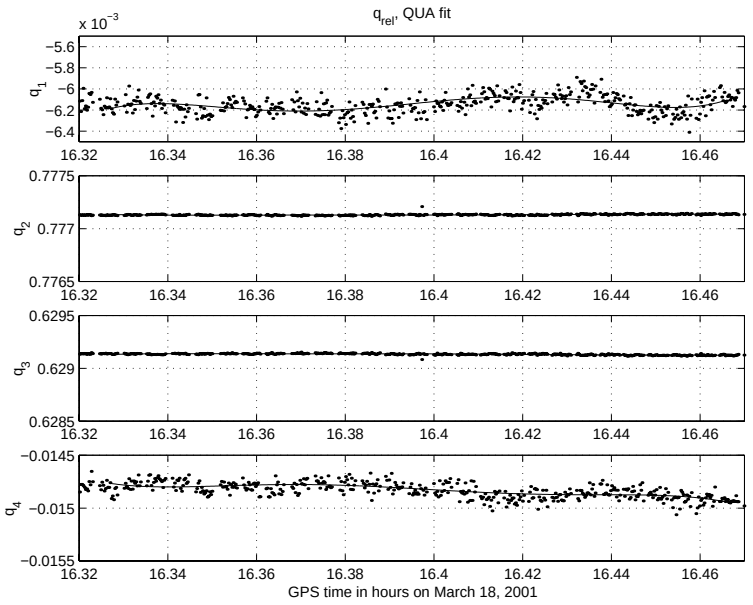

Figure 4.18: *Quaternion for the relative attitude between the two ASC coordinate systems, shown are raw simultaneous estimates (dots) and the fitted model (solid line).*

Improvement of attitude estimate: From the models of the relative attitude determined above the attitude of ASC2 is transformed to the ASC1 system. The standard deviations estimated from the polynomial fits to the Euler angles are transformed to the quaternion representation in the ASC1 system according to the method presented in section 2.5.2. Finally the weighted average is performed. An example of the obtained average attitude is shown in Figure 4.19. The standard deviations for the

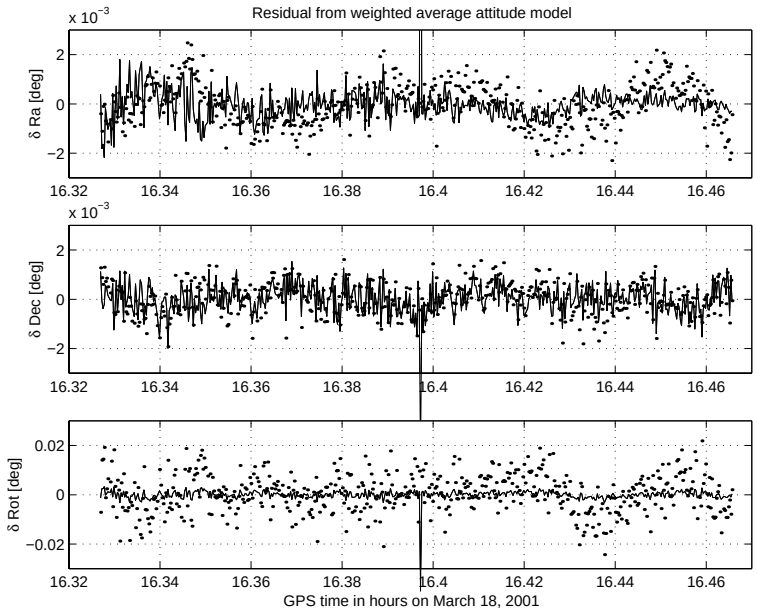

Figure 4.19: *Residual of improved attitude estimate. Shown are the residuals from a 5^{th} order model, for the ASC1 attitude (dots) and for the combined estimate from ASC1 and ASC2 (solid line).*

considered example are listed in Table 4.4.

It is seen that both the ASCs have a higher noise in the rotation angle, as expected. However, for ASC2 it is half the value of the one for ASC1. For the combined estimate, expressed in the ASC1 system, it is seen that there is an improvement of the noise in all three attitude angles. The

Table 4.4: Results of the combined CHAMP attitude estimate.

	Standard deviations [arcsec]		
	Ra	Dec	Rot
ASC1	4.45	4.13	52.47
ASC2	2.67	2.48	26.96
ASC1+2	3.65	2.29	7.98
Relative Improvement	0.82	0.55	0.15

Shown are the standard deviations for the individual ASC attitudes and the for the combined estimate along with the relative improvement.

boresight pointing direction noise (Ra and , Dec) is lowered by a factor 0.87 and 0.55 respectively. The estimate of the rotation angle on the other hand is lowered by a factor 0.15 corresponding to approximately a seven-fold reduction of the noise level. The larger reduction of the noise rotation angle is exactly what is expected and desired, since the accurately determined pointing direction of the ASC2 boresight helps in determining the ASC1 rotation angle when the combined attitude estimate is preformed using the modeled relative attitude.

4.4 N instruments

The inter-calibration of more than two instruments is often encountered on satellites. However it has not been possible to obtain a data set including more than two instruments since this part of the thesis work was initiated. Thus the general inter-calibration between N instruments is exemplified with a single, synthetic case, the SWARM type satellite.

4.4.1 SWARM

The four-instrument scientific payload proposed for the SWARM mission is a good example of the N-instrument inter-calibration. The project is still on the drawing board, thus the analysis of this configuration has to be tested with synthetic data. The aim is to test the influence of

various factors (i.e. the number of measurements, the distribution of data, magnetic offsets and error of the initial guess) on the convergence and quality of the inter-calibration.

Synthetic data

The synthetic data are constructed using a conceptual calibration setup similar to the one used in the Ørsted and SAC-C cases. The instrument package is rotated in the earth magnetic field while a fixed auxiliary magnetometer provides information about the magnetic field variations. The magnetic field is simulated by an average vector plus a normal distributed, random noise with zero mean and standard deviation $\sigma_{B,noise}$. The calibration site is chosen to be the TMO site, thus the average field in the NEZ system is known from the Ørsted and SAC-C measurements and is approximately $(24319.1, 5966.7, 42484.8)$nT. A number ($N_{obs}$) of different orientations is chosen for the instrument package. Since the boresights of the three ASCs are so far apart (approximately 113.5^o) it is not possible to make simultaneous measurements with the ASCs. Therefore the payload orientations are chosen so that each ASC has equally many valid observations. All ASC measurements are calculated but observations with a zenith distance larger than 40^o are given an invalid flag. The instrument package orientations are arranged with the ASC pointing randomly within a cone around Zenith, the opening angle of the cone (maximum Zenith distance) is $\sigma(z)$. The orientation of the instrument package specify the satellite system with respect to the local NEZ system i.e. R^{SAT}_{NEZ}. The individual instrument orientations with respect to the SAT system depend on the SAT system chosen, this choice is somewhat arbitrary. Letting the vector magnetometer be perfectly aligned with the SAT system, the instrument orientations are, as outlined in section 3.2.3 described by the following 323-Euler angles:

$$\begin{aligned}
\mathbf{R}^{CSC}_{SAT} &= R_{323}(\quad 0,\ 0, 0) \\
\mathbf{R}^{CHU1}_{SAT} &= R_{323}(\quad 0, 75, 0) \\
\mathbf{R}^{CHU2}_{SAT} &= R_{323}(120, 75, 0) \\
\mathbf{R}^{CHU3}_{SAT} &= R_{323}(240, 75, 0)
\end{aligned}$$

The total rotation from NEZ to the individual instruments are then found as:

$$\mathbf{R}_{NEZ}^{INST} = \mathbf{R}_{SAT}^{INST}\mathbf{R}_{NEZ}^{SAT} \tag{4.10}$$

The magnetic field (including the added noise) is rotated to the package magnetometer system. An example of the synthetic magnetometer data is shown in Figure 4.20. To investigate the influence of an offset in the mag-

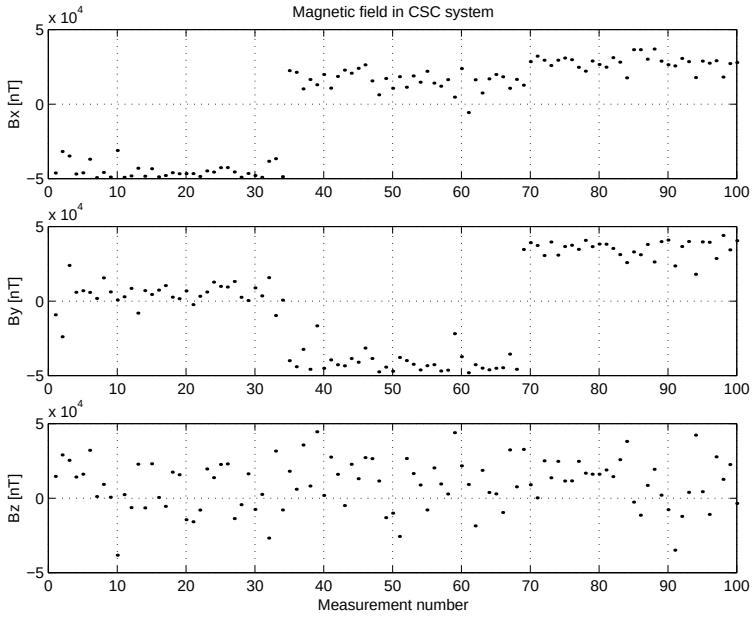

Figure 4.20: *Synthetic magnetometer data for the SWARM inter-calibration. The three regions, each with one ASC pointing close to zenith are clearly visible.*

netic field between the locations of the two magnetometers a randomly generated, constant vector offset ($\mathbf{b}_{offset}$) is added to the measurements of the auxiliary magnetometer. The attitudes of the three ASCs are generated from knowledge of the Earth rotation. The transformation from NEZ to $CHUn$ (R_{NEZ}^{CHUn}), which is given by the chosen instrument package

orientations can also be written as:

$$R_{NEZ}^{CHUn} = R_{SAT}^{CHUn} R_{NEZ}^{SAT} \quad (4.11)$$
$$= R_{CIS}^{CHUn} R_{CTS}^{CIS} R_{NEZ}^{CTS} \quad (4.12)$$

Here R_{NEZ}^{CTS} is given by the chosen location of the calibration site, R_{CTS}^{CIS} is given from theoretical knowledge of the Earth rotation. R_{CIS}^{CHUn}, which is the ASC measurement, can then be calculated. All of the above is done using the matrix formalism for rotations and a final conversion of the ASC attitude to 323-Euler angles is performed to make the data resemble actual observed data. An example of the synthetic ASC data is shown in Figure 4.21. Since the objective of this investigation is to study the

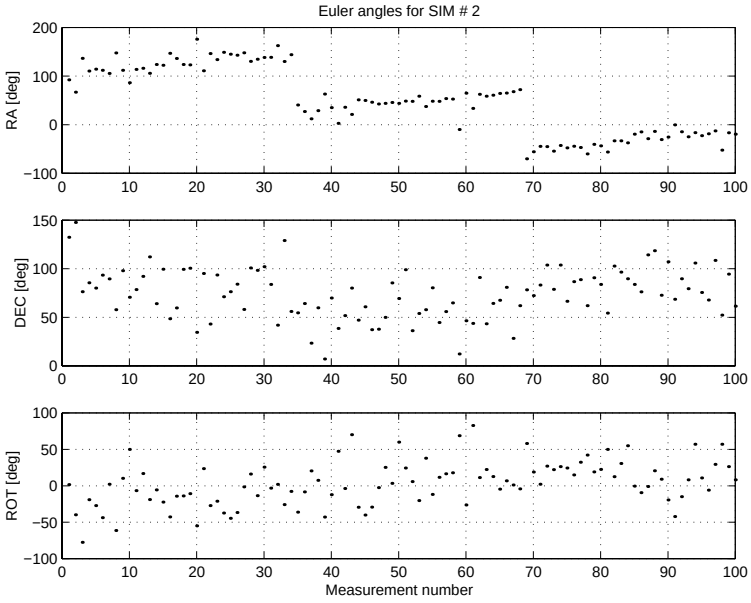

Figure 4.21: *Synthetic ASC data for the SWARM inter-calibration.*

influence of various parameters on the inter-calibration results, datasets with varying the number of positions (N_{obs}), norm of the magnetic offset ($|\mathbf{b}_{offset}|$) and maximum zenith distance $\sigma(z)$ have been produced.

Calibration procedure and experiments

The aim of the calibration of the synthetic data is to study the influence of various parameters on the quality of the obtained solutions.

The inter-calibration of the SWARM instrument package is somewhat different from the Ørsted and SAC-C cases. Partly because this inter-calibration has been fitted into a general inter-calibration procedure and partly because this inter-calibration is performed using the quaternion formalism. The matrix formalism was used for Ørsted and SAC-C. For the synthetic data the measurements are also considered instantaneous, so there are no effects of averaging data over various intervals of time.

However, there are also similarities with the Ørsted and SAC-C calibrations. Due to the payload geometry and the imposed limitations on the maximum zenith distance of the ASC readings, simultaneous measurements can only be obtained for the magnetometer and one ASC at a time.

Since none of the ASCs give valid data for all the measurements the inter-calibration differs somewhat from what was suggested in section 2.2.2 and sketched in Figure 2.6. It is not possible to select one of the ASCs $(O3)$ systems as determining the transition from absolute reference system to satellite system for all measurements. Instead the transition sketched in Figure 4.22 is used, for all the valid data. Should two ASCs have performed simultaneous measurements the magnetic measurements for this setting would thus appear twice in the construction of the error vector, once for each valid ASC attitude. The unit norm demand for the quaternions to represent attitudes is also added in the error function by adding a punishing term for deviations of quaternion norm from unity.

Results

The results of the various tests are listed in Tables 4.5 to 4.8. The Tables show the following. The first column of these tables show the value of the quantity varied i.e. $\sigma(q_0), N_{obs}, |B_o|, \sigma(z)$. Columns 2-5 give the quality of the obtained result, by the overall RMS value, the norm of the error of the obtained quaternion ($|\delta q|$), the maximal error of the corresponding Euler angles in arcsec. (δv). and the formal standard deviation on the Euler angles $\sigma(v)$. The standard configuration from which variation are

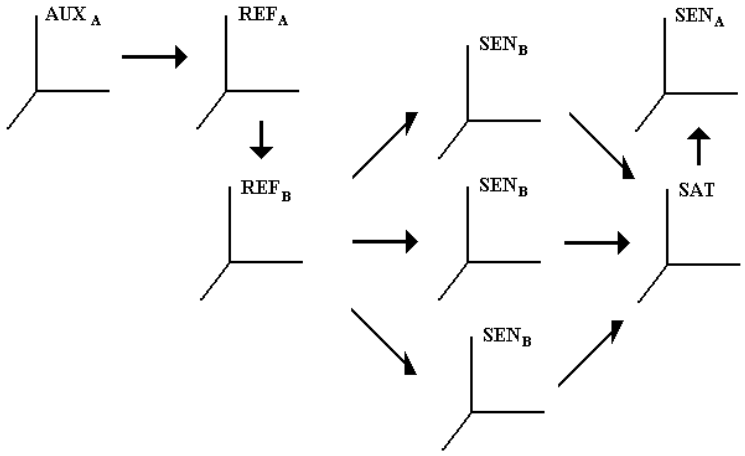

Figure 4.22: *SWARM inter-calibration principle.*

made is

$$\sigma(q_0) = 0.1 \qquad N_{obs} = 102$$
$$|B_o| = 0nT \qquad \sigma(z) = 20^o$$

The first test (Table 4.5) regards a varying error on the initial guess. The norm of the random quaternions added to each of the starting guesses has been varied from 0.01 to 1. The latter leads to a totally randomized starting guess. It is seen that the quality of the obtained solution is independent on the starting guess.

The second test (Table 4.6) concerns the number of observations. Here it is seen that the residual grows with the number of observations. This is a result of the fact that a fixed number of parameters can not equally model a larger number of data with random noise. The important feature is that both the formal and actual deviations from the correct solution are smaller for higher number of observations. This is due to the fact that the solution is better restricted the more measurements are available.

The offset between reference and payload magnetometers is varied in the third test (Table 4.7). It is seen that the offset is to some extent captured by the model in the inter-calibration, but not fully. Also the

Table 4.5: Results of synthetic SWARM inter-calibration. $\sigma(q_0)$ varied.

Varried quantity	Quality of obtained result			
$\sigma(q_0)$	RMS [nT]	$\lvert\delta q\rvert$	δv [arc sec]	$\sigma(v)$ [arc sec]
0.01	0.0011	$2.3 \cdot 10^{-8}$	0.006	38
0.1	0.0011	$2.3 \cdot 10^{-8}$	0.006	78
0.2	0.0011	$2.3 \cdot 10^{-8}$	0.006	34
0.5	0.0011	$2.3 \cdot 10^{-8}$	0.006	12
1.0	0.0011	$2.3 \cdot 10^{-8}$	0.006	46

Showing the obtained results for the synthetic SWARM inter-calibration for a varying $\sigma(q_0)$.

actual deviations of the solution from the actual values grows large (up to 276 arcsec.) as the offset increases. This demonstrates the importance of including the magnetometer offset in the modeling.

The last test carried out (Table 4.8) varies how far from zenith the three ASCs are pointing. Here it is seen that the solution is better restricted the larger the variation of the pointing.

In all the tests carried out show that the initial guess is not crucial. That more observations along with more varied (larger $\sigma(z)$) observations lead to a better determination of the relative attitude. And finally that offsets should be included.

This concludes the case studies. In the following conclusions and recommendations will be given.

Table 4.6: Results of synthetic SWARM inter-calibration. N_{obs} varied.

Varried quantity	Quality of obtained result			
N_{obs}	RMS [nT]	$\lvert\delta q\rvert$	δv [arc sec]	$\sigma(v)$ [arc sec]
6	0.00062	$1.01 \cdot 10^{-6}$	0.4	95
12	0.00100	$1.12 \cdot 10^{-7}$	0.04	129
21	0.00094	$7.94 \cdot 10^{-8}$	0.002	99
51	0.00098	$2.18 \cdot 10^{-8}$	0.004	36
102	0.00150	$2.12 \cdot 10^{-8}$	0.006	28
201	0.00150	$2.32 \cdot 10^{-8}$	0.005	18
300	0.00191	$8.71 \cdot 10^{-9}$	0.002	17

Showing the obtained results for the synthetic SWARM inter-calibration for a varying number of observations, N_{obs}.

Table 4.7: Results of synthetic SWARM inter-calibration. $\mathbf{b}_{offset}$ varied.

Varried quantity	Quality of obtained result			
$\lvert\mathbf{b}_{offset}\rvert$ nT	RMS [nT]	$\lvert\delta q\rvert$	δv [arc sec]	$\sigma(v)$ [arc sec]
0	0.001	$5.77 \cdot 10^{-8}$	0.02	39
5	0.88	$7.74 \cdot 10^{-5}$	15	25
10	2.64	$1.14 \cdot 10^{-4}$	26	29
20	6.31	$3.08 \cdot 10^{-5}$	6	25
50	7.19	$8.71 \cdot 10^{-4}$	187	45
100	24.57	$1.15 \cdot 10^{-3}$	276	60

Showing the obtained results for the synthetic SWARM inter-calibration for a varying $\mathbf{b}_{offset}$.

Table 4.8: Results of synthetic SWARM inter-calibration. $\sigma(z)$ varied.

Varried quantity	Quality of obtained result			
$\sigma(z)$	RMS	$\lvert\delta q\rvert$	δv	$\sigma(v)$
deg	[nT]		[arc sec]	[arc sec]
5	0.0012	$8.1 \cdot 10^{-8}$	0.029	167
10	0.0018	$6.8 \cdot 10^{-8}$	0.017	24
20	0.0011	$4.5 \cdot 10^{-8}$	0.014	66
30	0.0011	$3.0 \cdot 10^{-8}$	0.006	25
40	0.0011	$3.0 \cdot 10^{-8}$	0.006	28

Showing the obtained results for the synthetic SWARM inter-calibration for a varying $\sigma(z)$.

Chapter 5

Conclusion

Methods for determining the relative orientation between attitude sensitive instrument sensors have been described, implemented and tested with real cases.

Three attitude representations have been applied. In several aspects (e.g. computational ease and applicability in modeling) the quaternion representation is best suited for the described inter-calibration work.

It has been demonstrated that the Ørsted type geomagnetic instrumentation can be pre-flight inter-calibrated with accuracy in the arc second range. Also it has been demonstrated that this inter-calibration can be performed with the use of a variometer as the reference magnetometer.

A generalized implementation of the inter-calibration has been performed. However, case specific features are often so many that specialized implementations are to be preferred.

Generally high accuracy measurements demand high accuracy data analysis in order to avoid loss of accuracy. In the considered cases the inclusion of the aberration and refraction effects is necessary when treating the observations of the Advanced Stellar Compass. Otherwise the full accuracy of the relative attitude will not be obtained.

It has been demonstrated that it is possible to improve attitude estimates

by combining measurements from more sensors with inhomogeneous noise distributions. The principle has been demonstrated for two ASCs on the CHAMP satellite.

The matching of stars between astronomical images and reference catalogs has been used to obtain stellar coordinates on the images. This has further been used to show the principle of the inter-calibration necessary for a telescope guider system.

Chapter 6

Recommendations for future work

Having studied the field of accurate determination of relative attitudes between attitude sensitive instruments through this work some subjects, which deserves more attention have emerged. The primary subjects are listed here.

1. Outlier rejection in general and its influence on the inter-calibration results, needs to be studied.
2. The N-instrument inter-calibration needs a case study with real data. Also a study of cases with a broader variety of sensor types could be fruitful.
3. For the attitude improvement by combination of several sensor measurements, alternative methods to the polynomial fit should be investigated.
4. The Telescope Guidance System could benefit from a new set of inter-calibration measurements. This would also allow the study and modeling of the variation of the relative attitudes of the TGS.
5. On a somewhat different branch, the ASCfit tool could be applied to study the accuracy of the determination of the position of non-stellar objects. This would find application in the proposed asteroid detection mission "Bering".

Which of these items are the most pressing for further study, depends of cause to some extent on personal interests and preferences. However, a further study of the improvement in attitude estimate from two or more attitude sensors will find immediate, and in the future growing, application as more and more spacecraft are equipped with several high accuracy attitude instruments.

From personal interest, the construction of a working TGS with an automated procedure for inter-calibration is a future goal.

Appendix A

Details of the ASCfit package

The ASCfit package is developed for UNIX platforms and can be downloaded from `http://www.ifa.hawaii.edu/users/pickles`.

A.1 FITS keywords for World coordinates

The following FITS keywords, suggested by [44], are updated in the FITS header to store information about the world coordinates ($i, j \in \{1, 2\}$).

`CRVALi`	coordinate value at reference pixel (real floating)
`CRPIXi`	reference pixel coordinate (real floating – ASCfit uses 0
`CRTYPEi`	axis type (8 characters) `RA---CAR` or `DEC--CAR`
`CDi_j`	coordinate transformation matrix (real floating)

These keywords are read by viewing tools like SAOimage, which use the information to display on screen coordinates.

A.2 FITS keywords read by ASCfit

ASCfit reads a number of keywords from the FITS header. The following keywords are read.

IMAGETYP
RA
DEC
RA_OFF
DEC_OFF
EQUINOX
GAIN
SECPIXi (or PIXSCALi)
NAXISi ($i, j \in \{1, 2\}$)

The script allows for several commonly used keywords to be searched in order for most required FITS values. ASCfit ignores files with IAMGETYP set but not containing the word "OBJECT", ignoring "FLAT" or "BIAS" for example. If scaling information (SECPIXi) is not in the header, it must be supplied through the ASCfit option `-scale <as/pix>`.

A.3 Syntax and flag options for ASCfit

ASCfit is run from a bash shell, with synopsis:

```
ascfit infile [-s] [-f outfile] [-plot] [-ir] [-showoff]
[-verbose (int)] [-wide (float)] [-wdec (float)]
[-scale (float)] [-tolerance (float)] [-edge (int)]
[-nstar (int)] [-refstar (int)] [-estar (int)]
[-perr (float)] [-roff (float)] [-doff (float)]
[-mra (float)] [-mdec (float)]
[-box (int) (int) (int) (int) (0/1)]
[-color (float)] [-diffuse (float)] [-threshold (float)]
```

The flags have the following implications:
-s Save updated FITS file as "a_infile".
-f outfile Specify the name of the saved output file as "outfile".
-plot Output additional files that can be plotted in SM with macros in `ascfit.sm`.

-ir Select the infrared 2MASS point source catalog instead of the optical USNO-A2 catalog to search for reference stars.
-showoff Show the offsets from the nominal (header) position.
-verbose 1 Verbose mode, 1 for timing outputs, 2 for more elaborate output, default 0.
-wide 0.1 Set field width (RA & DEC) in degrees (default from header).
-wdec 0.1 Set field width (DEC only) in degrees (default from header).
-scale 0.54 Set pixel scale in arcsec (default from header).
-tolerance 0.1 Set allowed scale variance as LN[actual/assumed] (default 0.15 - effectively in %).
-edge 10 Specify number of pixels to be cut from the edge of the image search. Default 30.
-nstar 25 Set minimum number of bright IMAGE & REF stars (default 20).
-refstar 30 Set minimum number of bright REF stars only (default 20).
-estar 3 Exclude bright IMAGE stars (default 0).
-perr 100 Pointing error of telescope in arcsec. Will expand the area extracted from the reference catalog. Default 0.
-roff 20 & -doff 10.0 User specified RA and DEC offsets from pointing in header given in arcsec. Default 0.
-mra 120 -mdec -110 User specified RA/DEC offsets in arcsec of first mosaic chip 1 (default -140 -280). Offsets between UH8K mosaic chips are in the script, but can be modified for other cameras.
-box 10 1000 10 1000 1 Specify box boundary: xmin xmax ymin ymax 0/1 (0 exclude box, 1 include only box).
-color 1 MAG = R + color×(B-R) Change to another color (default 0.0). MAG = H + color×(J-H) Change to another ir color (default 0.0).
-diffuse 0.05 Specify the cutoff in the *SExtractor* galaxy/star classification parameter. High values are pointlike, low values are diffuse. Most untrailed stars have values > 0.5, but lower values are necessary to accept non-sidereal trailed stars (default 0.03).
-threshold 5 Specify the *SExtractor* threshold in sigma above background to detect objects in the image. A lower value will find more stars, default 10.

A.3.1 Multiple files

When a filename is passed to *ascfit* it first checks to see if that is the rootname of multiple files, and will work on all of them if it is, thus:

```
ascfit ccd.030 - will fit one file
ascfit ccd.03  - will expand list & fit ccd.030-039
ascfit ccd.0   - will expand list & fit ccd.000-099
```

A mosaic array is a particular case of this, thus for a case like the UH8K where the pointing axis has been moved off center:

```
ascfit 8k -roff 140 -doff 140
File list:  8k.0 8k.1 8k.2 8k.3 8k.4 8k.5 8k.6 8k.7
8k.0:12h42:51.08+0.535X-0.0020Y -01d20:36.2+0.538Y+0.0005X: 16/25/50*,0.47"RMS
8k.1:12h43:09.87+0.539X-0.0012Y -01d20:36.8+0.540Y+0.0014X: 14/21/42*,0.46"RMS
8k.2:12h43:09.31-0.537X+0.0003Y -01d02:07.8-0.538Y-0.0027X: 22/41/42*,0.49"RMS
8k.3:12h43:28.33-0.541X+0.0001Y -01d02:06.3-0.539Y-0.0017X: 13/23/42*,0.38"RMS
8k.4:12h44:06.04-0.536X+0.0020Y -01d02:06.6-0.538Y+0.0003X: 10/35/28*,0.47"RMS
8k.5:12h43:47.25-0.540X+0.0003Y -01d02:08.0-0.537Y+0.0002X: 10/28/40*,0.52"RMS
8k.6:12h43:47.72+0.538X-0.0003Y -01d20:36.1+0.539Y+0.0028X:  9/28/15*,0.46"RMS
8k.7:12h43:28.78+0.541X-0.0011Y -01d20:37.3+0.540Y+0.0009X: 17/23/38*,0.57"RMS
```

A.4 Options for the starfit program

The *starfit* program will use the two catalog files (`asc_ref.cat` and `asc_sextr.cat`) generated by *crect* or *msqbin* and *SExtractor* and can be run without the ASCfit script on these two files. A default setup for running *starfit* from the script is used. Modification of its operations may be obtained by using the following list of the flags accepted by *starfit*:

-d Default options, must be used if no other options are selected.
-plot Output additional files that can be plotted in SM with macros in `ascfit.sm`.
-silent Produce no commandline output from *starfit*.
-final Produce one line final output (if neither `-silent` nor `-final` is selected, output includes lists of the matched stars and the magnitude fit).

-mag writes final magnitude output.
-nstar 25 Set minimum number of bright IMAGE & REF stars (default 20).
-refstar 30 Set minimum number of bright REF stars only (default 20).
-estar 3 Exclude bright IMAGE stars (default 0).
-edge 10 Specify number of edge pixels to be excluded (default 30).
-scale 0.45 Pixel scale arcsec/pixel, (default 0.22).
-tolerance 0.1 Set allowed scale variance as LN[actual/assumed] (default 0.15 - effectively in %).
-color 1 MAG = R + color×(B-R) Change to another color (default 0.0).
MAG = H + color×(J-H) Change to another ir color (default 0.0).
-xpix 2048 -ypix 4096 Size of image in X and Y directions, used for the cropping of pixels near the edge and for the pinhole projection (default 2100 2068).
-box 10 1000 10 1000 1 Specify box boundary: xmin xmax ymin ymax 0/1 (0 exclude box, 1 include only box).
-diffuse 0.05 Specify the cutoff in the *SExtractor* galaxy/star classification parameter. High values are pointlike, low values are diffuse. Most untrailed stars have values > 0.5, but lower values are necessary to accept non-sidereal trailed stars (default 0.03).
-debug 3 Specify debug output level 1-5 for increasing debugging output.

A.5 Data for the infrared test case

The infrared example of the operation of the ASCfit program is shown below. What should be noted is the small number of objects detected in the image, this is often the case with infrared images.

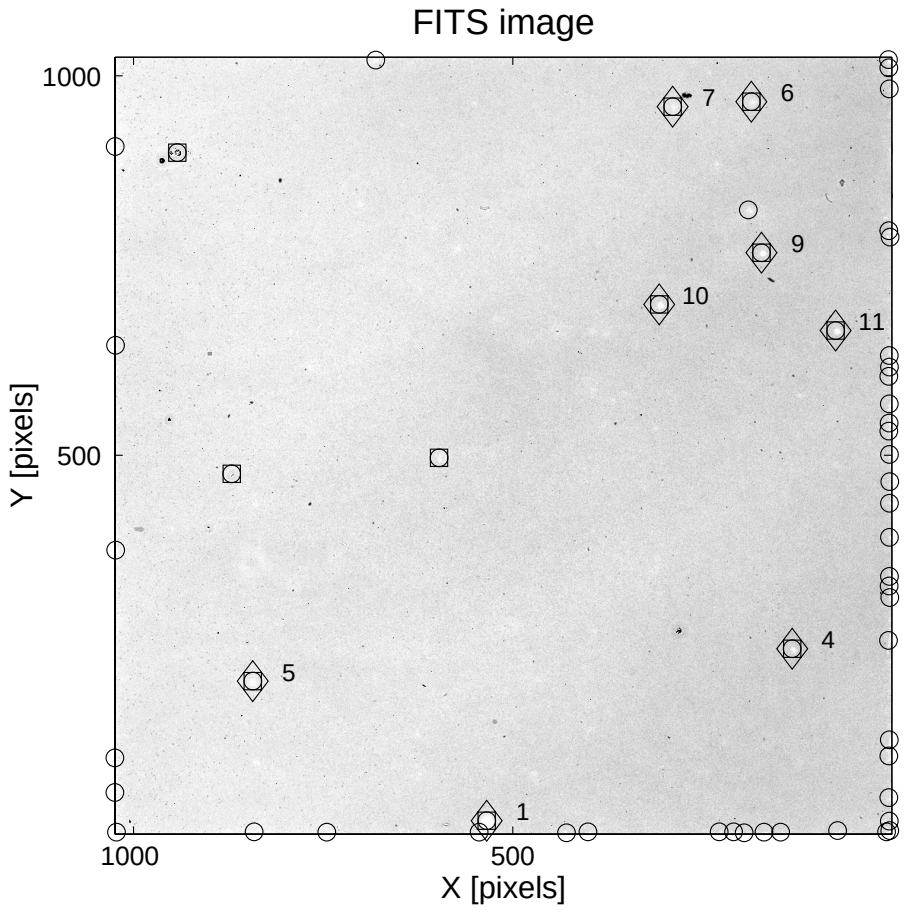

Figure A.1: *A FITS image taken using the infrared QUIRC camera. Detected stars are marked by circles, brightest stars by squares and the matched stars by diamonds.*

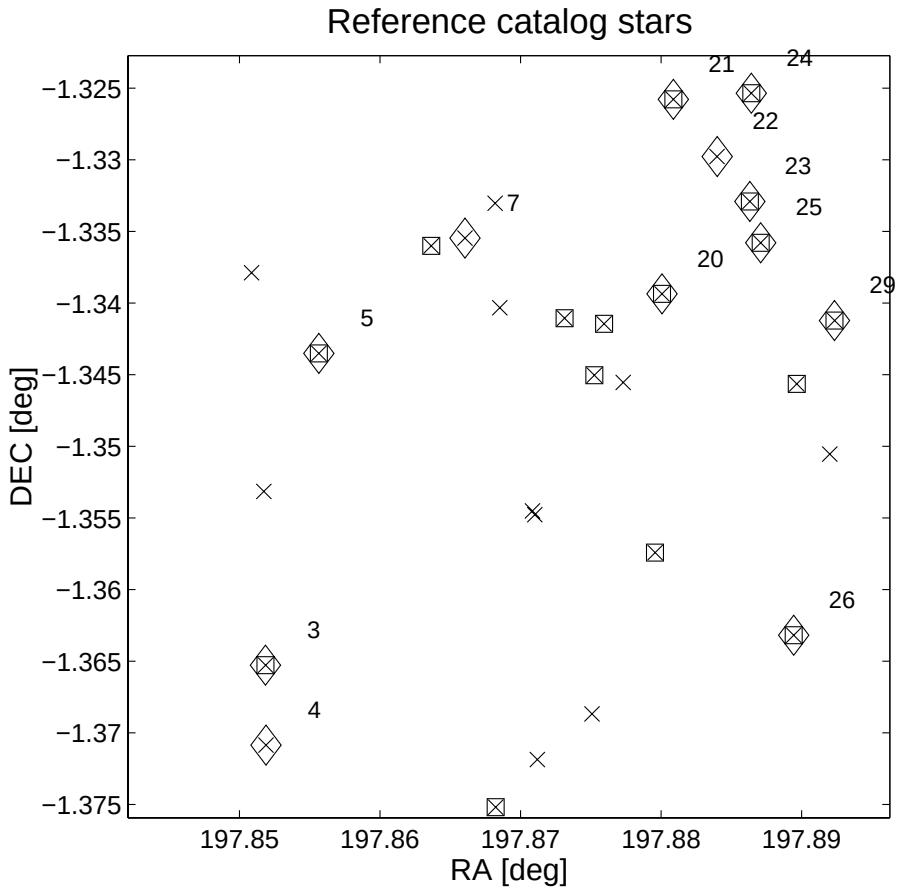

Figure A.2: *The reference catalog stars (crosses). Brightest stars are marked by squares and matched stars by diamonds.*

Appendix B

UH-24-inch TGS inter-calibration data

B.1 Results for the $O3$-$O3$ IC

Image 213:

$$\mathbf{R}_{ASC}^{TEL} = \begin{bmatrix} 0.73379890 & -0.67934380 & 0.00558202 \\ 0.67934397 & 0.73381681 & 0.00215667 \\ -0.00556130 & 0.00220954 & 0.99998209 \end{bmatrix}$$
$$(az, ze) \approx (-40^o, 55^o), v = 0.3429''$$

Image 216:

$$\mathbf{R}_{ASC}^{TEL} = \begin{bmatrix} 0.72281152 & -0.69103803 & -0.00315202 \\ 0.69101437 & 0.72281483 & -0.00615176 \\ 0.00652943 & 0.00226847 & 0.99997610 \end{bmatrix}$$
$$(az, ze) \approx (-100^o, 30^o), v = 0.3960''$$

B.2 Log of obtained images

Table B.1: Log of images taken for the UH 24-inch ASC inter-calibration on July 9, 2001. UT times refers to July 10, 2001.

Image ID	Ra [hh:mm:ss]	Dec [dd:mm:ss]	UT exp start	SAO number	Exposure time [s]
204	14:15:39.7	+19:10:56	05:46	100944	60
205	14:15:39.7	+19:10:56	05:46	100944	60
206	13:23:55.7	+55:54:17	05:56	28738	60
207	17:56:36.3	+51:29:19	06:04	30653	60
208	11:01:50.5	+56:22:55	06:13	27876	60
209	11:14:14.3	+15:25:45	06:21	99512	60
210	11:11:39.4	−22:49:23	06:27	179624	60
211	15:04:04.1	−25:16:54	06:33	183139	60
212	18:02:51.0	−24:16:56	06:39	186163	0.02
213	18:02:51.0	−24:16:56	06:44	186163	10
214	18:08:45.4	+20:48:51	06:51	85769	0.1
215	18:08:45.4	+20:48:51	06:51	85769	0.1
216	18:08:45.4	+20:48:51	06:56	85769	60
217	13:25:29.0	−43:01:00	07:07	NGC5128	60

Bibliography

[1] P. S. Jørgensen, J. M. G. Merayo, T. Risbo, A method for the determination of three euler angles for the SAC-C magnetic mapper probe instrument package, Sensors and Actuators A 95 (2001) 1–7.

[2] P. S. Jørgensen, A. Pickles, T. Betto, M. Riis, Ascfit - automatic stellar coordinate fitting package, in: ASP conference Series, Vol. ADASS XI Conference, Victoria BC, Canadal, in press, 2001.

[3] J. M. G. Merayo, P. Brauer, F. Primdahl, P. S. Joergensen, T. Risbo, J. Cain, The spinning Astrid-2 satellite used for modeling the Earth's main magnetic field, IEEE Transactions on Geoscience and Remote Sensing 40 (4) (2002) 898–909.

[4] M. D. Shuster, A survey of attitude representations, The Journal of the Astronautical Sciences 41 (4) (1993) 439–517.

[5] J. L. Synge, Handbuch der Physik, Springer Verlag, 1960, Ch. Classical Dynamics pp 1-223, in Band III/1, Prinzipien der Klassischen Mechanik und Feldtheorie.

[6] T. Risbo, Ørsted-2 vector magnetometer calibration I CSC magnetometer coil facility results - Ørsted technical note TN-347, Tech. rep., University of Copenhagen, Niels Bohr Institute AFG, Juliane Mariesvej 30, DK-2100 Copenhagen Ø (September 2000).

[7] Parkinson, Introduction to Geomagnetism, Scotish Academic Press, 1983.

[8] J. R. Wertz, Spacecraft Attitude Determination and Control, Kluwer Academic Publishers, 1978.

[9] O. V. Nielsen, J. R. Petersen, F. Primdahl, P. Brauer, B. Hernando, A. Fernandez, J. M. G. Merayo, P. Ripka, Development, construction and analysis of the 'Ørsted' fluxgate magnetometer, Meas. Sci. Technol. 6 (1995) 1099–1115.

[10] J. Jørgensen, A. Eisenman, C. Liebe, G. Jensen, The advanced stellar compass onboard the Ørsted satellite, in: 3rd ESA Symp. on Spacecraft Guidance, Navigation and Control Systems, ESTEC, ESA, 1997.

[11] T. Brahe, Astronomiæ Instauratæ Mechanica, Wandsbek 1598, english translation by H. Ræder, E. Strömgren and B. Strömgren: Tycho Brahes's Description of his instruments and Scientific Work, Copenhagen 1946, 1598.

[12] M. D. Shuster, D. S. Pitone, G. J. Bierman, Batch estimation of spacecraft sensor alignments I. relative alignment estimation, The Journal of the Astronautical Sciences 39 (4) (1991) 519–546.

[13] R. Desjardins, In-orbit startracker misalignment estimates on the OAO, in: Proceedings, Symposium of Spacecraft Attitude Determination, El Segundo, California, September 20-October 2, 1969, pp. 143–153.

[14] G. Abshire, R. McCutcheon, G. Summers, F. Vanlandingha, G. Meyers, High precision attitude determination for Magsat, in: Proceedings, ESA International Symposium on Spaceflight Dynamics, Darmstadt, Federal Republic of Germany, 1981.

[15] G. M. Lerner, M. D. Shuster, In-flight magnetometer calibration and attitude determination for near-earth spacecraft, Journal of Guidance and Control 4 (1981) 518–522.

[16] M. D. Shuster, D. M. Chitre, D. P. Niebur, In-flight estimation of spacecraft attitude sensor accuracies and alignments, Journal of Guidance, Control and Dynamics 5 (1982) 339–343.

[17] G. J. Bierman, M. D. Shuster, Spacecraft alignment estimation, in: Proceedings of the 27th Conference on Decision and Control, 1988, pp. 856–859.

[18] M. D. Shuster, D. S. Pitone, Consistent estimation of spacecraft sensor alignments, in: Proceedings of the 1990 American Control Conference, 1990, pp. 1389–1395.

[19] G. M. Lerner, Attitude sensor calibration using scalar observations, The Journal of the Astronautical Sciences 38 (2) (1990) 201–213.

[20] M. D. Shuster, D. S. Pitone, Batch estimation of spacecraft sensor alignments II. absolute alignment estimation, The Journal of the Astronautical Sciences 39 (4) (1991) 547–571.

[21] W. Davis, Hashmall, J. Garrick, R. Harman, Postlaunch calibration of spacecraft attitude instruments, Advances in the Astronautical Sciences 84 (1993) 1085–1099.

[22] D. B. Reid, Calibration of the Milstar attitude determination system, in: Proceedings of the American Control Conference, Albuqerque, New Mexico, June 1997, 1997, pp. 557–563.

[23] T. Risbo, N. Olsen, Attitude intercalibration of the star imager and the spherical compact sensor magnetometer for the Ørsted geomagnetic satellite mission, Proceedings of the SPIE - The International Society for Optical Engineering, 2810 (1996) 230–8.

[24] K. Gödderz, H. Lühr, M. Rother, R. Bock, CHAMP optical bench star camera/vector magnetometer inter-calibration, Workshop on Calibration of Space-Borne Magnetometers, Braunschweig march 9, 1999. "Ground and In-Flight Space Magnetometer Calibration Techniques" (1999).

[25] The Astronmical Almanac for the Year 1997, Her Majesty's Nautical Almanac Office, Royal Greenwich Observatory, London, 1997.

[26] W. Torge, Geodesy, 2nd Edition, deGruyter, New York, 1991.

[27] W. Menke, Geophysical Data Analysis: Discrete Inverse Theory, Vol. 45 of International Geophysics Series, Academin Press, 1989.

[28] W. H. Press, W. T. Vetterling, S. A. Teukolsky, B. P. Flannery, Numerical Recipes in Fortran, Cambridge University Press, 1994.

[29] J. Kovalevsky, Modern Astrometry, Springer-Verlag, Berlin, 1995.

[30] A. Chapman, Astronomical Instruments and Their Users, Variorum, 1996.

[31] R. P. Feynman, R. B. Leighton, M. Sands, The Feynman Lectures on Physics, Vol. 1, Addison-Wesley Publishing Company, 1977, sixth printing.

[32] R. Bock, H. Lühr, CHAMP attitude aberration correction, Tech. Rep. CH-GFZ-TM-2702, GFZ Potsdam (2001).

[33] G. Seeber, Satellite Geodesy, de Gruyter, Berlin, 1993.

[34] B. Pedersen, O. Rasmussen, Installation og kalibrering af et refference magnetometer på TMO 23-25 oktober 1996, Danish Meteorological Institute, in danish (1997).

[35] Mignard, Report of the IAU working group on ICRS, in: K. J. Johnston, D. D. McCarthy, B. J. Luzum, G. H. Kaplan (Eds.), Towards Models and Constants for Sub-Microarcsecond Astrometry, Proceedings of the IAU Colloquium 180, 2000.

[36] E. Bertin, S. Arnouts, Sextractor: Software for source extraction, Astronomy and Astrophysics, Supplement Series 117 (1996) 393–404.

[37] E. J. Groth, A pattern-matching algorithm for two-dimensional coordinate lists, The Astronomical Journal 91 (5) (1986) 1244–1248.

[38] F. Primdahl, The fluxgate magnetometer, Journal of Physics E: Scientific Instruments 12 (1979) 241–53.

[39] F. Primdahl, P. Anker Jensen, Compact spherical coil for fluxgate magnetometer vector feedback, Journal of Physics E: Scientific Instruments 15 (1982) 221–226.

[40] P. Brauer, The ringcore fluxgate sensor, Ph.D. thesis, Technical University of Denmark (1997).

[41] J. M. G. Merayo, P. Brauer, F. Primdadhl, J. R. Petersen, O. V. Nielsen, Scalar calibration of vector magnetometers, Measurement science and technology 11 (2000) 120–132.

[42] T. Risbo, P. Brauer, J. M. G. Merayo, O. V. Nielsen, J. R. Petersen, F. Primdahl, N. Olsen, Ørsted calibration mission: The thin shell method and spherical harmonic analysis, Workshop on Calibration of Space-Borne Magnetometers, Braunschweig march 9, 1999. "Ground and In-Flight Space Magnetometer Calibration Techniques" (1999).

[43] S. W. Shepperd, Quaternion from rotation matrix, Journal of guidance and control 1 (1978) 223–224.

[44] E. W. Greisen, M. Calabretta, Representation of world coordinates in FITS, Astrophysics .

[45] J. Hodapp, K.-W. abd Hora, D. Hall, L. Cowie, M. Metzger, E. Irwin, K. Vural, L. Kozlowski, S. Cabelli, C. Chen, D. Cooper, G. Bostrup, R. Bailey, W. Kleinhans, The Hawaii infrared detector arrays: testing and astronomical characterization of prototype and science-grade devices, New Astronomy 1 (2) (1996) 177–96.

[46] G. Luppino, M. Metzger, N. Kaiser, D. Clowe, I. Gioia, S. Miyazaki, Observations of weak lensing in clusters with an 8192*8192 CCD mosaic camera, Astronomical Society of the Pacific Conference Series 88 (1996) 229–32.

[47] D. Monet, B. A., B. Canzian, C. Dahn, H. Guetter, H. Harris, A. Henden, S. Levine, C. Luginbuhl, A. K. B. Monet, A. Rhodes, B. Riepe, S. Sell, R. Stone, F. Vrba, R. Walker, The USNO-A2.0 catalogue, U.S. Naval Observatory, Washington DC (1998).

[48] T. Jarrett, T. Chester, A. Cutri, S. Schneider, M. Skrutskie, J. Huchra, 2MASS extended source catalog: overview and algorithms, Astronomical Journal Vol.119 Issue 5 (2000) 2498–531.

[49] J. M. G. Merayo, Magnetic gradiometry, Ph.D. thesis, Technical University of Denmark (1999).

[50] J. Jørgensen, Private comunications.